SYNTHESIS AND APPLICATION OF SILICA BASED MESOPOROUS MATERIALS FOR REMOVAL OF ENDOCRINE DISRUPTING COMPOUNDS IN AQUEOUS SOLUTION

SHANMUGA SUNTHARAM A/L KITTAPPA

DEPARTMENT OF CIVIL ENGINEERING
FACULTY OF ENGINEERING
UNIVERSITY OF MALAYA
KUALA LUMPUR

2015

SYNTHESIS AND APPLICATION OF SILICA BASED MESOPOROUS MATERIALS FOR REMOVAL OF ENDOCRINE DISRUPTING COMPOUNDS IN AQUEOUS SOLUTION

SHANMUGA SUNTHARAM A/L KITTAPPA

DESSERTATION SUBMITTED IN FULFILMENT OF THE REQUIREMENTS FOR THE DEGREE OF MASTER OF ENGINEERING SCIENCE

DEPARTMENT OF CIVIL ENGINEERING
FACULTY OF ENGINEERING
UNIVERSITY OF MALAYA
KUALA LUMPUR

2015

UNIVERSITY OF MALAYA

ORIGINAL LITERARY WORK DECLARATION

Name of Candidate: Shanmuga Suntharam a/l Kittappa (I.C No:

Matric No: KGA 130024

Name of Degree: Master of Engineering Science

Title of Dissertation ("this Work"): Synthesis and Application of Silica Based Mesoporous Materials for Removal of Endocrine Disrupting Compounds in Aqueous Solution.

Field of Study: Environmental Engineering

I do solemnly and sincerely declare that:

(1) I am the sole author/writer of this Work;

(2) This Work is original;

(3) Any use of any work in which copyright exists was done by way of fair dealing and for permitted purposes and any excerpt or extract from, or reference to or reproduction of any copyright work has been disclosed expressly and sufficiently and the title of the Work and its authorship have been acknowledged in this Work;

(4) I do not have any actual knowledge nor do I ought reasonably to know that the making of this work constitutes an infringement of any copyright work;

(5) I hereby assign all and every rights in the copyright to this Work to the University of Malaya ("UM"), who henceforth shall be owner of the copyright in this Work and that any reproduction or use in any form or by any means whatsoever is prohibited without the written consent of UM having been first had and obtained;

(6) I am fully aware that if in the course of making this Work I have infringed any copyright whether intentionally or otherwise, I may be subject to legal action or any other action as may be determined by UM.

Candidate's Signature Date:

Subscribed and solemnly declared before,

Witness's Signature Date:

Name:

Designation

ABSTRACT

The economical synthesis route of silica based mesoporous materials using eco-friendly and cheaper chemicals and material was studied. Three mesoporous silica-based materials were successfully synthesized and applied for the removal of endocrine disrupting compounds (EDCs): mesoporous silica materials (MSMs) synthesized by reacting pore templating agent Pluronic P123® with silica (SiO_2) powder instead of organometallic precursors [i.e. tetraethyl orthosilicate (TEOS)]; magnetised nanocomposite silica material (MNCM) synthesized by incorporating MSMs with nano magnetite; and N^1-(3-Trimethoxysilylpropyl) diethylenetriamine (Tris) coated magnetised nanocomposite silica materials (MNCMT) synthesized by incorporating MNCM with Tris. The synthesized materials were characterized by X-ray diffraction (XRD), Brunauer–Emmett–Teller (BET)/Barrett-Joyner-Halenda (BJH) surface and pore size distribution analysis, fourier transform infra-red spectroscopy (FTIR), magnetometer, zetasizer, field emission scanning electron microscopy (FESEM) and transmission electron microscopy (TEM).

In the first phase, MSMs were synthesized at different calcination temperatures and tested for the removal and drug loading capacities of ibuprofen (IBP). The results of isotherms and kinetics of IBP removal indicated that MSM calcined at 500 ^oC (MSM–500) had the highest sorption capacity and speed than other MSMs, SBA–15 and zeolite. The IBP removal mechanism was identified as a hydrophilic interaction between the carboxylic group (COO–) of IBP and silanol (Si–OH) of the pore surface.

In the second phase, to further improve the separation process, MNCMs were prepared using SiO_2 and nano-magnetite (Fe_3O_4) via a new synthetic route, and applied to remove methylene blue (MB). Among the synthesized materials (MNCM-0.25, -0.5 and -1),

MNCM-1 was found to have the magnetic property (2.9 emu/g) and highly sharp pore size distribution. It also had high and fast adsorptive ability to remove MB. The removal of MB by MNCM-1 is a physisorption process and thermodynamically favourable at higher temperatures. The process involves an electrostatic interaction between negatively charged silanol ($Si\text{-}O^-$) and positively charged MB. Conversely, the removal of other EDCs such as BPA, CFA and IBP with MNCM-1 was not very effective.

In the third phase, MNCM was functionalized by incorporating 1 mmol, 2 mmol and 3 mmol of N^1-(3-Trimethoxysilylpropyl) diethylenetriamine (Tris), and the products were denoted as MNCMT-1, -2 and -3, respectively. The synthesized MNCMTs products were used to remove ibuprofen (IBP), bisphenol A (BPA) and clofibric acid (CFA). Whilst, the resulting MNCMT-3 revealed the highest adsorption capacity (182 mg/g) for the removal of BPA followed by MNCMT-2 and -1, MNCMT-1 was demonstrated to have higher adsorption capacity than MNCMT-2 and -3 for IBP and CFA. The removal mechanism of BPA, IBP and CFA was influenced by the hydrophobicity behaviour and the surface charge of MNCMT, which was dominantly affected by the $\pi-$ hydrogen bonding between the adsorbate and adsorbent. A cost analysis study revealed that MSM, MNCM and MNCMT were much cheaper than any other mesoporous silica material for the removal of EDCs.

ABSTRAK

Dalam penyelidikan ini, telah dilaporkan sintesis silika mesoporous dengan menggunakan bahan mesra alam dan murah. Tiga bahan mesoporous silika telah berjaya disintesis untuk penyingkiran "endocrine disrupting compound" dengan menggunakan agent pembentukkan Pluronic P123 dan silika (SiO_2) mengantikan organometalik precursor iaitu [i.e (tetraethyl orthosilicate (TEOS)]; bahan magnetic nano komposit (MNCM) di sintesis dengan menggunakan nanomagnet and mesoporous silika; (MNCMT) magnetic nano material disadur dengan Tris (N^1- (3-Trimethoxysilylpropyl) diethylenetriamine) dihasilkan dengan menggunakan Tris dan mesoporous silika nano komposit (MNCM) . Buat pertama kali, bahan silika mesoporous (MSM) telah disintesis menggunakan Pluronic P123® dan serbuk silika (SiO_2). Bahan kimia organologam seperti TEOS telah digantikan dengan bahan kimia lain. Keadaan eksperimen seperti suhu, jisim magnetit dan jumlah Tris telah dioptimumkan untuk menghasilkan bahan terbaik ciri-ciri fizikalnya. Bahan-bahan yang disintesis dicirikan melalui penggunaan x-ray pembelauan (XRD), BET dan BJH permukaan dan saiz liang analisi, Fourier Transform infra-merah spektroskopi (FTIR), magnetometer, Zetasizer, Field pelepasan mikroskop imbasan elektron (FESEM) dan penghantaran elektron mikroskopi (TEM).

Peringkat pertama penyelidikan ini adalah penghasilan bahan mesoporous silica (MSM) pada suhu sintesis yang berlainan. Isotherma dan kinetik penyingkiran ibuprofen (IBP) menunjukkan bahawa MSM−500 mempunyai kapasiti penjerapan yang paling tinggi berbanding dengan bahan silika lain seperti SBA−15 dan zeolite. Berdasarkan analisis FTIR, mekanisme tindak balas telah dikenal pasti sebagai interaksi hidrofilik antara kumpulan karboksilik (COO-) pada IBP dan silanol (Si-OH) atas permukaan liang.

Peringkat kedua adalah penghasilan bahan MSM yang boleh diasingkan dengan menggunakan magnet supaya memudahkan proses penyingkiran . Bahan magnetit yang dihasilkan dinamakan sebagai bahan magnetit nanokomposit silica (MNCM) yang telah disediakan dengan menggunakan silika (SiO_2) dan nano-magnetit (Fe_3O_4). Antara bahan-bahan disintesis, MNCM−1, yang disediakan dengan nisbah berat molekul Fe_3O_4 untuk SiO_2 0.14: 1, mempunyai struktur mesopore homogen dengan saiz liang min 4.68 nm, luas permukaan 576 m^2g^{-1}, dan isipadu liang 0.65 cm^3g^{-1}. MNCM−1 mempunyai kekuatan magnet (2.9 emu) dan kekuatan struktur yang baik. MNCM−1 menunjukkan penjerapan lebih tinggi dan lebih cepat terhadap metilena biru (MB) berbanding penyingkiran daripada bahan mesoporous lain. Didapati bahawa, penyingkiran MB oleh MNCM−1 adalah melalui proses penjerapan fizikal dengan interaksi elektrostatik antara silanol bercas negatif ($Si{-}O^-$) dan MB bercas positif.

Peringkat ketiga adalah untuk meningkatkan penyingkiran bahan-bahan EDCs pengubahsuaian bahan dilakukan dengan menggunakan N1- (3-Trimethoxysilylpropyl) diethylenetriamine. MNCMT dengan 1mmol, 2mmol dan 3mmol telah berjaya disintesis dengan menggunakan kaedah pasca sintesis. Bahan MNCMT telah digunakan untuk mengkaji penyingkiran pelbagai EDCs seperti ibuprofen (IBP), bisphenol A (BPA), asid clofibric (CLO) dan metilina biru (MB). MNCMT- 3mmol menunjukkan kapasiti tertinggi penjerapan 182 mg g^{-1} untuk penyingkiran BPA diikuti oleh 2mmol dan 3mmol MNCMT. Walau bagaimanapun dalam kes IBP dan CLO 1mmol MNCMT menunjukkan kapasiti penjerapan lebih tinggi daripada 2 dan 3mmol MNCM-T. Mekanisme telah disiasat untuk memahami keupayaan penjerapan yang berbeza menunjukkan bahawa cas permukaan MNCMT, hidrofobik and ikatan –hidrogen memainkan peranaan dalam penjerapan EDC. Kajian analisa kos telah mendedahkan bahawa MSM, MNCM dan MNCMT jauh lebih murah daripada bahan silika mesoporous lain untuk penyingkiran EDC.

ACKNOWLEDGEMENT

This thesis would have not been possible without the support, encouragement, love and motivation of many people, who have contributed to the completion of this study. Firstly, I would like to express my sincere gratitude to my supervisor, Professor Dr. Min Jang for his time, knowledge, support and guidance, which has been the great encouragement for me to complete this thesis.

My heartfelt gratitude goes to my beloved wife, Dr. Malarvili Shanmuga for her constant encouragement, support, patience and love, which has been a great motivation for me to continue my studies. My lovely boys, Saveen Raj and Yashveen Raaj, who have always been understanding and provide me their love and support during this challenging and stressful period. A special thanks to my beloved niece Keithanchali Mohananaidu, for her encouragement and motivation. Thanks to my fellow lab buddies especially, Ranjini, Sharmini, Mohsen, Farahin, Payam, Wong, Kang and Leong. Thanks also to the undergraduates, Farhan and Gerald, who have worked along with me in the laboratory. A special gratitude to some of the laboratory technicians and assistants, who have guided and helped me to conduct my experiments and analysis, especially Pn. Kalai, Pn Rozita and Cik Alya from the Department of Civil Engineering, En. Rahman from the Faculty of Science and En. Jasmi from the Institute of Postgraduate Studies. I would like to take this opportunity to acknowledge my sponsors the Ministry of Higher Education Malaysia and High Impact Research Malaysia (HIR) for providing me the financial assistance for this project

Last but no least “Thank you God for all your blessings, love and care in guiding me through to the completion of this thesis”.

TABLE OF CONTENTS

LIST OF FIGURES

LIST OF TABLES

LIST OF SCHEMATIC

LIST OF SYMBOLS AND ABBREVIATIONS

$	Dollar
%	Percent
°C	Degree celcius
1/n	Adsorption strength
2θ	2 Theta
Å	Ångström, 10^{-10} meter
AC	Activated carbon
ACS	American Chemical Society
AOPs	Advanced Oxidation Process
BOD	Biological oxygen demand
BET	Brunauer-Emmet-Teller
BJH	Barrett-Joyner-Halenda
BPA	Bisphenol A
C_0	Initial concentration
C_{eq}	Concentration at equilibrium
CFA	Clofibric acid
cm^3/g	Centimeter cube per gram
COD	Chemical oxygen demand
CNT	Carbon nano tubes
CO_2	Carbon dioxide
COO^-	Carboxylic ion

CPAC	Charcoal powdered activated carbon
emu	Electromagnetic unit
FESEM	Field Emission Scanning Electron Microscopy
FTIR	Fourier transform infrared spectroscopy
g	Gram
g/mol	Gram per mole
GAC	Granular Activated Carbon
h	hours
IBP	Ibuprofen
IUPAC	International Union of Pure and Applied Chemistry
K	Kelvin
K_2	Pseudo 2^{nd} order kinetic constant
K_L	Langmuir constant
K_F	Freundlich constant
KOe	Kilo-oersted
m^2/g	Meter square per gram
m^3	Meter cube
M41S	Mesoporous materials
MB	Methylene Blue
MCM-41	Mobil Composition of Matter No. 41
mg/g	Milligram per gram
mg/L	Milligram per litre

min	minutes
mL	Millilitre
mmol	Millimole
mmol/g	Millimole per gram
MNCM	Magnetized Nano Composite Material
MNCMT	Magnetised Nano Composite Material coated with Tris
MSM	Mesoporous silica material
mV	Millivolt
nm	Nanometre
NSAID	Nonsteroidal anti-inflammatory drug
O_2	Oxygen
pKa	Dissociation constant
POPs	Persistent organic pollutants
ppb	Part per billion
PPCPs	Pharmaceutical and personal care products
ppm	Part per million
q_{ecalc}	Adsorption calculated using pseudo 2^{nd} order kinetic
Q_{eq}	Adsorption at equilibrium
Qmax	Maximum adsorption capacity
Q_{max}	Maximum adsorption capacity
Q_t	Adsorption capacity at time t
q_t	Adsorption at time t

R^2	Coefficient of determination
RM	Ringgit Malaysia
rpm	Revolution per minute
SBA-15	Santa Barbara Amorphous material
SEM	Scanning Electron Microscopy
Si	Silica
SiO_2	Silicon dioxide
Si-OH	Silanol
t	time
TEM	Transmission electron microscopy
TEOS	Tetraethyl orthosilicate
TRIS	N1-(3-Trimethoxysilylpropyl) diethylenetriamine
TSS	Total suspended solidS
UV	Ultraviolet
v_o	Initial sorption rate
WHO	World Health Organization
XRD	X-ray diffraction
$\Delta_{ads}G$	Adsorption Gibbs free energy
$\Delta_{ads}H$	Adsorption Enthalpy
$\Delta_{ads}S$	Adsorption Entropy
ΔE_a	Arrhenius activation energy
π	Pi

1. INTRODUCTION

1.1 Water, environment and socioeconomic

Recently, water pollution has become the most important environmental concern. In year 2014, our country faced a long period of drought with many places facing water cuts, shortage and rationing. Klang Valley and Selangor have been the worst affected areas; residents encountered very tough time to get clean water to endure their daily lives. In a more global perspective, especially in third world countries water has been a major issue causing instability, socio-economic problem and in a worst case scenario, wars. Women and children are suffering from drinking contaminated water which contains high levels of toxins and pollutants. According to the World Bank data, our country receives abundance of rain fall around 200 to 300 mm every month. Our monsoon seasons are long and they bring a lot of rain to Peninsular Malaysia and the eastern states of Sabah and Sarawak. Nevertheless, getting clean water was difficult and the condition further deteriorates.

Main source for clean water comprises rivers, lakes and ponds that have been polluted severely. Some studies even mentioned that 80 % of the surface water in our country is already polluted and not suitable for drinking purpose. Malaysian rivers, at present are heavily contaminated with discharges from many different sources. These discharges are from industrial effluents, waste waters from factories, agricultural activities, domestic or municipal sources and also from some other unknown sources (Kadhum, Ishak, Zulkifli, & Roshaslinya , 2015; Md Paudi Abdullah, 2015).

1.2 Pollutants in the water source

Most of our river waters are already heavily polluted and the water quality has deteriorated. Main contaminants were found to be sourced from industrial and residential discharges to the water sources. Heavy metals, biological oxygen demand (BOD), chemical oxygen demand (COD) and total suspended solid (TSS) were discovered to be higher than their permissible level. Many studies over the last 10 years, focussed on these contaminants and their removals from water source.

1.3 Micropollutants

Many scientists have diverted their research focus to pollutants that are present at very low concentrations (i.e. ppb ~ ppt) in water, known as micropollutants. Although the concentration is low, these micropollutants cause potential health hazards and ecotoxicological effects to humans and other wild lives. In most countries, the discharge of organic pollutants from industrial effluents resulted in severe impact on the soil and water bodies. Industrial effluents containing micropollutants such as endocrine disrupting compounds (EDCs), pharmaceutical chemicals, disinfection by-products (DBPs), persistent organic pollutants (POPs), dyes and trace metal-organic complexes have significant negative effects on the water quality. Wastewater discharged from various industries, such as textiles, paper manufacturing, wool colouring, and paint production, contains not only micropollutants, but also high levels of organic dyes and heavy metals. (Xiao, Zhang, Feng, Deng, & Wang, 2015)

There are two main issues associated with micropollutants in waters: most of the existing approaches hinder the detection of micropollutants; most micropollutants were either not detected or below the detection limit, and the available current analytical equipment or remediation techniques are rather complicated and expensive. Each of

these issues has limitations, and they require serious remedial action and attention. Taking into account the technical limitations of currently used technologies, the complexity and high cost, an outcome for establishment of new simple methods and use of cheap materials that are environmentally friendly should be considered for remediation purpose. The use of these options not only will resolve the discussed shortcomings but also may resolve the secondary pollution problem and evade the water from being contaminated during and after the water treatment.

1.4 Research gaps

- There is a need to develop or modify materials that are able to remove various types of micropollutants.
- The materials must be cost efficient and should be commercially applicable and viable for water treatment purpose
- The materials should not cause any secondary contamination during the water treatment process

1.5 Objectives of this research

The main objective of this research was to develop mesoporous silica material (MSM), magnetized nano composite material (MNCM) and Tris incorporated magnetised nano composite material (MNCMT) through a simple synthesis route using eco-friendly and economical chemicals for the removal of selected micropollutants from water.

The specific objectives are listed:

1) To economically synthesize and optimize MSM, MNCM and MNCMT using SiO_2 instead of an expensive Si precursor, tetraethyl orthosilicate (TEOS).

2) To develop magnetized MNCM for an easy separation during water treatment process.

3) To synthesize functionalised MNCMT to enhance the removal of various EDCs.

4) To elucidate the removal mechanism of the materials using physical chemical analysis and various batch tests.

1.6 Thesis overview

This thesis is divided into six (6) different chapters. Chapter One (1) contains the introduction and objectives of this research. In Chapter Two (2), a detailed literature review is presented focussing on key micropollutants and materials. The experimental process and synthesis is explained in Chapter Three (3). In Chapter Four (4), all results and findings are presented and discussed. Chapter Five (5) concludes the findings of this study, while Chapter Six (6) contains references and followed by supplementary section of publications and conference details.

2. LITERATURE REVIEW

2.1 Pharmaceutical and Personal Care Products (PPCPs)

Pharmaceutical and Personal Care Products (PPCPs) are a group of chemicals originated from pharmaceutical drugs, cosmetic products, detergents, household chemicals, personal care products, toiletries, shampoo, soaps and many more. PPCPs are not fully metabolized or used in the body and the residues are excreted via urine and faeces (Serrano, Lema, & Omil, 2010). Hospitals and landfills are major sources of PPCPs, The leachates from these sources have been reported to contain high concentration of PPCPs, (micrograms to nanograms per litre) (Serrano et al., 2010). These leachates flow and mix with the nearest water sources such as river, lakes and ponds. Agricultural discharge of excess sludge contains hydrophobic PPCPs that may cause potential risk to the environment (Kimura, Hara, & Watanabe, 2007).

The removal of PPCPs in drinking water has been widely studied for the last 10 years. The main cause of this interest is mainly due to the high usage of pharmaceutical drugs by humans and the excretion process, which eventually pollute the drinking water system. In many countries surface water is the primary source of water, which is popularly used for drinking, agricultural and life stock rearing activities. However, due to the anthropogenic activities, these surface water sources became contaminated in many ways. Contaminated surface water can affect the health of human and animals when they consume, and for aquatic organisms, when they ingest the contaminated sediments.

2.2 Endocrine disrupting Compounds (EDCs)

EDCs can be defined as an exogenous substance or mixture that alters the function(s) of the endocrine system and causes adverse health effects in an intact organism or population (Organization, 2002). Research shows that pharmaceutical residues in water known as EDCs could bioaccumulate in human population. Research conducted in Europe and US have revealed that EDCs are the most common micropollutants found in many water sources and waste waters Many papers have reported the presence of PPCPs and EDCs in water sources particularly for drinking purpose (Cleuvers, 2004; Connors, 2013; Ternes et al., 2002). Exposure to EDCs in water has been associated with adverse health effects. Fent et. al has confirmed that EDCs, even at very low concentrations (ppb levels) can cause serious health risks to living organism (Fent, Weston, & Caminada, 2006). Also, other studies have reported that EDCs cause health effects such as early puberty and menopause, early breast growth and lactation; and uterine related diseases such as fibroids and endometriosis (Jones, Green, Voulvoulis, & Lester, 2007). These EDCs were not only found to affect the human endocrine system, but also the aquatic wild life, causing ecotoxicological effects (Jermann, Pronk, Boller, & Schäfer, 2009). Of particular concern is the effect in relation to fish reproduction caused by feminization and masculinization of fish in the aquatic wildlife (Jermann et al., 2009; McLachlan, Simpson, & Martin, 2006; Tsutsumi, 2005). 17 α-ethinylestradiol can give common contraceptive effects on the reproduction of zebra fish (Ternes, 2001). This can lead to the reduction of fish and other aquatic population growth in the water bodies. For this particular research, four (4) EDCs have been selected; IBP, BPA, CFA and MB. Table 2.1 listed some types of EDC compounds and their research focus as well as the highlights.

Table 2.1: Compilation of Selected Literature Reports on EDCs

Type of EDC	Research Highlights and Findings	Ref.
Ibuprofen (IBP)	Ibuprofen has been encapsulated in MCM-41 silica with different pore sizes. Interaction with silica surface and IBP was weak, which favours the fast drug release. Carboxylic acid group of IBP was in a chemical exchange state and IBP can be crystallized in the pores of MCM-41.	(Azaïs et al., 2006)
Ibuprofen (IBP) and Triclosan (TCL)	Single wall, multi wall and oxides multi wall carbon nano tubes were studied for the adsorption of IBP and TCL.	(Cho, Huang, & Schwab, 2011)
Naproxen and clofibric acid (CFA)	Endocrine disrupting compound has been removed using modified metal organic framework (MOF), MOF denoted as MIL-101 was able to remove the EDCs at much faster adsorption rates than activated carbon. The removal mechanism suggested was electrostatic interactions.	(Hasan, Jeon, & Jhung, 2012)
Ibuprofen (IBP)	The role of 3-aminoprpyltriethoxysilane in the preparation of mesoporous silica nanoparticles for IBP delivery. The effect on physiochemical properties and the removal mechanism were studied.	(Kamarudin et al., 2013)
Molsidomine	The phenyl modified silica was the most quantitatively and energetically favourable to remove molsidomine. The thermodynamic effects were discussed in detail.	(Nonna A Alyoshina & Elena V Parfenyuk, 2013)

Table 2.1: Continued

Type of EDC	Research Highlights and Findings	Ref.
Fluorescein and Mercury	Magnetic SBA-15 was used to remove the environmental wastes, which could be separated magnetically. The uptake of mercury was almost 97 % within 7 h. Fluorescein was adsorbed within minutes and solution became clear. Mag-SBA-15 has a great potential for application at large treatment plant.	(B. C. Kim et al., 2011)
BPA	Organic-inorganic hybrid mesoporous silica material was synthesized by co-condensation of phenyltriethoxysilane (Ph-MS) and tetraethoxysilane. Ph-MS adsorbed most amount of BPA faster than activated carbon. Highest adsorption capacity was 351 mg/g.	(Y.-H. Kim, Lee, Choo, & Choi, 2011)
Carbazepine Estrone CFA IBP Iopromide Diclofenac	Functionalized mesoporous SBA-15 was studied for the removal of 12 types of EDCs. The removals of hydrophobic and hydrophilic EDCs were investigated. Adsorption of nine EDCs by functionalized SBA-15 was higher than sole SBA-15.	(Bui, Kang, Lee, & Choi, 2011)
IBP	MCM-41 had higher drug loading capacity than SBA-3. The main interaction between silica surface and IBP is hydrogen bonding.	(Andersson, Rosenholm, Areva, & Lindén, 2004)

Table 2.1: Continued

Type of EDC	Research Highlights and Findings	Ref.
BPA	Phenyl functionalised mesoporous silicas (Ph-MSs) were synthesized and their removal of BPA was investigated. It was found that Ph-MSs removes BPA better due to the hydrophobic interaction between the adsorbent and adsorbate.	(Y.-H. Kim, Lee, Choo, & Choi, 2014)
MB	Mesoporous NiO/MCM-41 was prepared by chemical precipitation process. NiO/MCM-41 showed high adsorption capacity (22.4 mg/g) for MB.	(Xiao et al., 2015)
MB	A sandwich structured $ZeCe_{0.03}Fe_{1.97}@SiO_2@SBA\text{-}15$ was synthesized. It was rod like shape material with uniform mesochannels and had the maximum adsorption capacity (241 mg/g) of MB.	(Kuai & Nan, 2014)
MB	Nanoporous SBA-3 was successfully synthesized and the adsorption behaviour was studied. The adsorption equilibrium reached within 1 h and fitted well with Langmuir and pseudo-2^{nd} order kinetic model.	(Anbia & Hariri, 2010)
IBP	Using single step process, hollow mesoporous silica spheres with and without modification was synthesized. Highest ibuprofen storage (969 mg/g) has been achieved.	(Zhu et al., 2005b)

2.2.1 Ibuprofen (IBP)

Ibuprofen is classified as non-steroidal anti inflammation drug (NSAID) and is used widely as common pain killer, relieving pain, fever and inflammation (Cho et al., 2011; Sadecka, Čakrt, Hercegová, Polonský, & Skačáni, 2001; Zhu et al., 2005b). World Health Organization (WHO) assessment indicated IBP was the leading micropollutant found at the highest concentration in comparison to other micropollutants including erythomycin, bleomycin and others (WHO. 2001). Some studies in Europe have revealed that IBP can be found at concentration ranging from 60 to 3,400 ng/L in waste waters (Cho et al., 2011). The molecular size of IBP (<1 nm) could simply fit into pores of mesoporous silica material (X. Wang, Liu, & Tian, 2011). The above mentioned facts have been the primary reason for the selection of IBP as one of the model EDCs for this research.

Table 2.2: Physiochemical Properties of IBP

Compound	*Structure*	*Mw (g/mol)*	*S_w (mg/L)*	*Log K_w*	*pK_a*
Ibuprofen	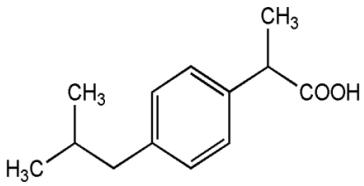	206.3	21	3.97	4.9

Source: http://pubchem.ncbi.nlm.nih.gov/

2.2.2 Bisphenol A (BPA)

Bisphenol A (BPA) is largely used in the manufacturing of polycarbonate plastics, epoxy resins, metal tin lining and many plastics materials manufacturing. Common plastic bottles, food containers, toys, thermal paper, sports equipment, CDs and DVDs are made by BPA. Plastic materials made using BPA are very tough and strong. BPA

became one of the most widely used chemicals in the world with 3.9 million tons in 2006 and 100 million BPA was released into the atmosphere. BPA has a chemical formula of $(CH_3)_2C(C_6H_4OH)_2$ with average molecular weight of 228 gram. BPA even at low concentrations was found to be health hazard and suspected carcinogenic (Y.-H. Kim et al., 2011; G. Li et al., 2015) .

Table 2.3: Physiochemical Properties of BPA

Compound	*Structure*	*(g/mol)*	S_w *(mg/L)*	*Log* K_w	pK_a
BPA	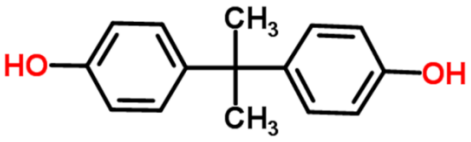	228	320	3.32	9.6

Source: http://pubchem.ncbi.nlm.nih.gov/

In the environment, BPA was released mainly by anthropogenic activities by humans. BPA was found in a very low concentration usually from nanogram to microgram per litre in water. BPA is naturally degradable under aerobic condition but still exists in the surface water and aquatic organism due to its slow biodegradation and good stability properties(Y.-H. Kim et al., 2011).

2.2.3 Methylene blue (MB)

Industrial waste waters contain high levels of MB, a synthetic organic dye pollutant. Paper and pulp mills, textiles, printing and dyeing of cloths have been major user of dyes and the used solution was discharged as waste into the water systems (Anbia & Hariri, 2010). Methylene blue belongs to a group called azo dyes and has a chemical formula of $[(CH_3)_2N(C_6H_3)NS^+(C_6H_3)N(CH_3)_2]$ with IUPAC name 7-(dimethylamino)

phenothiazin-3-ylidene-dimethylazanium chloride. Methylene blue has been reported to cause adverse health effects to humans, wildlife, and microorganisms, and also to increase dangers in the environment (Nonna A Alyoshina & Elena V Parfenyuk, 2013; Kuai & Nan, 2014; Xiao et al., 2015). In humans, MB can cause adverse health effects such as eye burns, cyanosis, methemoglobinemia, convulsions, tachycardia, dyspnea, and skin irritation (Xiao et al., 2015). Methylene blue has a complex aromatic molecular structure with high thermal, light stability and poor biodegradability features. These features make the MB difficult to be degraded. Methylene blue is also classified as EDC because it is used as a pharmaceutical drug to treat prophylaxis or therapy of infectious diseases. In some cases, MB is applied as an antidote for certain poisons. .

Table 2.4: Physiochemical Properties of MB

Compound	*Structure*	*Mw (g/mol)*	*S_w(mg/L)*	*Log K_w*	*pK_a*
MB	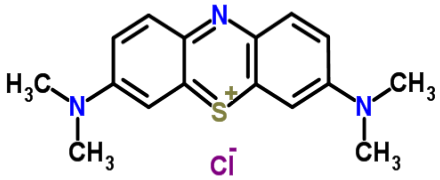	319.85	43600	5.85	3.8

Source: http://pubchem.ncbi.nlm.nih.gov/

2.2.4 Clofibric acid (CFA)

Clofibric acid (CFA) is a drug metabolites used as active lipid regulator (Qiangqiang Sun et al., 2015). Clofibric acid is very stable and estimated to be persistent in the environment for more than 20 years. Clofibric acid was first detected in a German treatment plant and later found in many water sources around the world. Recently, CFA was detected in sewage treatment facilities and rivers in many places.

Table 2.5: Physiochemical Properties of CFA

Compound	*Structure*	*Mw (g/mol)*	*Sw (mg/L)*	*Log Kw*	*pKa*
CA	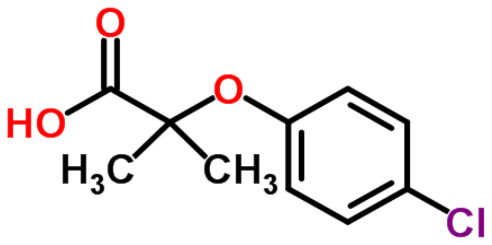	214.04	583	2.57	2.5

Source: http://pubchem.ncbi.nlm.nih.gov/

2.3 Water treatment system

Water treatment technologies for removing of micropollutants have been heavily researched over the last 20 years. New methods and technologies were developed to treat various types of pollutants. Technologies such as biological treatment, ozonation, advanced oxidation (AOPs) and physicochemical processes such as precipitation, filtration, ion exchange and adsorption were developed to remove micropollutants in the water. Ozonation requires expensive equipment and the rates of ozone generation decrease at a high temperature, resulting in a low efficiency output. Ozonation's energy and chemical consumption was high, which is a big hurdle in the actual scale of water treatment. As for the biological treatment, the activated sludge process has been known to have low treatment efficiencies for micropollutants. Due to these drawbacks, the existing conventional methods were not preferred and the attention was therefore directed to adsorption technologies. Adsorbents with larger sorption rate and capacity were more favoured because they have longer lifespan, and the amount needed was also less. Consequently, technology using silica and/or carbon based nano-engineered materials was explored and extensively studied

Conventional techniques such as coagulation, flocculation and sedimentation were reported less effective for the removal of pharmaceutical residue in water due to their polarity effects (Cho et al., 2011; Ternes et al., 2002). Conversely, advance oxidation process (AOP) and ionization have shown some good removal efficiencies for EDCs, but these methods were energy intensive and may produce residual by products (Hasan, Choi, & Jhung, 2013).

Advanced techniques such as membrane filtration removed the EDCs effectively, but the fouling effects reduced the efficiency and speed of the process, (Jones et al., 2007). Membrane bioreactor was generally effective in removal of EDCs, but the setting up cost was high and the implementation was difficult in many treatment facilities (Clara et al., 2005). On the contrary, adsorption process, which uses granular activated carbon (GAC) was reported simple and cost effective for remediating of EDCs, (Hasan et al., 2013; Hasan et al., 2012; Ana S Mestre et al., 2009; Serrano et al., 2010). Moreover, the adsorption process requires less energy consumption, produces minimum by-products and is easy to operate. The comparison between conventional material and nano-engineered material operating water treatment system is shown in schematic diagram 2.1. Nano engineered sorbents require less mass, small space and generate minimum waste. Based on the life-cycle assessment, nano-engineered material operating water treatment system requires smaller costs, and provide greater yield than other conventional system.

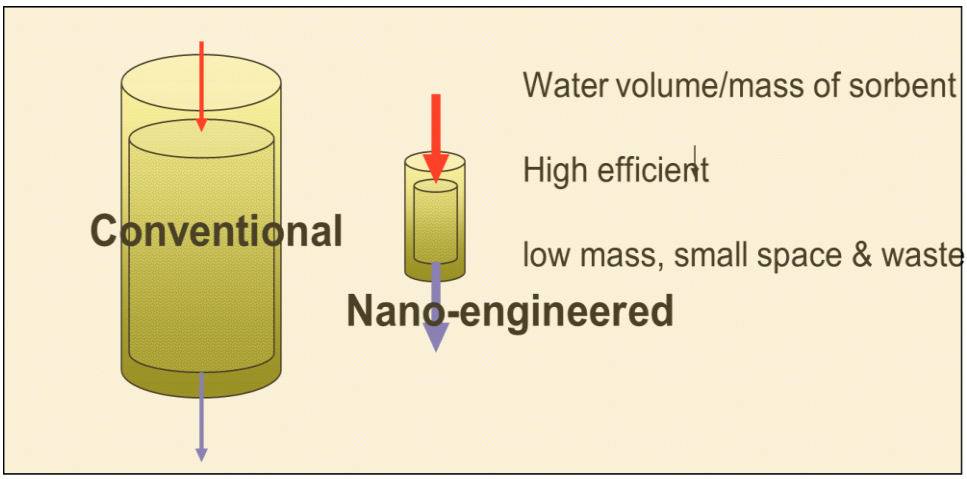

Schematic 2.1: Comparison of conventional and nano-engineered material

2.4 Adsorbent materials

2.4.1 Activated carbon

There are several types of adsorbents that have been used for the purpose of water treatment: mainly carbon, silica or zeolites based materials. Activated carbon (AC) is of the most common type of adsorbent used in the application of water treatment, gas purification, sewage treatment and filters in gas masks. Activated carbon is readily available and the price is very cheap. Activated carbon materials can be obtained from different sources such as palm fibres, corn flakes and coconut shells (Hameed, Tan, & Ahmad, 2009; Islam, Tan, Benhouria, Asif, & Hameed, 2015). Activated carbon is produced in two step process. Step one is the pyrolysis of carbon material such as palm fibres or wood under a high temperature in an inert atmosphere. Second step is the activation process, where the materials are oxidized with a mild oxidizing agent such as CO_2 or O_2. Although AC is popularly used for removing EDCs such as benzafibrate, clofibric acid, diclofenac and carbamazepine, the treatment time is rather very long. It takes about 100 to 130 days for total removal .(Ternes, Joss, & Siegrist, 2004). Also, the adsorption capacity is greatly reduced in the presence of natural organic matters (NOMs) and is difficult to regenerate(Bui & Choi, 2009a).

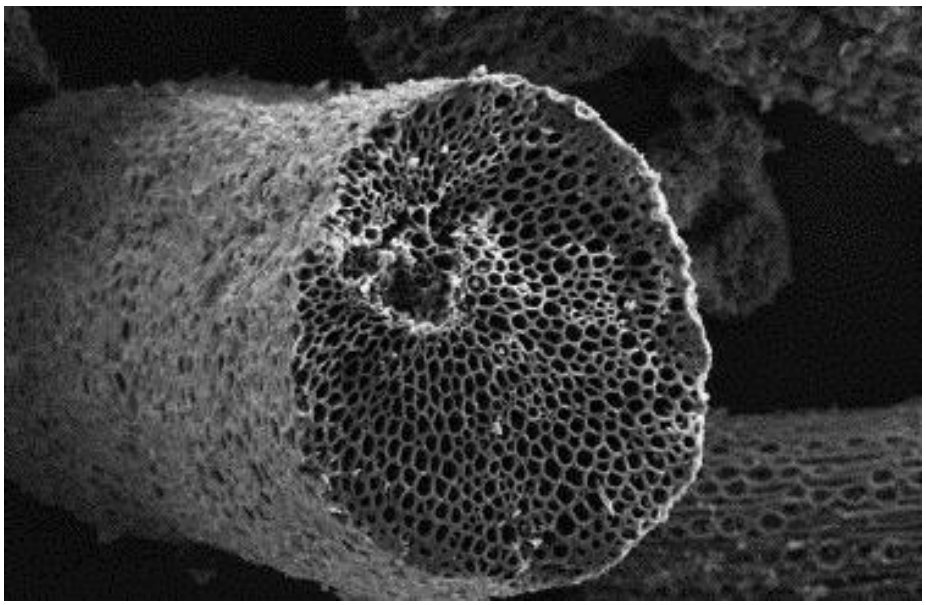

Figure 2.1: Activated carbon SEM image, source: Equilibrium and kinetic studies on basic dye adsorption by oil palm fibre activated carbon
Source : (Tan, Hameed, & Ahmad, 2007)

2.4.2 Carbon nano-tubes (CNT)

Carbon nano-tubes were first discovered in year 1991. Carbon-nano tubes have an excellent and unique tubular structure with outstanding mechanical and chemical properties. Their tubular forms and hollow cavity behave as an excellent nanostructure reactor. Their application is wide and is used as catalyst, super capacitors, biological sensors and batteries. It is further enhanced by functionalized surface area (Shan, Chen, Yu, & Gao, 2010). Carbon nano-tubes coated with magnetic materials using magnetic wires, nanoparticles and magnetic shell have high adsorption capacity for organic micropollutants (Lei Zhang et al., 2013). They could potentially be used as both fixed-phase and dispersed phase adsorbents, and can aid to transport micropollutants (Cho et al., 2011). Single walled and multi walled CNTs (typically 1-30 nm in diameter) have been investigated for their effectiveness as adsorbents for IBP (Cho et al., 2011). Due to their large specific surface areas and small material sizes, CNT provides a high adsorption capacity against the weight ratio, 126 to 475 m^2/g (Cho et al., 2011; Cho,

Smith, Wnuk, Fairbrother, & Ball, 2008). Zhishong and Ao Xia have reported that magnetization of CNT materials will increase the speed of separation drastically, when applied to a magnetic separator (Xu, Xia, Wang, Yang, & Fu, 2007). However, the production cost of CNT is very high, which is a limiting factor to the application of CNT in large scale water treatment process.

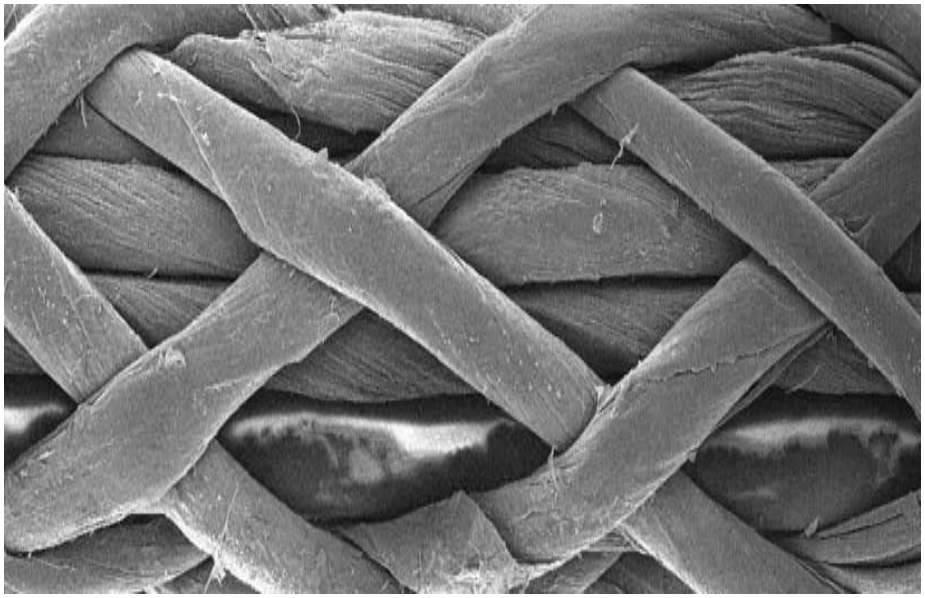

Figure 2.2: Carbon Nano Tubes SEM image
Source: Nanocomp technologies incorporated

2.4.3 Zeolites

Zeolites are naturally occurring minerals and contain mainly aluminosilicate. Zeolites are used commercially as adsorbents and catalysts. They were first discovered by Swedish mineralogist Axel Fredrik Cronstedt in year 1756. Zeolites have pore structures that can accommodate various types of cations such as Na^{+}, K^{+}, Ca^{2+} and Mg^{2+}. Zeolites possess a well-defined microporosity (pore size from 0.5 to 2.0 nm). It separates the adsorbates according to their sizes. Zeolites can be functionalized easily using simple ion exchange process to change the surface charge of material. The

specific functionalization enables the material to be more selective towards certain species of molecules (Cabrera-Lafaurie, Román, & Hernández-Maldonado, 2014).

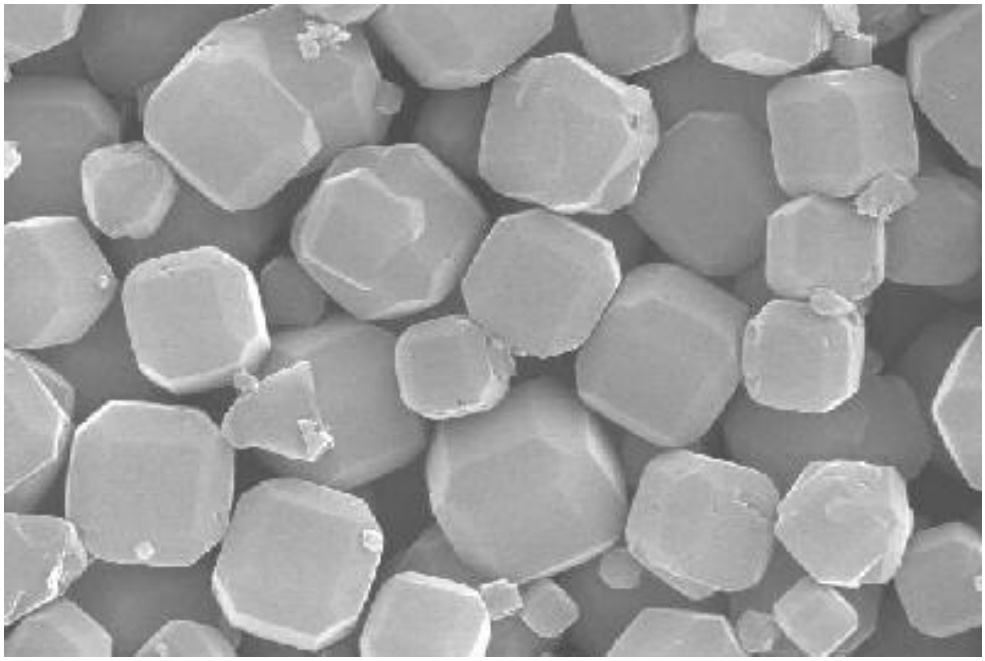

Figure 2.3: Cubic shaped zeolites
Source: hompi.sogang.ac.kr

2.4.4 Mesoporous Materials

Mesoporous material is a porous material and the pore size can range from 2 to 50 nm (Ciesla & Schüth, 1999). Materials with smaller pore size less than 2 nm is called microspores and larger than 50 nm is macrospores. Mesoporous material has a large ordered and narrow pore size distribution, as well as high surface areas. Moreover, the pore size and functionality of mesoporous materials can easily be tailored (Park, Han, & Kim, 2012). These aspects support its adsorption, catalysis and sensing applications.

2.4.5 Mesoporous Silica Material

In 1992, Mobil corporation scientist successfully synthesized a mesoporous silica material, known as Mobil Crystalline Materials, denoted as MCM-41 and MCM-48,

which turn out to be an important milestone in the development of mesoporous silica material. The MCM-41 and MCM-48 in figure 2.4 (a) and (b) have a unique feature to modify the pore size. The type of structural forms depends on various factors such as surfactant type, pH, temperature and additives. The most common structures are hexagonal and cubic, as shown in figure 2.4.

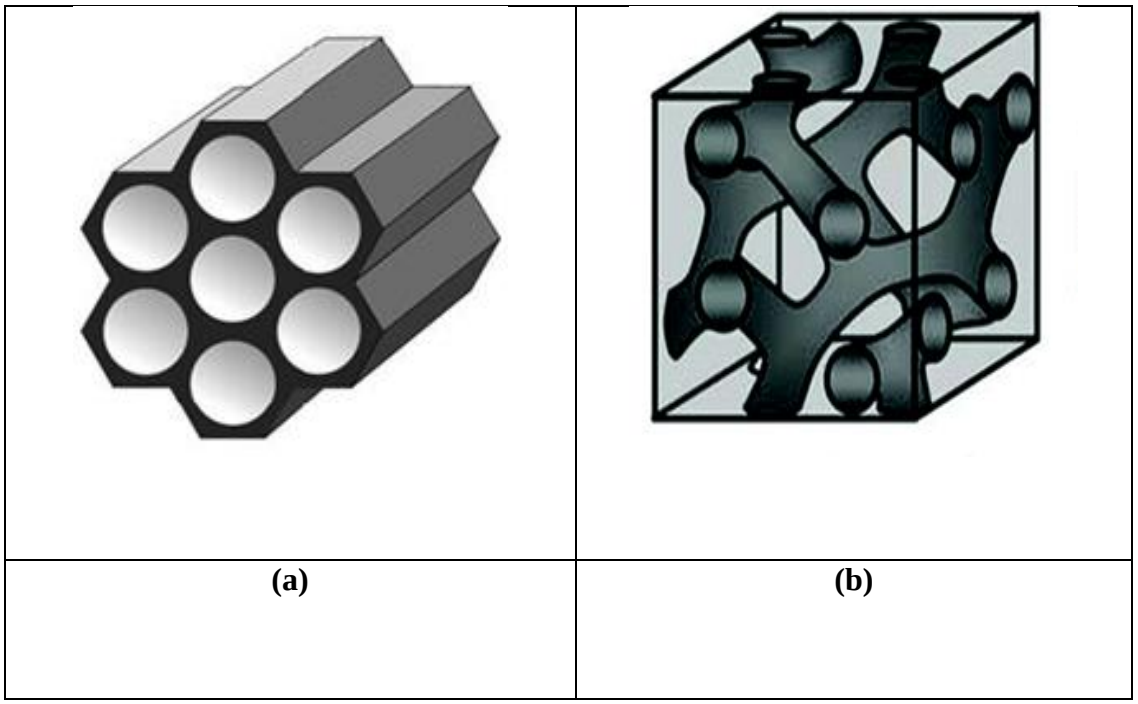

Figure 2.4: Micelle aggregation into the (a) hexagonal MCM-41 and (b) cubic MCM-48
Source: pubs.rsc.org

The M41S family of mesoporous silicate molecular sieves opened new possibilities in the fields of catalysis, sensors, and adsorbents. According to IUPAC, porous materials can be classified into several kinds by their size: microporous (< 2.0 nm), mesoporous (2.0 ~ 50.0 nm), and macroporous (> 50.0 nm). The mesoporous materials synthesized with a self-assembled molecular array of surfactant molecules produce a very sharp and ordered pore. These materials have a large internal surface area of up to 1,000 m^2/g, a pore volume of about 0.8 ~ 1.2 cm^3/g and uniform pore channels. In addition, the pore sizes and inorganic framework of these mesoporous materials can be tailored by

choosing the suitable synthesis conditions in order to meet the objectives of the application. Organic mono-layers functionalized mesoporous silica materials were developed for removing mercury and other heavy metals. For example, self-assembled monolayers on mesoporous supports (SAMMS) could adsorb 700 mg of mercury per gram of material. SAMMS had very rapid kinetics and high distribution coefficient (K_d) (108 mL/g). These features enhanced the removing of Hg, which is approximately 1,000 times higher than that of the GT-73 resin. The Hg-laden SAMMS also had high hydrothermal stability and passed the EPA's TCLP (Toxicity Characterization Leaching Procedure) tests. Based on laboratory equilibrium data of SAMMS, manufacturer's extrapolation data of GT-73 and the full-scale column performance of activated carbon, the total life-cycle cost of SAMMS is about 9.8 and 367.6 times lower than those of GT-73 and activated carbon, respectively.

Zhao et. al from the University of California-Santa Barbara developed an important mesoporous silica material known as SBA-15 (Santa Barbara Amorphous-15)(D. Zhao, Feng, et al., 1998) .

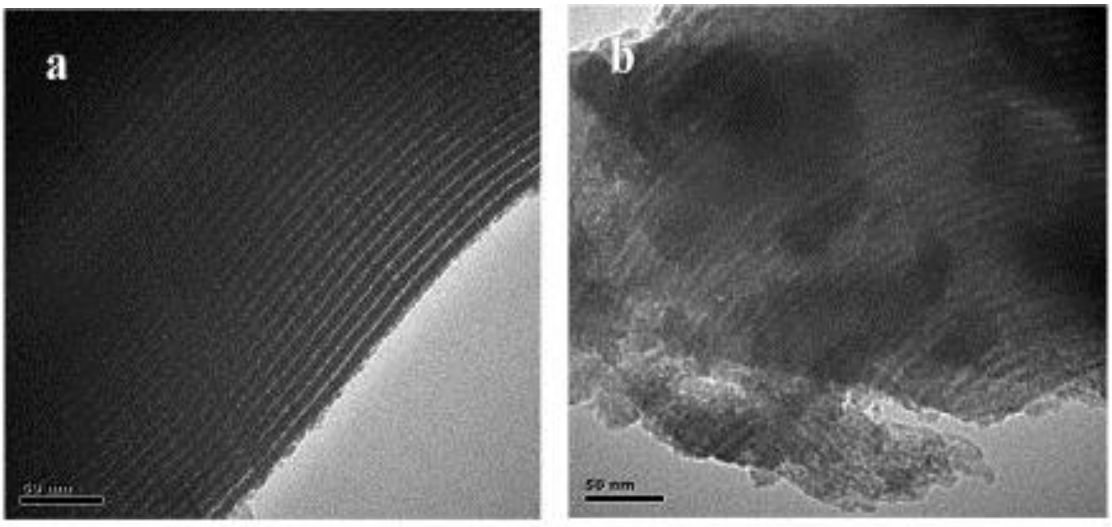

Figure 2.5: TEM image (a) and FESEM (b) of SBA-15
Source : (Yu, Yang, & Wang, 2015)

SBA-15 is one of the most widely used mesoporous silica material. Since its discovery in 1998, SBA-15 has been vastly tested for adsorption of noble metals, immobilization of enzymes, drug carrier and hosting. The surface of SBA-15 was modified and functionalized using various types of functional groups. This was executed in order to generate materials with different affinities towards the organic or inorganic compounds. More recently, SBA-15 was studied as the host material for drug storage and control release properties, which are important aspects in the biomedical field (Katiyar, Yadav, Smirniotis, & Pinto, 2006).

2.4.6 Recent development in mesoporous silica material

Many studies have reported mesoporous silica materials focusing on adsorption capacities of emerging organic pollutants (Katiyar et al., 2006; Zhu et al., 2005a). However, SBA-15 and MCM-41 were the most studied commercial mesoporous materials (Katiyar et al., 2006; Vallet-Regí, Balas, & Arcos, 2007). These materials were mainly synthesized using TEOS, an organic cross linking agent, reported effective but costly and toxic (Nakashima, Omae, Sakai, Yamazaki, & Sakurai, 1994)

2.4.7 Magnetized mesoporous silica material

Several scientists tried to develop highly porous magnetized mesoporous silica materials that can be used to enhance the separation and recovery process of the adsorbent (Fu, Chen, Wang, & Liu, 2011). A facile separation technique using magnetised material is important for industrial application as it reduces the chances of secondary contamination. Magnetic material provides an easy and convenient method for removal of EDCs or drug delivery of specific compounds. The combination of mesoporous silica materials physical advantages and magnetic properties were important to develop a novel adsorbent material for water treatment (W. Zhao, Gu, Zhang, Chen, & Shi, 2005).

2.6 Adsorption Isotherm and Kinetic Models

2.6.1 Langmuir Isotherm Model

In year 1918, Irving Langmuir published his concept of adsorption in the American Chemical Society (ACS) journal. Langmuir concept was based on the single layer of gas molecule adsorption on the solid surface. He published two papers proving his claim that the adsorption thickness is not more than single molecule.

The Langmuir model fits the data of isotherm, when the adsorption is held monolayer and uniform on the surface of materials. Maximum adsorption capacity is achieved when all sorption sites are saturated. The linear form of Langmuir model can be depicted as:

$$q_{eq} = \frac{Q_{\max} K_L C_{eq}}{1 + K_L C_{eq}} \quad (1)$$

Where q_{eq} is the amount of solute adsorbed per unit weight of adsorbent (mg/g), C_{eq} is the equilibrium concentration of solute in the bulk solution (mg/L), Q_{max} is the maximum adsorption capacity (mg/g), and K_L is the Langmuir constant related to the energy of adsorption (Kittappa et al., 2015).

2.6.2 Freundlich Isotherm Model

In the cases, where the adsorptions are held onto the heterogeneous surface of adsorbent, the Freundlich model fits well to the isotherm data. In the Freundlich model, chemisorption and physisorption are pertinent to monolayer and multilayer adsorption, respectively. The linear form of Freundlich equation is expressed as:

$$\log q_{eq} = \log K_F + \frac{1}{n} \log C_{eq} \quad (2)$$

where K_F and n are Freundlich isotherm constants related to adsorption capacity and adsorption intensity, respectively.

2.6.3 Pseudo 1st order Kinetic Model

Pseudo 1st order reaction is used in the prediction of kinetic in the adsorption process.

Pseudo 1st order kinetic model is interpreted from the equation (3),

$$Rate = k[A][B] \quad (3)$$

[A] and [B] is the initial concentration of the reactants. We assume that reactant A's concentration will be much higher than B in the reaction. The reactant A concentration will remain almost constant in the experiment and its consumption is very small and almost negligible compared to [B]. Hence, the 3 can be expressed as $k' = k\,[A]$ and the new rate equation is stipulated as shown in 4.

$$Rate = k'[B] \quad (4)$$

The new rate constant is used as 1st order reaction constant.

Langergren has introduced a linear form of pseudo 1st order kinetic and is represented by the equation (5) described below (Anbia & Hariri, 2010)

$$\log(q_{eq} - q_t) = \log q_{eq} - \frac{k_1 t}{2.303} \quad (5)$$

As per above equation, q_{eq} is defined as adsorption capacity at equilibrium, q_t is the adsorption at time t and k_1 is the pseudo 1st order adsorption rate constant (L/ min)

2.6.4 Pseudo 2nd order Kinetics Model

Recently, many adsorption process were well matched with pseudo 2nd order kinetic models (Y. Ho & Wang, 2004; Y.-S. Ho & McKay, 1999).

Pseudo 2nd order kinetic model is represented using the equation below:-

$$\frac{t}{q_t} = \frac{1}{K_2 q_{eq}^{\ 2}} + \frac{t}{q_{eq}} \qquad (6)$$

The adsorption kinetics is investigated using pseudo 2nd order kinetic model, in which (t/q) versus t is plotted to obtain rate parameters.

Using the kinetic data, a pseudo 2nd order kinetic model equation is applied to obtain the kinetic constants of the reaction.

K_2 is the rate constant of pseudo 2nd order adsorption (g/mg·min), $K_2\ q_{eq}^{\ 2}$ or v_0 (mg/g·min) is the initial adsorption rate, and q_t is the amount of adsorbate adsorbed at time t (min).

2.6.5 Intraparticle Diffusion (IPD) Model

IPD model was presented by Weber and Moris in 1962 and was applied in three different forms:

I. q_t (the amount of adsorption at any time) is plotted against $t^{1/2}$ (the square root of time) to get a straight line that is forced to pass through the origin (Wu, Tseng, & Juang, 2009)

II. Multi-linearity in q_t vs. $t^{1/2}$ plot is considered , when two or three steps involved in the adsorption process (Qingye Sun & Yang, 2003): external surface adsorption or instantaneous adsorption occurs in the first step; the second step is the gradual adsorption step, where intraparticle diffusion is controlled; the third step is the final equilibrium step, where the solute moves slowly from larger pores to micropores causing a slow adsorption rate. The time required for the second step usually depends on the variations of the system (including solute concentration, temperature, and adsorbent particle size), which is difficult to be predicted or controlled; q_t is plotted against $t^{1/2}$ to obtain a straight line, but does not necessarily pass through the origin because there is other factors affecting the rate of reactions besides the diffusion effect.

III. q_t vs. $t^{1/2}$ plotted to obtain a straight line, did not pass through the origin but there is an intercept. Most of the intercepts listed in the literatures are positive indicating a rapid adsorption process (Juang, Wu, & Tseng, 2002; Wu et al., 2009) .

The IPD model can be represented by equation (7) (Dinu & Dragan, 2010).

$$q_t = k_{ip} t^{0.5} + I \qquad (7)$$

Where k_{ip} (mg/g·min$^{1/2}$) is the intraparticle rate constant, q_t is the amount of dye adsorbed at time t, and I is a constant associated with the thickness of the boundary layer.

2.7 Temperature effect and thermodynamics

Thermodynamics of adsorbate adsorption onto MSM was investigated using Gibbs free energy (ΔG), enthalpy (ΔH) and entropy change (ΔS) parameters.

adsorbate in solution ↔ adsorbate adsorbed

The thermodynamic calculation and interpretation mentioned (E8) was adapted from previously reported mechanism and calculation (Nonna A Alyoshina & Elena V Parfenyuk, 2013). This adsorption process is represented by a reversible heterogeneous equilibrium as stated below. The equilibrium constant is defined using the following equations (Liu & Liu, 2008; Walas, 1985)

$$K = \frac{a_{ads}}{a_s} = \frac{\gamma_{ads} \times q_e}{\gamma_s \times C_s} \quad (8)$$

From E8, a_{ads}, γ_{ads}, γ_s, and a_s are the activities and coefficients of IBP in the solution, q_e and C_s are concentrations of adsorbed adsorbate, respectively.

In equilibrium $\gamma_{ads} = 1$, the equation is represented as

$$K = \frac{q_e}{\gamma_s \times C_s} \quad (9)$$

Standard thermodynamic constant of adsorbate and adsorbent is defined as

$$K^{\circ} = \lim_{Cs \to 0} \frac{q_e}{\gamma s \times c_s} \tag{10}$$

When $C_s \to 0$ $\gamma_s \to 1$, K^o is equal to the intercept value of the plot q_e/C_s verses C_s plot.

Gibbs free energy $\Delta_{ads}G$, enthalpy $\Delta_{ads}H$ and entropy $\Delta_{ads}S$ were determined using the following equations 11 and 12.

$$\Delta adsG^{\circ} = -RT \ln K^{\circ} \tag{11}$$

$$\ln K = \frac{\Delta_{ads}S^{\circ}}{R} - \frac{\Delta_{ads}H^{\circ}}{RT} \tag{12}$$

R and T are gas constant and absolute temperature, respectively.

$\Delta_{ads} H^o$ and $\Delta_{ads} S^o$ is obtained from the slope and intercept of the line plotted by $\ln K^0$ versus 1/T.

The change of enthalpy of the system is contributed by different processes occurring in the system, dehydration of the adsorbent surface and adsorbate molecule, adsorbent and adsorbate specific and non-specific interaction.

2.8 Summary of the literature review

Numerous physicochemical treatment techniques, such as chemical oxidation (Jurado, Fernandez-Serrano, Nunez-Olea, Luzon, & Lechuga, 2006; Salem & El-Maazawi, 2000) ultrafiltration (Doke & Yadav, 2014), photodegradation (Kuo & Ho, 2001), extraction (Regel-Rosocka & Szymanowski, 2005), and adsorption (Fu et al., 2011) have been developed to treat micropollutants. Among these methods, adsorption was demonstrated very promising for the removal of micropollutants because the technique is simple, economical, and energy saving. To date, activated carbons, nanoporous silicas, zeolites, and iron oxides were extensively studied for the removal of micropollutants. However, the application of these materials in waste water treatment is limited due to separation difficulties, low sorption capacities, and the risk of secondary environmental contamination caused by fine particles.

Over the last decade, mesoporous silica materials have been of great interest in the field of water treatment. MCM-41, MCM-48, and SBA-15 were studied as possible adsorbents because of their simple preparation process and high stability feature (J. Wang, Lu, Yang, Xiao, & Wang, 2012; S. Wang & Li, 2006). The high surface area, large pore volume, even pore size distribution, and open pore structures, make them suitable adsorbents for large sized organic pollutants such as dyes (Anbia & Hariri, 2010; Hong, Lin, Jiang, Chen, & Chang, 2013; Y. Kim et al., 2014; Xiao et al., 2015). However, the synthesis of these mesoporous silica materials involves the use of expensive silica sources, such as TEOS (Kuai & Nan, 2014; Xiao et al., 2015). The materials, although have been used in the application of drug loading and unloading, in the field of water treatment the utilities are limited. This was due to the costly materials used in the synthesis process; and the process itself is energy-intensive, time-consuming and complicated.

Moreover, these mesoporous, have very fine particle size, which makes the separation process difficult and expensive (B. C. Kim et al., 2011). It is therefore, important to develop sorption materials with high sorption capacities, low production costs, high reusability, and thermal stability. Also the synthesized mesoporous silica materials should be suitable for large scale production.

3. MATERIALS AND METHOD

3.1 Chemicals and materials

The following chemicals were commercially available and used.

Pluronic® P123 ($EO_{20}PO_{70}EO_{20}$) and silicon dioxide (SiO_2) were obtained from Sigma-Aldrich (USA) and R & M (United Kingdom). Sodium hydroxide (NaOH) and hydrochloric acid (HCl) (37%) were purchased from MERCKS (Germany). Methanol was purchased from Fisher Scientific. Analytical grade IBP was purchased from ALFA AESER (United Kingdom). Iron (II) sulphate heptahydrate ($FeSO_4 \cdot 7H_2O$) and potassium permanganate ($KMnO_4$) were purchased from MERCKS. Methylene blue (MB) powder was purchased from R & M. N^1-(3-Trimethoxysilylpropyl) diethylenetriamine (Tris) , analytical grade BPA and CFA were purchased from Sigma-Aldrich (USA).

3.2 Synthesis of MSM

MSMs were synthesized by reacting Pluronic® P123 with SiO_2 in the presence of NaOH and HCl. SiO_2 (1 M) was dissolved in a 1 M NaOH solution and stirred using a magnetic stirrer at 45 °C for 20 h. The pore-templating agent was prepared separately using 4 g of Pluronic® P123, which was dissolved in 120 mL of a 2 M HCl solution with continuous stirring at 45 °C. These two solutions were mixed and stirred for 3 h at 45°C and then for an additional 12 h at room temperature. The molar ratio of chemicals used in the synthesis of MSM was 1 SiO_2:1 NaOH: 5.28 HCl: 0.015 Pluronic®:200 H_2O. The solution was then aged in a Teflon bottle at 90 °C for 20 h. The precipitated solid product was recovered by filtering the solid using 0.45-µm-pore-size cellulose acetate membrane filters. Finally, the material was washed with deionized (DI) water and ethanol (50%) and dried at 60 °C for 24 h. A WESTERN® furnace was used to calcinate

the dried samples at temperatures ranging from 500 to 900 °C for 4–6 h (Kittappa et al., 2015).

3.3 Synthesis of nano-magnetite and MNCM

The synthesis method of nano-magnetite was modified from Schwertmann and Comell (2000). Forty gram (40 g) of $FeSO_4 \cdot 7H_2O$ was dissolved in 500 ml of DI water at room temperature. The solution was heated to 80°C and alkaline solution was slowly added. The alkaline solution was prepared separately using 22.4 g NaOH and 3.3 KNO_3 in 415 ml of DI water. The colour of solution changed from yellowish to dark purplish and black. The temperature was maintained at 80°C for 1 h and left stirring overnight at room temperature. The nano-magnetite was washed with deionized water several times and dried in the oven at 60 °C. The prepared nano-magnetite was used for synthesis of MNCM in the following section.

The silica source was prepared using SiO_2 powder dissolved in 1M NaOH solution, stirred at 45 °C for 20 h. Separately 0.25 to 1 g of nano-magnetite was added into the solution containing pore templeting agent Pluronic® P123 and HCl (2 M) and heated to 45 °C. Then, 30 ml silicate solution was added into 60 ml solution containing nano-magnetite. The mixed solution was stirred at 200 rpm from 40 to 45 °C for 3 h. The mixture was stirred vigorously at room temperature overnight. The synthesis ratio for 1 g MMSM was 0.14 Fe_3O_4:1 SiO_2:1 NaOH: 0.1 HCl: 0.013 Pluronic®:167 H_2O. The solution was transferred to an autoclave container and aged at 90 °C for 20 h. The suspension was centrifuged at 2000 rpm and the solution was decanted. The recovered solids was washed with DI water and ethanol (50%) and dried at 60 °C for 24 h. The dried samples were calcinated at 500 °C for 6 h using a WESTERN® furnace.

3.4 Synthesis of MNCMT

Silicon dioxide (SiO_2) was dissolved in 1 M NaOH and stirred at 45 °C for 20 h. A predetermined mass (1 g) of nano-magnetite was added into the acidic solution containing the pore-templating agent Pluronic P123 and HCl (2 M). The suspension was heated to 45°C. Then, 30 mL of the prepared silicate solution was added to the 60 mL suspension. The mixed solution was stirred at 200 rpm from 40–45 °C for 3 h. After stirring for an additional 24 h at room temperature, the mixture was transferred to an autoclave container and aged at 90 °C for 20 h. The precipitated solid and liquid were centrifuged (2,000 rpm) and the solution was decanted. The solids obtained were washed with DI water and ethanol (50 %), and dried at 60 °C for 24 h. The dried samples were calcined at 500 °C for 6 h using a Western furnace. The MNCM was coated with 1, 2 and 3 mmol of Tris using an incipient wetness impregnation method. The material was designated as MNCMT-1,-2 and -3. Then MNCMT was dried in the oven at 60 °C overnight, The synthesis ratio for MNCMT was 0.14 Fe_3O_4:1 SiO_2: 1 NaOH: 0.1 HCl: 0.013 Pluronic: 167 H_2O: 0.01/0.02/0.03 Tris.

3.5 Adsorption method for IBP removal of by MSM

Adsorption isotherms and kinetics were determined for four synthesized MSMs calcinated at 500, 600, 700, and 900 °C, denoted as MSM–500, –600, –700, and –900, respectively.

Two hundred milligrams (200 g) of IBP tablets (Nurofen®) were crushed to powder using a laboratory mortar and pestle. The required amount of IBP powder was dissolved in 10 % of methanol and dissolved in DI water in a 250 mL volumetric flask. The mixture was stirred for 12 h, sonicated for 2 h, and filtered using a 0.45-µm-pore-size cellulose acetate membrane filter. Sodium chloride (NaCl) solution was added to the

filtrate to create an ionic strength (0.01 M) in the solution. The pH was adjusted to 7 using sodium phosphate (Na_3PO_4) solution.

In a typical isotherm reaction, 10–500 mg of MSM and 10 mL of IBP solution (150 mg /L) were added to individual 20 mL vials. The vials were placed into an electric shaker and agitated at 250 rpm and 25 °C. The suspension was filtered using a 0.45-µm-pore-size cellulose acetate membrane filter (Bui & Choi, 2009b). The obtained filtrate was analysed for IBP. The data were fitted into Langmuir and Freundlich isotherms.

Kinetic experiment was performed using IBP solution (200 mL) of 100 mg/L added to four separate beakers containing 1000 mg MSM. The beakers were stirred constantly at 200 rpm at room temperature for 200 min. At time intervals, the sample from each beaker was collected, filtered, and analysed for IBP. After obtaining the kinetic data, a pseudo-second-order kinetic model equation was applied to obtain the kinetic parameters of the reaction.

3.6 Adsorption method for MB removal by MNCM

In a conical flask, 200 mL of MB was prepared at 20 mg/L. The initial pH of the MB solution was adjusted from 2–10, and 15 mg of MNCM-1 was dispersed in the solution. The pH adjustment was conducted using either 0.1 M HCl or NaOH solutions. The conical flasks were placed into an electric shaker and agitated at 200 rpm and 25 °C for 100 min. At regular intervals, samples were collected and the suspended solids were separated using a magnet.

To investigate the concentration effect and isotherm of MB removal, further batch tests were conducted using MB solutions with 20–40 mg/L. The initial pH was adjusted to

10, and other experimental conditions were maintained similar to those described in earlier paragraph. The solution after adsorption was tested for the remaining MB concentration using a UV-vis spectrophotometer Shimadzu, Japan.

Regeneration test were conducted using the same condition of the isotherm test described earlier and repeated for 5 times. After each adsorption the adsorbent MNCMM was separated using magnet and calcined in the furnace at 300 °C for 3 h and reused for adsorption test.

3.7 Adsorption method for BPA, IBP and CFA removal by MNCMT

A total of 50 mg adsorbent media (MNCMT-1, MNCMT-2 and MNCMT-3) was added to a conical flask containing 200 ml of BPA solution (20 mg/L), and shaken at 200 rpm for 24 hours. The solution and media was separated using a simple laboratory magnet and the required amount of samples was taken from the conical flask. The solution was analysed for the concentration of pollutants left in the solution. This experiment was repeated for IBP or CFA solutions of different concentrations, ranging from 10 to 250 mg/L.

EDCs solution of 20 mg/L was added to three separate conical flasks containing 20 mg media. The mixture was stirred at 200 rpm at room temperature. At time intervals, samples from three flasks were collected and separated quickly by magnet and analysed using a UV spectrometer. After obtaining the kinetic data, kinetic models were applied to determine rate parameters of the reaction.

3.8 Measurement and instrumentation

3.8.1 Preparation of MB, BPA, IBP and CFA standard calibration graph

Required amounts of MB/BPA/IBP/CFA powder were accurately weighed and dissolved in water/ methanol and diluted with DI water in a volumetric flask. The aqueous solution was stirred for 3 h to completely dissolve in the DI water. A standard calibration graph for MB, BPA, IBP and CFA was plotted, ranging from 1 to 250 mg/L, with the determination coefficiency (R^2) of 0.995-0.999. A UV-vis spectrometer, (Shimadzu, Japan) at wavelength, 660, 276, 222 and 227 nm was used to analyse the standard and samples.

3.8.2 Measurement and instruments

The following analytical equipment and instruments were used for this research: A PANalytical Empyrean X-ray diffractometer (Panalytical, Netherlands) was used to determine the presence of mesostructure in the synthesized materials. The scanned angle was from 0.5–5.0 ° of 2θ, and the step size and scanning time were 0.0070° and 19.9260 s, respectively. Small-angle X-ray scattering (SAXs) was performed to determine the particle size distribution of the nano-magnetite. Nitrogen adsorption and desorption isotherms were measured using a Micromeritics TriStar II 3020 system (Micromeritics Instrument Corporation, United States). The samples were analysed at 77.35 K. Brunauer-Emmett-Teller (BET) theory was used to determine the specific surface area of the samples. The Barrett-Joyner-Halenda (BJH) method was used to measure the pore size distributions and pore volumes of the samples. IR spectra were obtained using a NICOLET IS 10 spectrometer (Thermo Scientific, USA). Microscopic images of nano-scale pore structures were taken using transmission electron microscopy (Hitachi HT 7700 TEM, Japan) at 120 kV. An ultra-high-resolution FESEM (Hitachi SU 8000, Japan) fitted with an EDX analyzer was used to capture the images of the samples. A

Netzsch-brand TGA (Netzsch Holdings, Germany) was used to perform the thermal analysis of the samples, scanning from 25 to 1100°C. The zeta potential of the samples was measured using a Malvern Zetasizer nano-series (Malvern Instrument, UK). A magnetometer was used to determine the magnetic properties of the sample.

4. RESULTS AND DISCUSSION

4.1 Characterization of MSM

Figure 4.1 (A) shows a low-angle XRD diffraction pattern of selected MSMs. Among the synthesized media, as-synthesized MSM, MSM-500, and MSM-600 showed well-resolved peaks indexed at *d*(100) reflection. Additionally, MSM-500 had two more weak peaks at 2θ angles of 1.08 and 1.58°, indexed at *d*(110) and *d*(200), respectively. These types of XRD reflection patterns can be assigned to a well-ordered mesoporous structure with *P*6*mm* hexagonal symmetry (Bui & Choi, 2009b; X. Wang et al., 2011; D. Zhao, Feng, et al., 1998).

The XRD results indicated that MSM-500 had the highest peak intensity compared with the other MSMs, reflecting the formation of more uniform mesopores (X. Wang et al., 2011; Zhu et al., 2005b). The shifting of peaks to lower 2θ values with higher calcination temperature shows an increase in the pore sizes of the MSMs, indicating the possibility of MSM-500 having larger pores than MSM-600 and -700. However, MSMs calcined at >700 °C showed no XRD diffraction peak, demonstrating the collapses of the pore structure (X. Wang et al., 2011). This phenomenon was investigated further using N_2 adsorption–desorption analysis.

Figure 4.1 (B) shows the N_2 adsorption–desorption isotherms of the various MSMs. According to the IUPAC classification, the as-synthesized MSM, MSM-500, and MSM-600 had a type-IV sorption pattern (S. S. Kim & Pinnavaia, 2001; Kresge, Leonowicz, Roth, Vartuli, & Beck, 1992), whereas MSMs calcined at >700 °C showed no sorption profile. At a relative pressure of $P/P_o < 0.2$, MSM-500 had more primary micropores (< 2nm) than MSM-600. Reversible sorption of N_2 gas for MSM-500 and -600 occurred up to a P/P_o of 0.6, whereas for as-synthesized MSM happened much earlier, at a P/P_o of

0.2. These results indicate that MSM-500 and -600 had more uniform pores with a hysteresis loop pattern type H_1, similar to SBA-15 (Jaroniec, 2002; Thommes, 2010). However, their behaviour differed from MCM-41, where the adsorption-desorption isotherm processes were fully reversible (Kruk, Jaroniec, & Sayari, 1997).

Using the BJH method, the pore-size distribution was obtained for as-synthesized MSM, MSM-500, and -600 (figure. 4.1(C)). These results showed that MSM-500 had the narrowest pore-size distribution, with a primary peak at 6.2 nm, while MSM-600 displayed a broader distribution and a primary peak at 5.6 nm. This indicates that MSM-500 had a larger pore structure and pore volume than MSM-600, consistent with the XRD results in figure 4.1(A).

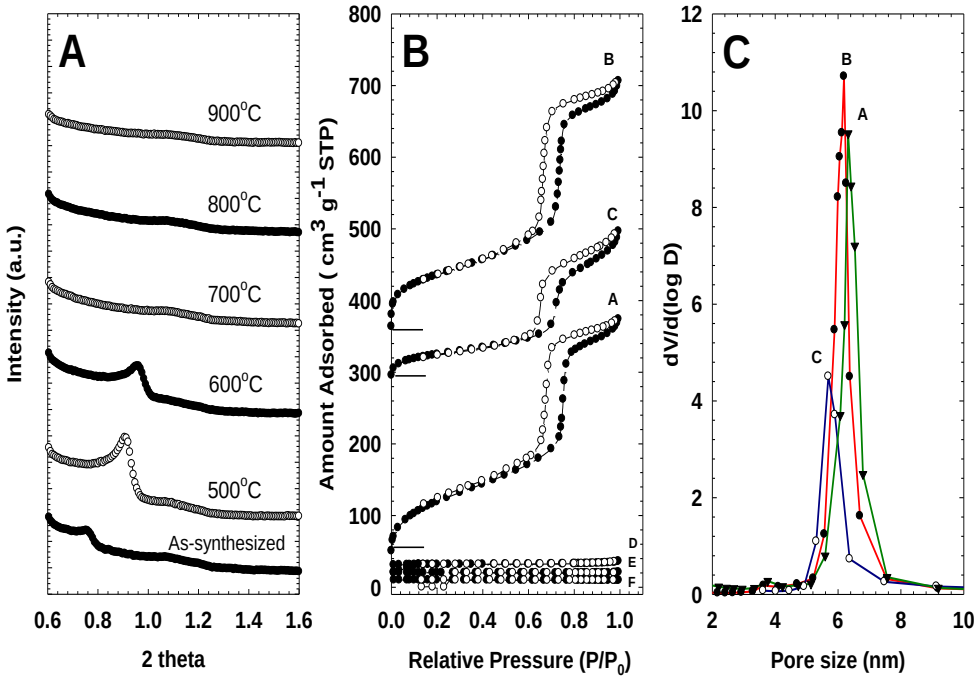

Figure 4.1: (A) XRD patterns of as-synthesized mesoporous material and MSMs calcined at different temperatures, (B) the N_2 sorption isotherm, and (C) pore-size distribution of the MSMs (A: MSM-as synthesized, B: MSM-500, C: MSM-600, D: MSM-700, E: MSM-800, and F: MSM-900).

The pore structure characteristics of MSMs and other referenced media are summarized in Table 4.1. Among the calcined MSMs, MSM-500 had the highest BET specific surface area (310 m^2/g) and pore volume (0.541 cm^3/g). The BET specific surface area and pore volume decreased substantially, when the calcination temperature increased from 500 to 900 °C. A significant decrease was noted at 700 °C, with the BET specific surface area reduced to <10 m^2/g. Generally, the MSMs synthesized had smaller BET specific surface areas and pore volumes than reported for SBA-15 (Doadrio et al., 2004; Kittappa et al., 2015; Yang, Huang, Kong, Lin, & Fu, 2007)

Table 4.1: The structural parameters as –synthesized and calcinated MSM

MSM	*D* spacing (nm)	Mean Pore diameter [a] (nm)	Wall thickness[b] (nm)	Surface area[c] (m^2g^{-1})	V_t Pore volume ($cm^3\ g^{-1}$)	V_m Micropore %	Ref.
As-synthesized	11.90	6.21	7.6	326	0.541	5.09	This work
500 ^oC	9.68	6.74	4.5	310.	0.565	1.80	This work
600 ^oC	9.33	7.56	3.3	160	0.339	3.40	This work
700 ^oC	n/a	4.76	n/a	6.30	0.0089	n/a	This work
800 ^oC	n/a	1.98	n/a	1.70	0.0039	n/a	This work
900 ^oC	n/a	n/a	n/a	0.70	0.0006	n/a	This work
MSU-H	10.60	9.30	2.9	625	0.9700	n/a	(S.-S. Kim, Pauly, & Pinnavaia, 2000)

Table 4.1: Continued

MSM	*D* spacing (nm)	Mean Pore diameter [a] (nm)	Wall thickness[b] (nm)	Surface area[c] (m^2g^{-1})	V_t Pore volume ($cm^3\ g^{-1}$)	V_m Micropore %	Ref.
MCM-41	4.80	3.30	n/a	1200	1.0000	n/a	(Andersson et al., 2004)
HMSCs	n/a	2.71	n/a	1244	1.2340	n/a	(Zhu et al., 2005a)
MSU-F	n/a	22.5	n/a	759	1.8700	n/a	(S.-S. Kim et al., 2000)
MSH	97.10	5.50	5.71	866	0.9500	n/a	(Margolese, Melero, Christiansen, Chmelka, & Stucky, 2000)

[a]Calculated from the desorption of N_2 Isotherm, [b]Determined from the difference between the unit cell parameter ($a_o = 2d_{100}/\sqrt{3}$) and the frame work pore size. Surface area (BET) calculated from the adsorption of N_2 Isotherm, Vp and V_m total and micro pore volume calculated using BJH

The corresponding unit cell parameter (a_o) and mean BJH desorption pore diameter were used to determine the wall thickness of the MSMs. The wall thickness was calculated as the difference between a_o, where $a_o = 2 \times d(100)/\sqrt{3}$, and the mean BJH desorption pore diameter (Lim & Stein, 1999; D. Zhao, Feng, et al., 1998). The mean BJH desorption pore diameter increased during the calcination process at 500 °C and 600 °C (6–7 nm) for MSMs and was smaller than that of SBA-15 (~10 nm). At the same temperature, the MSMs *d*-spacing and wall thickness decreased from 11.9 to 9.3 nm and 7.6 to 3.3 nm, respectively. This reduction in wall thickness is a result of silicate condensation during calcination (D. Zhao, Huo, Feng, Chmelka, & Stucky, 1998). Calcination at temperatures >700 °C caused a significant decrease in the wall thickness and the framework to collapse (D. Zhao, Feng, et al., 1998; X. Zhao, Lu, Whittaker, Millar, & Zhu, 1997). In this research, MSMs were found to have lower thermal stability (up to 600 °C), which could be due to the formation of weaker bonds between the condensed silica walls. In contrast, Tung et al. reported that SBA-15 and a few other mesoporous silica-based materials had high thermal stabilities of up to 850 °C (Bui & Choi, 2009b).

4.2 Mechanism of synthesis of MSM

In the current synthesis method, MSMs were prepared under acidic conditions (pH <1), a clear white precipitate was formed immediately after the silicate ($HSiO_3^-$) and acidified Pluronic® P123 solutions were mixed together. The precipitate was treated using hydrothermal process, where it was heated and condensed to form MSM. This method allows the excess hydrogen (H^+) and chlorine (Cl^-) to electrostatically coordinate between the non-ionic pore-templating agent (S^o) and the hydrogen-associated silicic acid [I^o, $Si(OH)_4$], which finally may lead to the formation of $S^oH^+Cl^-I^o$. Considering the above mentioned facts, the reaction mechanism of this synthesis can

be represented using reactions R1, R2, and R3, respectively (Kittappa et al., 2015). Firstly, the mixing of NaOH and SiO_2 may lead to formation of silicate ions ($HSiO_3^-$) (R1).

$$SiO_2 + NaOH \rightarrow Na^+ + HSiO_3^- \qquad (R1)$$

Secondly, when both silicate and acidic Pluronic® solution are mixed together, silicic acid [Si $(OH)_4$] is formed under acidic conditions (R2).

$$HSiO_3^- + HCl + H_2O \rightarrow Si(OH)_4 + Cl^- \qquad (R2)$$

Finally, through hydrothermal process, two silicic acids gets condensed and form a silicate dimer, which further polymerizes to form the framework of MSMs (R3).

$$Si(OH)_4 + Si(OH)_4 \xrightarrow[\Delta 90^oC]{} Si_2O(OH)_6 + H_2O \qquad (R3)$$

This was different compared to the result reported by Park et al. in the synthesis of mesoporous materials at pH >10, which yielded a white gel that transformed into a mesoporous material due to hydrothermal process (Park et al., 2012).

4.3 Removal of Ibuprofen by MSM

4.3.1 Adsorption isotherms of IBP by MSMs

The IBP adsorption isotherms were conducted using MSMs calcinated at different temperatures. The results of adsorption at equilibrium (Q_{eq}) against concentration were plotted in figure 4.2

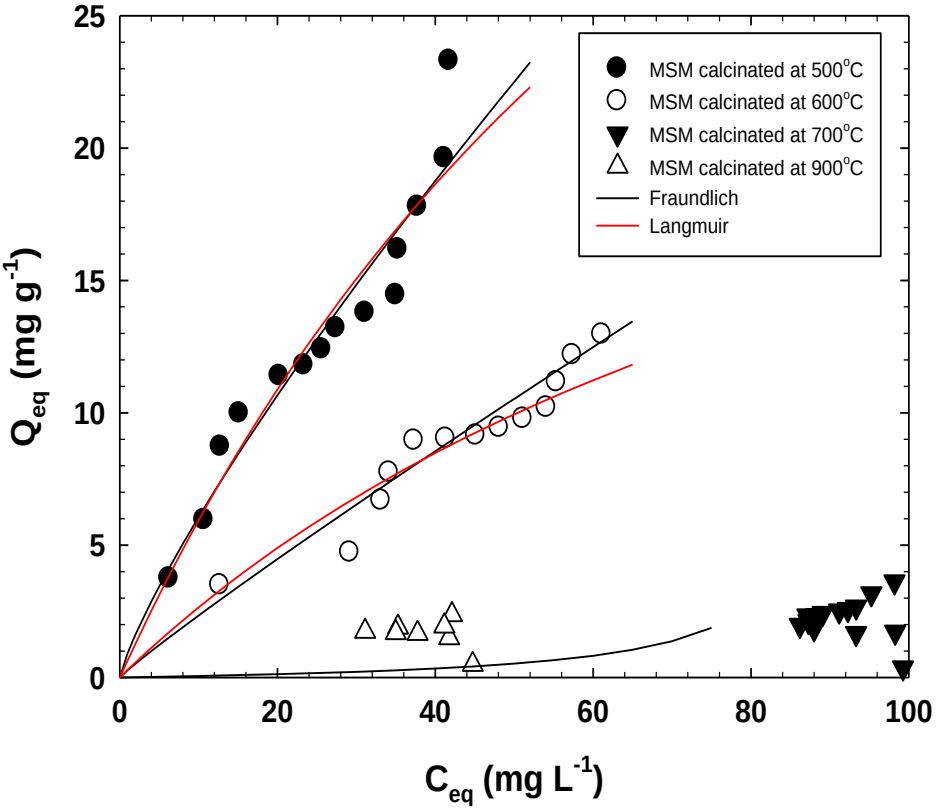

Figure 4.2: Isotherm of IBP removals by MSM

The Q_{eq} of IBP by MSM–500 and –600 increased with increasing C_{eq}, although there were differences in the adsorption capacities. However, MSM–700 and –900 did not show any significant adsorption, which the outcome matches with the physical property result presented using XRD and N_2 adsorption–desorption analysis. To understand the adsorption phenomenon of these MSMs, Langmuir and Freundlich model line were fitted with the experimental data of MSM–500 and –600 using equation (E1) and (E2).

The Langmuir and Freundlich parameters along with determination coefficients (R^2) of the linear plots, were calculated and the results are presented in Table 4.2.

Table 4.2: Isotherm parameter of MB adsorption fitted with Langmuir and Freundlich model

Sample	Langmuir equation				Freundlich Equation			Ref.
	pH	K_L (L/mg)	Q_{max} (mg/g)	R^2	[a]k_F	$1/n$	R^2	
MSM–500	7	0.010	64.8	0.97	0.93	1.22	0.95	This study
MSM–600	7	0.009	31.9	0.74	0.27	1.08	0.75	This study
SBA–15	5	13.330	0.41	0.97	1.50	0.78	0.97	Bui,Choi2009

The adsorption capacities (Q_{max}) for MSM–500 and –600 varied greatly, with 64.8 mg/g for MSM–500 and 31.9 mg/g for MSM–600.

As the value of K_L increases, the adsorption affinity of IBP by the adsorbent increases. The result shows, MSM–500 had a higher affinity than MSM–600 due to higher K_L value (Table 4.2). However the adsorption tests of MSMs were conducted in neutral pH so that it was difficult to compare with the reported K_L value with most of the experiment was conducted in acidic condition.

At higher pH, two important factors such as ionization and surface charge of adsorbent may affect the adsorption process. The acid dissociation of IBP molecules occurs at a pH higher than the pK_a value (4.9), which may stimulate the IBP solubility. As a result, a weaker interaction between the MSM surface and IBP could possibly occur, and the adsorption capacity is reduced significantly. However, interestingly, the Q_{max} *of* MSM-500 was higher than that of SBA-15 Q_{max}.

As a function of adsorption strength, the constant values of 1/*n*, obtained by the Freundlich model for IBP removal by MSM–500 and –600, were 1.22 and 1.08, respectively. These values were relatively larger than the constant values of other media except for commercial GAC (Table 2). If 1/*n* equals 1, then the partition between the two phases is considered independent of concentration. A value of 1/*n* less than 1 demonstrates normal adsorption. A value of 1/*n* greater than 1 indicates cooperative adsorption. Therefore, based on the evaluation of 1/*n*, it can be inferred that the adsorptive removal of IBP by MSM–500 and –600 is favourable (Foo & Hameed, 2010; Tonghuan, Guojian, Xiaojiang, Wangsuo, & Ying, 2013). The adsorption density per unit surface area for MSM–500 and –600 were similar, 0.21 and 0.20 mg/m^2, respectively. These values were comparable to those reported values (0.28–0.32 mg/m^2) for SBA–15 (Andersson et al., 2004; Vallet-Regi, Balas, & Arcos, 2007).

4.3.2 Adsorptive kinetics of IBP by MSMs

Figure 4.3 depicts the kinetics of IBP removal by MSMs at pH 7. A rapid adsorption of IBP by MSM–500 and –600 was observed for the first 5 min, reaching a plateau stage after 15 min. After 60 min, the IBP adsorption increased again, suggesting the possibility of IBP molecules forming a dimer (Andersson et al., 2004; Babonneau, Camus, Steunou, Ramila, & Vallet-Regi, 2003; X. Wang et al., 2011). Thus, the contact time needed for MSM–500 and –600 was much shorter than for the activated carbon that requires about ~ 4 h. The faster adsorption of MSM–500 and –600 may relate to their pore structures. MSMs have mostly mesopores and only 3–5 % micropores, while AC has dominantly micropore as high as 70 %, thus limits the diffusion. The pore size of MSMs (~ 7 nm) is uniform and large, sufficient for penetration of IBP molecules (~ 1 nm). The pore size of MSMs allows the IBP molecules to diffuse easily and adsorb onto the surface of MSMs within a shorter time. This implies that MSM–500 and –600 can

be advantageous in terms of designing a compact water treatment system and enhance their application economically for commercial use. The adsorption kinetics was investigated using the pseudo 2nd order kinetic model, in which Q_t versus t was plotted to obtain the rate parameters. The results showed that the fit of model to the data had a good determination coefficient (0.99).

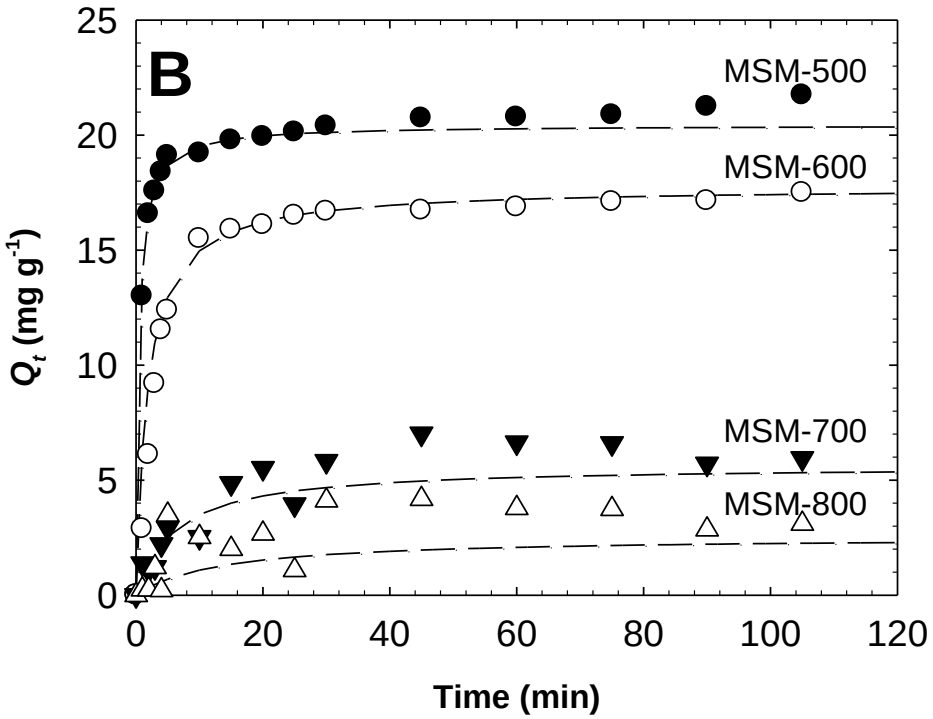

Figure 4.3: Kinetic data of ibuprofen adsorption onto MSM

Table 4.3 lists the important parameters obtained from the current kinetic study and other references. The K_2 values for MSM–500 and –600 were 0.10 and 0.03 g/mg min, respectively. A higher K_2 value for MSM–500 indicates that the media is much faster in adsorbing IBP then other MSMs. Although several types of AC have higher K_2 values than MSMs most of these tests were conducted under acidic conditions at pH ~4. Amazingly, at pH 7, MSM–500 had about 100 times higher sorption speed than the commercial GAC, which had a K_2 value of 0.001147 g/mg min. Zeolites had a higher K_2 value than MSMs, but its Q_{max} was only 0.0976 mg/g.

Table 4.3: Kinetic parameters of pseudo 2nd order model for IBP adsorption

Sample	C_0	**pH**	K_2	R^2	$K_2 q_{eq}^2$ or v_0	$q_{e,calc.}$	**Ref.**
MSM–500	100	7	0.10	0.999	43.5	20.4	This study
MSM–600	100	7	0.03	0.999	9.58	17.7	This study
MSM–700	100	7	0.02	0.965	0.92	5.6	This study
MSM–900	100	7	0.01	0.622	0.19	2.5	This study
[a]CAC	90	~4	0.07	0.999	834	112.4	Mestre et al. 2009
[b]CPAC	90	~4	0.23	0.999	2500	106.4	Mestre et al. 2009
Honey comb AC	50	2–5	0.049	0.993	n/a	16.7	Dubey et al. 2010

Table 4.3: Continued

Sample	C_0	**pH**	K_2	R^2	$K_2 q_{eq}^2$ or v_0	$q_{e,calc.}$	**Ref.**
Olive waste AC	n/a	4.1	1.491	1	n/a	9.1	Baccar et al. 2012
[c]Zeolites MNCZ	0.1	7	0.214	0.999	n/a	0.098	Salem Attia et al. 2013
Commercial GAC	n/a	7	0.0011	0.952	n/a	69.95	Guedidi et al. 2013
Cork Based GAC	90	4	0.07	0.999	834	112.4	Neng et al. 2011

Units, C_0= (mg/L) $K_2 q_{eq}^2$ or v_0 = (mg/g min) $q_{e,calc.}$ = (mg/g)

4.3.3 Thermodynamics of IBP removal

Figure 4.4 shows kinetic data of IBP adsorption at 299, 309 or 319 K, and fit-lines of pseudo 2nd order kinetic model. The q_{eq} (adsorption at equilibrium) of IBP uptake by MSM−500 was 22.8 mg/g at 299 K, but decreased to 18.28 and 7.7 mg/g at 309 and 319 K, respectively.

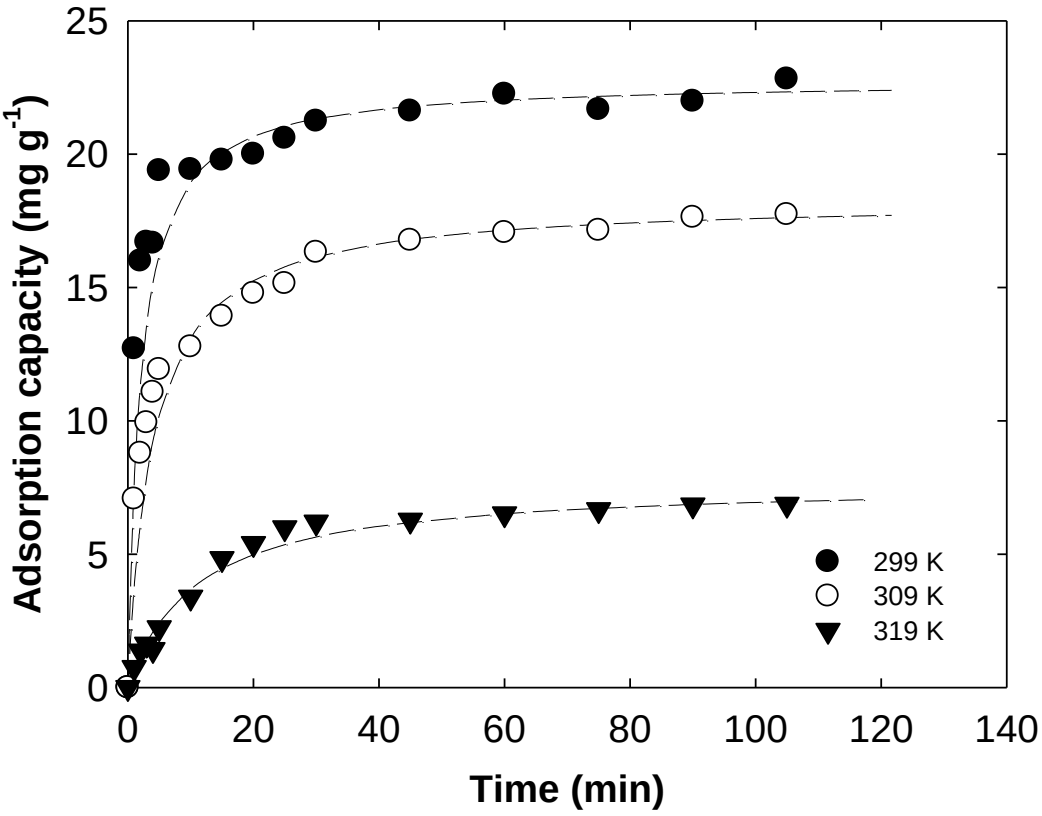

Figure 4.4: Temperature effect of IBP adsorption onto MSM−500

This phenomenon has been revealed at several studies on various EDC removals by silica based media and multi-wall carbon nano-tube (MWCNT) (Al-Khateeb, Obaid, Asiri, & Salam, 2014; N. A. Alyoshina & E. V. Parfenyuk, 2013; Reijenga, Ingelse, & Everaerts, 1997; L. Zhang et al., 2013). Based on the calculation for thermodynamic parameters, the $\Delta_{ads}G^0$ values were -10.4, 1.01 and 11.3 kJ/mol at 299, 309 and 319 K, respectively. Thus, the IBP adsorption is a spontaneous physical process at room

temperature, but becomes non-spontaneous at higher temperatures. Besides $\Delta_{ads}G^0$, $\Delta_{ads}H^0$ and $\Delta_{ads}S^0$ were also calculated. The calculated $\Delta_{ads}H^0$ was -23.0 kJ/mol. This indicates that the IBP adsorption onto MSM−500 is an exothermic reaction. This effect could lead to a decrease in the IBP randomness because the degree of freedom or mobility of IBP is limited compared to IBP in the solution. Meanwhile, the $\Delta_{ads}S^0$ was found to be -0.07 J/mol K, which is an interesting finding, as the $\Delta_{ads}S^0$ is much smaller than other reported references. The small value represents that lesser energy is required to restore the system back into its original state. The negative $\Delta_{ads}H^0$ and $\Delta_{ads}S^0$ suggest that the removal process of IBP can be considered as an enthalpy-driven process.

4.3.4 Regeneration of MSM

Figure 4.5 reveals the kinetic data of five times adsorption of IBP by MSM−500 and fit-lines of pseudo 2nd order kinetic model. Figure 4.5 shows the q_{eq}, K_2 and v_0 at each cycle, with the first cycle having the highest q_{eq} (22.8 mg/g). This result is similar to the results of kinetic tests conducted previously, suggesting that experiments were reproducible under the same condition. All consecutive cycles exhibited 19~19.8 mg/g of q_{eq} which were slightly lower than the q_{eq} at first cycle. Based on the first q_{eq}, MSM−500 had 83~87% of recovery efficiencies.

At the first cycle, 90% of q_{eq} for IBP uptake was achieved at 5 min. But, the uptake slowed down to about 30 min at third and fourth cycles. When compared, the values of K_2 and v_0 were similar in first and second cycles, but the values dropped largely at third cycle and decreased further at fourth and fifth cycle

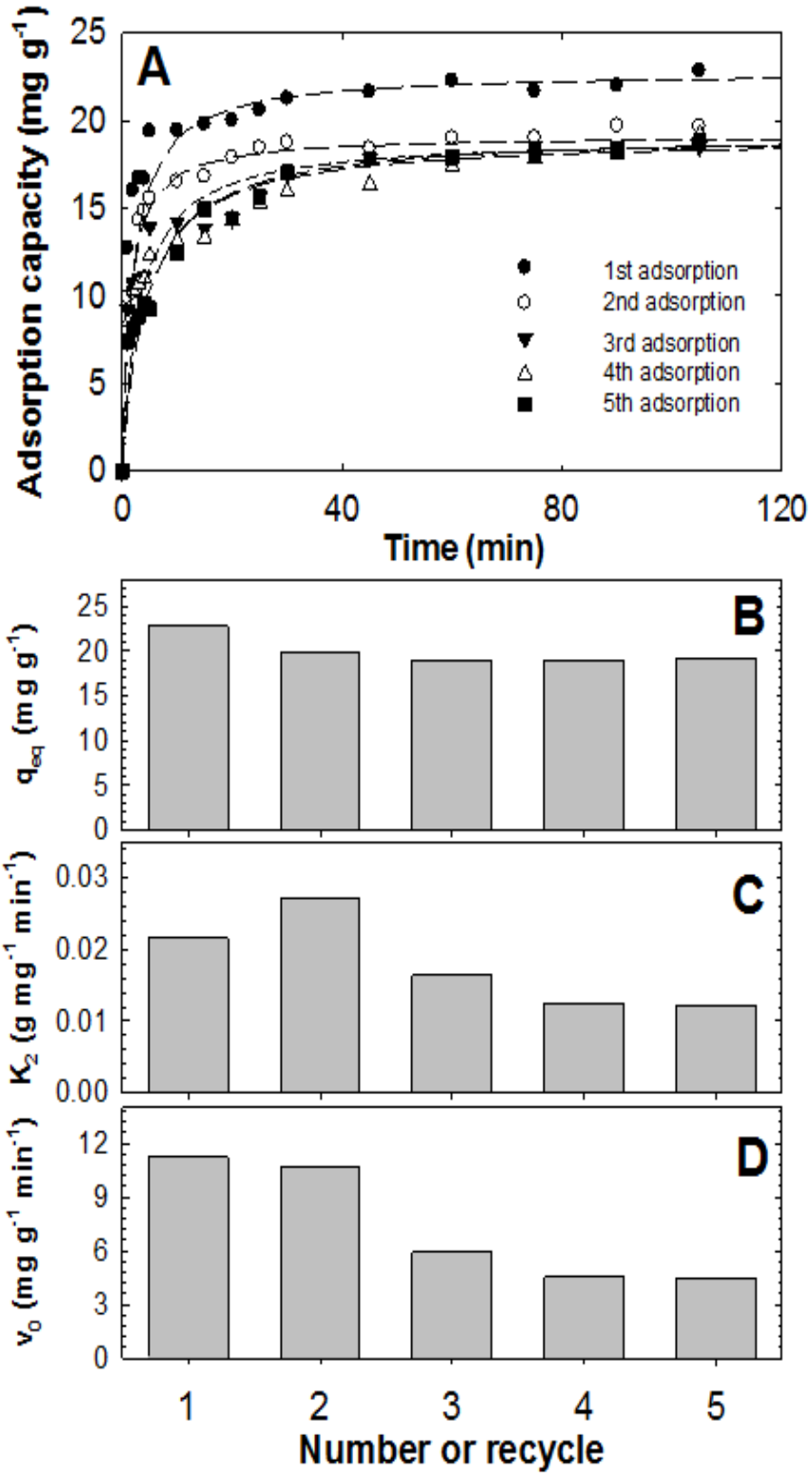

Figure 4.5: Adsorption and re-adsorption of ibuprofen onto MSM−500

The experimental data verified that the reduction trends of IBP uptake capacity and speed were different. These differences could be due to the deformation of pore structure or the partial existence of IBP molecules trapped in the pores after extraction by methanol. Activated carbon is mostly composed of micropores, whereas the IBP molecules are adsorbed at supermicropores, with the critical dimension of 0.72 nm (Mestre et al., 2014). Hence, the extraction-based regeneration is not practical for AC due to the relatively high adsorption energy required. Generally, the loaded AC is regenerated ex-situ using heat or steam, which is a high energy-consuming process, and during this process, a large portion of AC could potentially be lost (A. S. Mestre et al., 2009). Indeed, in terms of regeneration, MSM−500 have more merits than AC because the process is simple and can be regenerated fast using methanol.

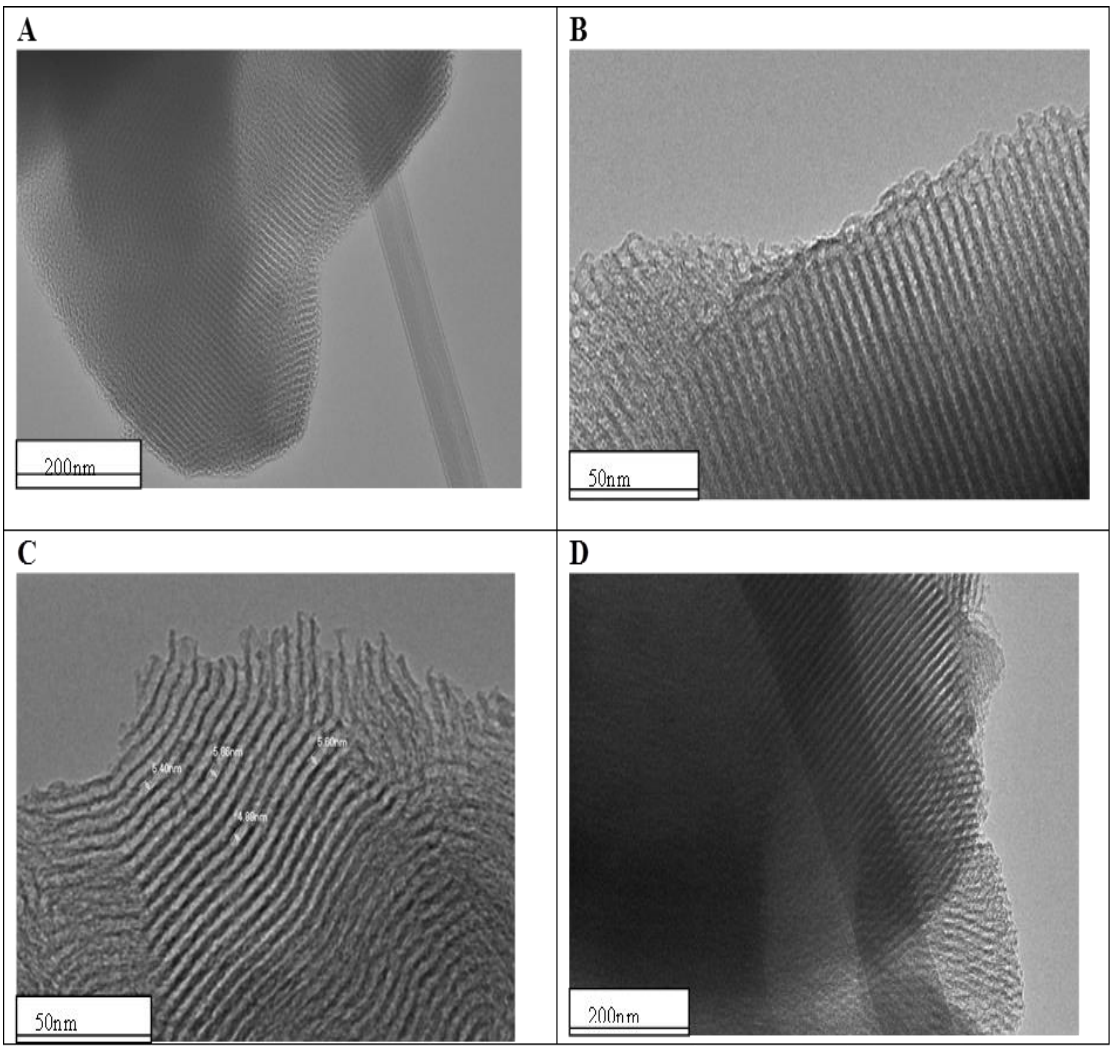

Figure 4.6: TEM images of the MSM−500 before (A), (B) and (C) after adsorption of IBP (D)

Figure 4.6 shows the TEM images of MSM–500 before and after 5th adsorption of IBP. As shown at figure 4.6, MSM–500 had homogeneous pore and wall structures, especially, the measured pore size was in the range of 5.44 ± 0.4 nm, which is about 11 % smaller than the primary pore size (6.2 nm) determined by N_2 gas isotherm. The TEM image taken for MSM–500 obtained after 5th adsorption shows a slight deformation at the inlet side of pore structure without any major defect. Therefore, this result might be strongly linked to the kinetic results for re-adsorption.

4.3.5 Mechanism of adsorption of IBP by MSM

Figure 4.7 shows the FTIR spectra (4000 to 500 cm^{-1}) of all the MSMs prepared at different calcination temperatures, as well as that of IBP-retained MSMs. The as-synthesized MSM had obvious bands of OH (~3400cm^{-1}), H_2O (1644 cm^{-1}), Si–O–Si [symmetric stretching vibrations (*vs*) at 1057 cm^{-1} and ~800 cm^{-1}], Si–OH (*vs* at ~950cm^{-1}), and O–Si–O [deformation vibration (δ) at 435cm^{-1}]. Si–O–Si (lines a and c in figure. 3) and Si–OH (line b) of MSM–500 and –600 show FTIR spectra typical of MSM (Yang et al., 2007). The intensity of the Si–O–Si peak for MSM calcined at > 600 °C is reduced drastically, representing the dissociation of the Si–O–Si bond during calcination.

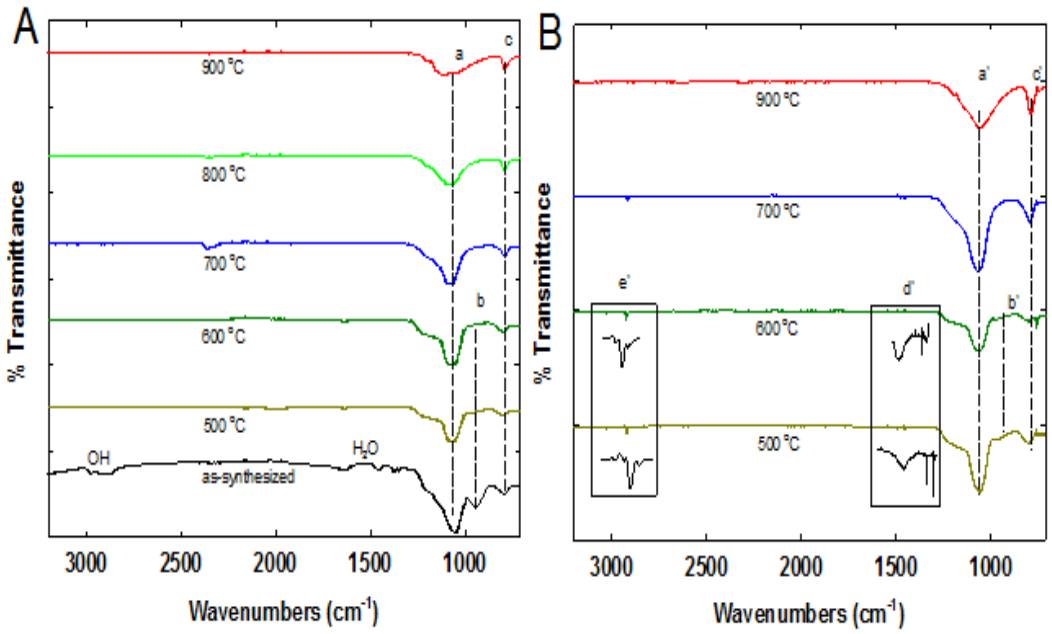

Figure 4.7: FTIR spectra of MSM materials before (A) and after adsorption (B) of IBP.

After the IBP adsorption, the Si–O–Si (lines a′ and c′ in figure 4.7) and Si–OH (line b′) peaks were preserved in the MSMs, showing the stability of the pore structure. A new band centred at 1630 cm^{-1} (box labelled d′) can be attributed to the asymmetric vibration

of carboxylic functional group (COO^-). Two more sharp peaks located at 1435 and 1500 cm^{-1} were assigned to the C–H bonding of carbon atoms. The peak at 2920cm^{-1} (box labelled e′) is assigned to a strong C–H bond, confirming the adsorption of IBP into the channels of MSM–500 (Munoz, Ramila, Perez-Pariente, Diaz, & Vallet-Regi, 2003; Vallet-Regi et al., 2007; Yang et al., 2007). Conversely, MSM–600 had a weaker adsorption peak, as shown in the d′ and e′ boxes, while the other MSMs did not show any peaks around this range. The FTIR data suggests that the reaction mechanism between IBP and MSM is a hydrophilic reaction (Bui & Choi, 2009b). At pH 7, the hydrogen of the carboxylic group of IBP is dissociated to form a COO^- functional group.

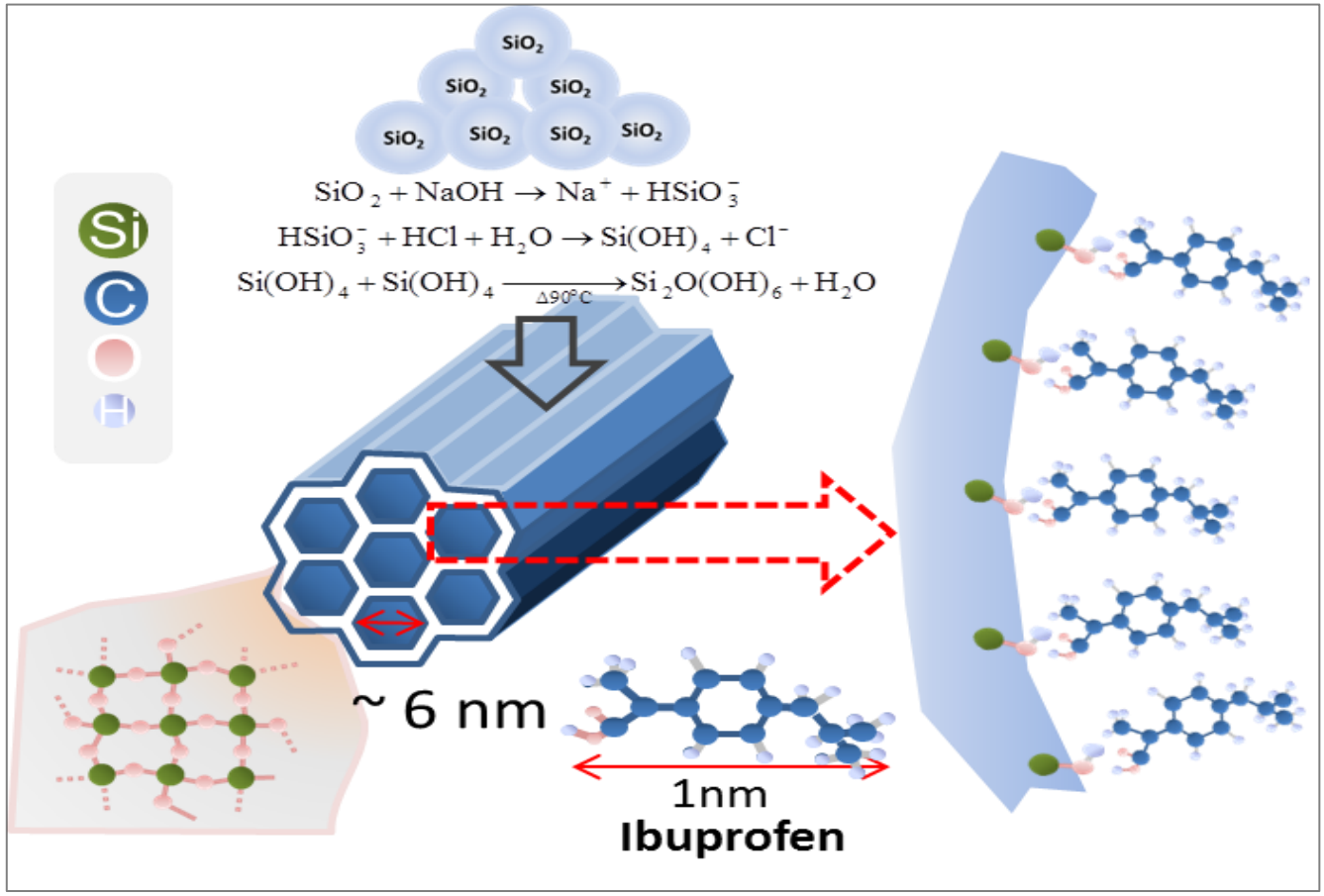

Schematic 4.1: The synthesis and removal mechanism of MSM

Schematic 4.1 clearly shows the mechanism MSM synthesis and the removal of IBP in details. The formation of hydrogen bonding reaction between the COO^- of IBP and silanol groups on the pore surface is favourable because it requires a lower activation energy (Andersson et al., 2004; Bui & Choi, 2009b).

$$\equiv Si - OH + {}^{-}OOC - B \cdots CH \rightarrow \equiv Si - O \cdots H \cdots OOC - B \cdots CH$$

Where ≡Si–OH and $^{-}$OOC–B···CH are silanol and IBP, respectively.

4.4 Characterization of MNCMs

Figure 4.8 (A) shows a low-angle XRD diffraction pattern of all synthesized samples. MNCM-1 displayed a well-resolved peak at ~1° of 2θ, corresponding to diffraction of d(100).

The peak intensity of MNCM-1 was much higher than those of the other samples, indicating the formation of uniform and homogenous mesopore structures. Compared with MSM, MNCM-1 had a peak shift toward higher 2θ values. This indicated a decrease in the d-spacing, caused by the introduction of the nano-magnetite in the pore frameworks, but the pore structure was largely maintained (Xiao et al., 2015). However, the MNCM synthesized with the addition of less than 1g of nano-magnetite (MNCM-0.25 or -0.5) did not form mesopore structures. This indicated that the amount of nano-magnetite plays an important role in the formation of the mesopore material. The mechanism of MNCM formation was further examined and reported in section 4.4.2

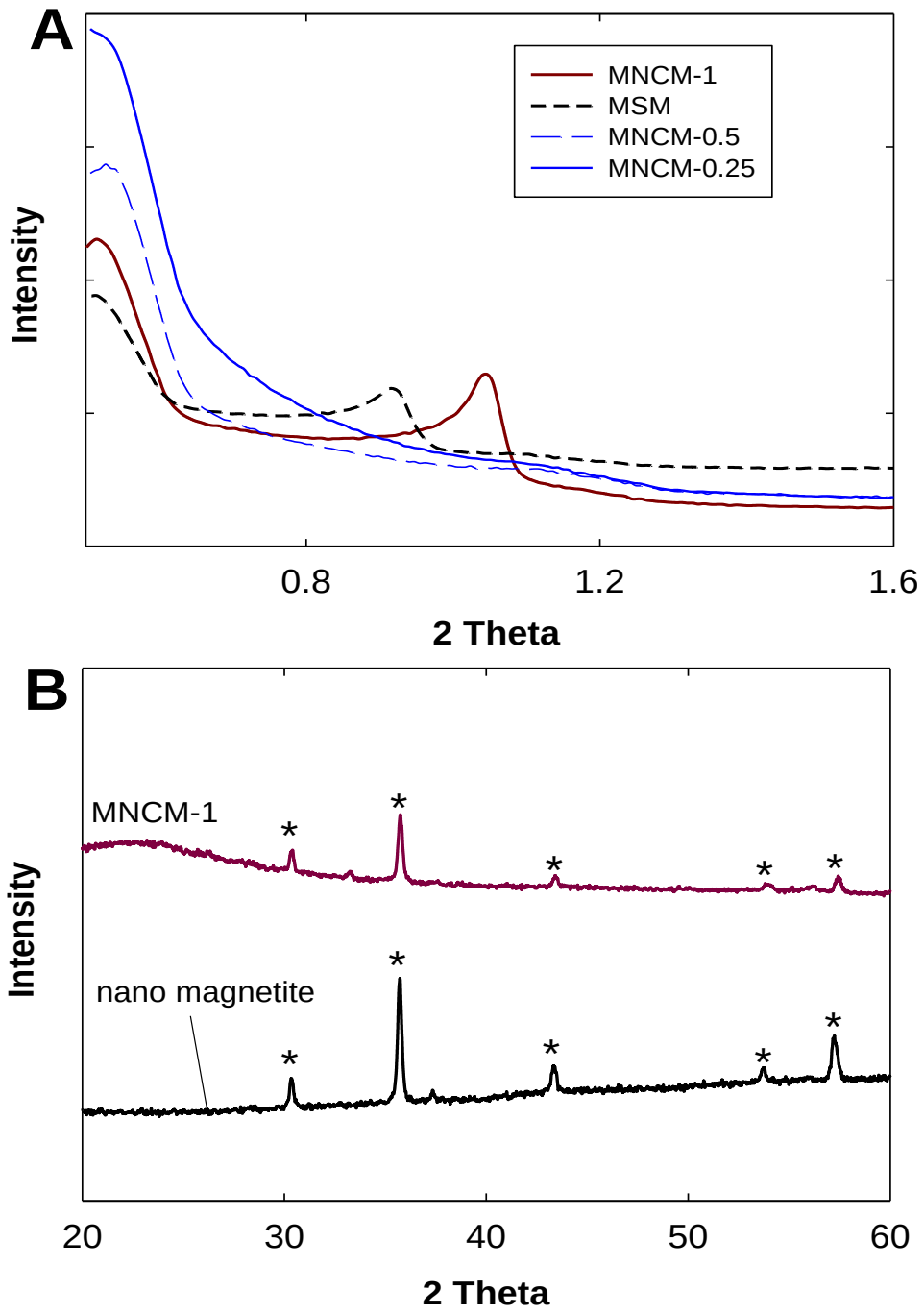

Figure 4.8: (A) Low angle XRD patterns of MNCMs and MSM, (B) wide angle XRD patterns of nano magnetite and MNCM-1

The wide-angle XRD peak of nano-magnetite and MNCM-1 are shown in figure 4.8 (B), with diffraction peaks corresponding to (220), (311), (440), (511), and (440). A broad peak between 20° and 30° was observed, which can be attributed to amorphous SiO_2 (Kuai & Nan, 2014; Xiao et al., 2015). These results confirmed that the nano-magnetite in MNCM-1 was coated around by SiO_2. The diffraction patterns of MNCM-1 and nano-magnetite were rather similar, suggesting that the nano-magnetite was retained after the synthesis and was stable in the hydrothermal process. Nevertheless, the intensity of the peaks was reduced due to the SiO_2 coating (Kuai & Nan, 2014).

Figures 4.9 (A) and (B) display the nitrogen gas isotherm and pore size distribution of the samples. MNCM-1 and MSM exhibited type IV hysteresis loop patterns, similar to MCM-41 and SBA-15, demonstrating the formation of mesopore structures. Other samples exhibited hysteresis loop patterns of macropore structures. Among the synthesized materials, MNCM-1 had the sharpest pore size distribution with a primary pore size of 5.7 nm, highest BET surface area of 576 m^2/g, and pore volume of 0.65 cm^3 /g. MNCM-0.5 had a broader pore size distribution than MNCM-1, but it was homogeneous compared with MNCM-0.25. Thus, the primary pore size shifted from macropore to mesopore as the amount of nano-magnetite increased. The wall thickness (5.84 nm) was calculated as the difference between corresponding unit cell parameter (a_o), where $a_o = 2 \times d(100)/\sqrt{3}$, and the mean BJH desorption pore diameter (Kuai & Nan, 2014).

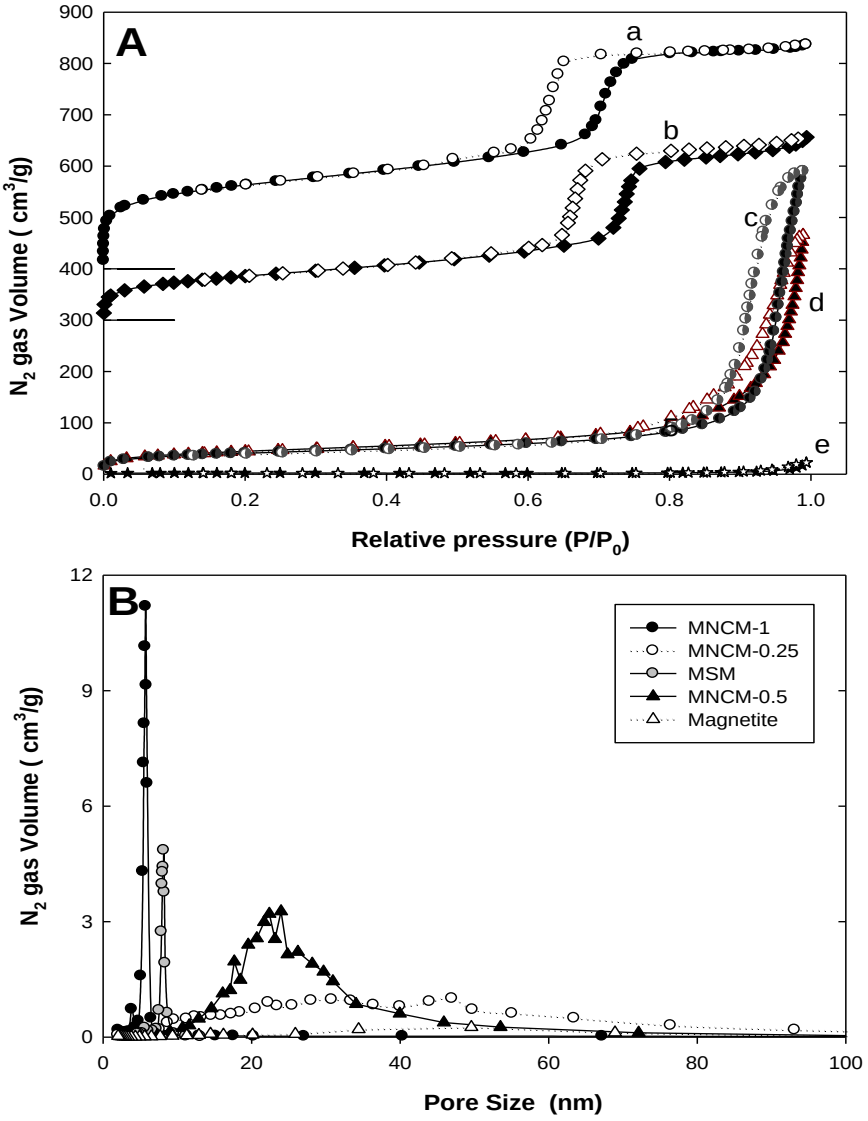

Figure 4.9: (A) Nitrogen adsorption-desorption isotherm of (a) MNCM–1, (b) MSM, (c) MNCM–0.5, (d) MNCM–0.25, (e) nano magnetite, (B) pore size distributions of all media

MNCM-1 had a slightly smaller wall thickness than MSM (7.96 nm). The reduction in wall thickness might have been caused by the interruption of nano-magnetite during the synthesis process. However, the wall thickness of MNCM-1 was close to the reported values of SBA-15 (5.27 nm) (Huang, Chang, Ou, Chiang, & Wang, 2011) and MCM-41 (5.0 nm) (Kruk et al., 1997), demonstrating the MNCM-1 is thermally stable. This wall thickness result indicates that MNCM-1 have better thermal stability compared to other synthesized materials.

Table 4.4: Comparison of Pore structural parameters of MNCM-1 with other materials

Materials	*d*-spacing [a] (nm)	Mean pore diameter [b] (nm)	Wall thickness [c] (nm)	BET Surface area [d] ($m^2 g^{-1}$)	V_t Pore volume [e] ($cm^3 g^{-1}$)	V_m, Micropore ($cm^3 g^{-1}$)	Ref.
SBA–15	9.73	5.27	5.96	659	0.83	n/a	(Huang et al., 2011)
MCM–41	4.8	3.3	5.0	1200	1.00	0.020	(Kruk et al., 1997)
Magnetic meso-SiO_2	n/a	5.9	n/a	362	0.48	n/a	(B. C. Kim et al., 2011)
$ZnCe_{0.03}Fe_{1.97}O_4$@SiO_2@SBA-15	n/a	5.4	n/a	481	0.53	n/a	(Kuai & Nan, 2014)
MSM	11.9	5.78	7.96	326	0.54	0.025	This work
MNCM–1	9.1	4.68	5.84	576	0.65	0.083	This work

[a]Calculated from the desorption of N_2 Isotherm, [b]Determined from the difference between the unit cell parameter ($a_o = 2d_{100}/\sqrt{3}$) and the frame work pore size. Surface area (BET) calculated from the adsorption of N_2 Isotherm, Vp and V_m total and micro pore volume calculated using BJH

The FESEM image in figure 4.10 clearly shows the formation of mesoporous material in MNCM-1 as a composite material with nano-magnetite and mesoporous SiO_2.

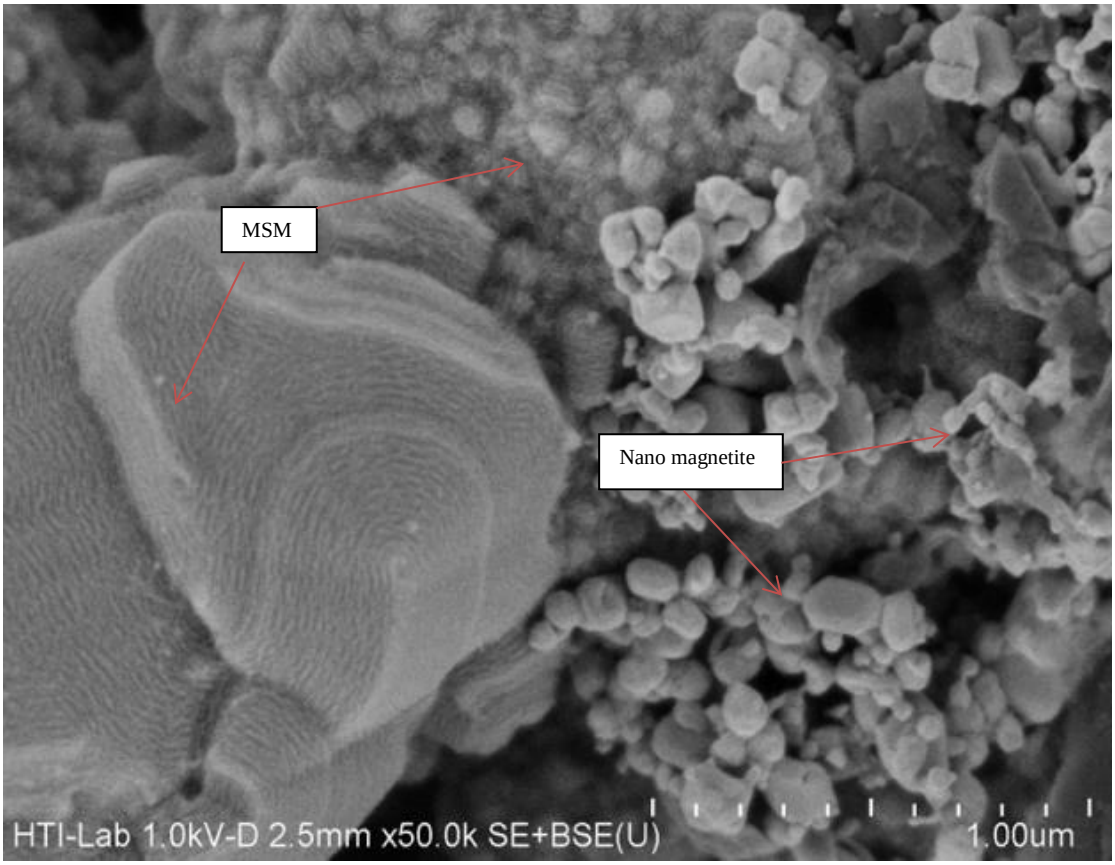

Figure 4.10: FESEM images of MNCM-1 formation of composite material

TEM results (figure 4.11), showed that nano-magnetite was impregnated into the mesopore structures. Coagulated nano-magnetite material formed backbone like structure, with well-organized and aligned mesopores.

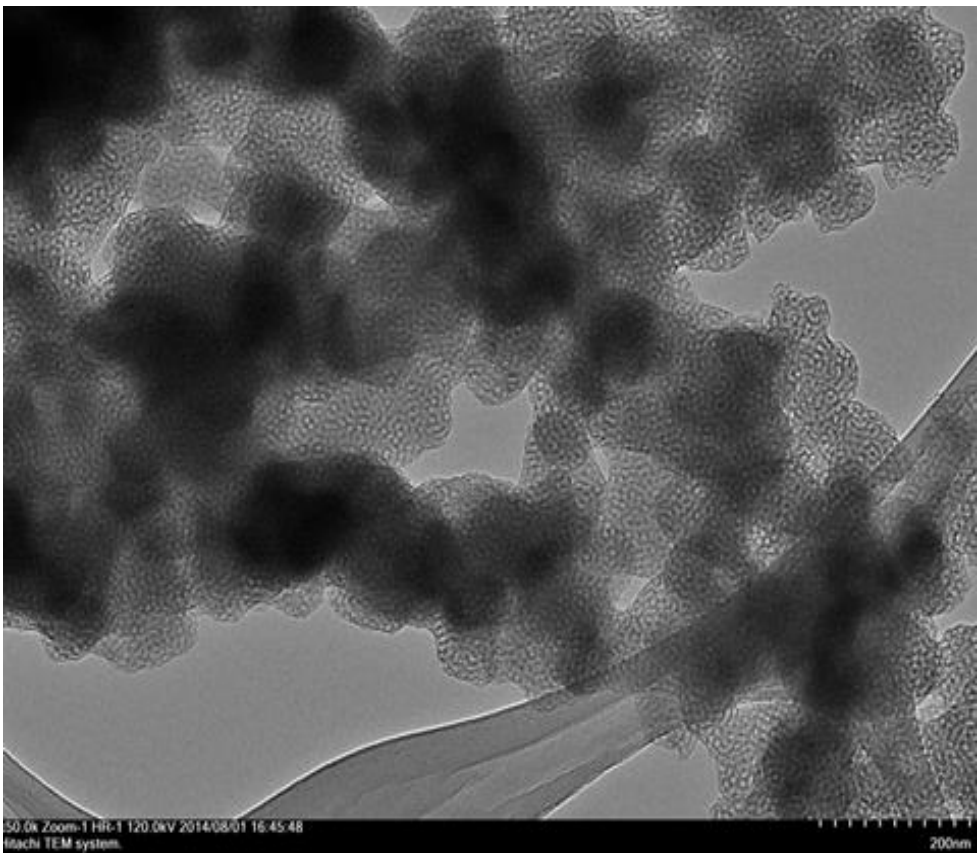

Figure 4.11: TEM image of nano magnetite impregnated MNCM-1

The measured pore size of MNCM-1 was ~5 nm, similar to the results obtained for the BJH pore size distribution (figure 4.9 B). As shown in the FESEM and TEM images, nano-magnetite existed in both the frameworks of mesoporous SiO_2 and coagulated particles (200–400 nm). In the TEM result, the coagulated size of nano-magnetite incorporated in mesoporous SiO_2 was measured at ~100–300 nm. To confirm the coagulation of nano-magnetite, the particle size distribution of nano-magnetite was determined by SAXs shown in figure 4.12.

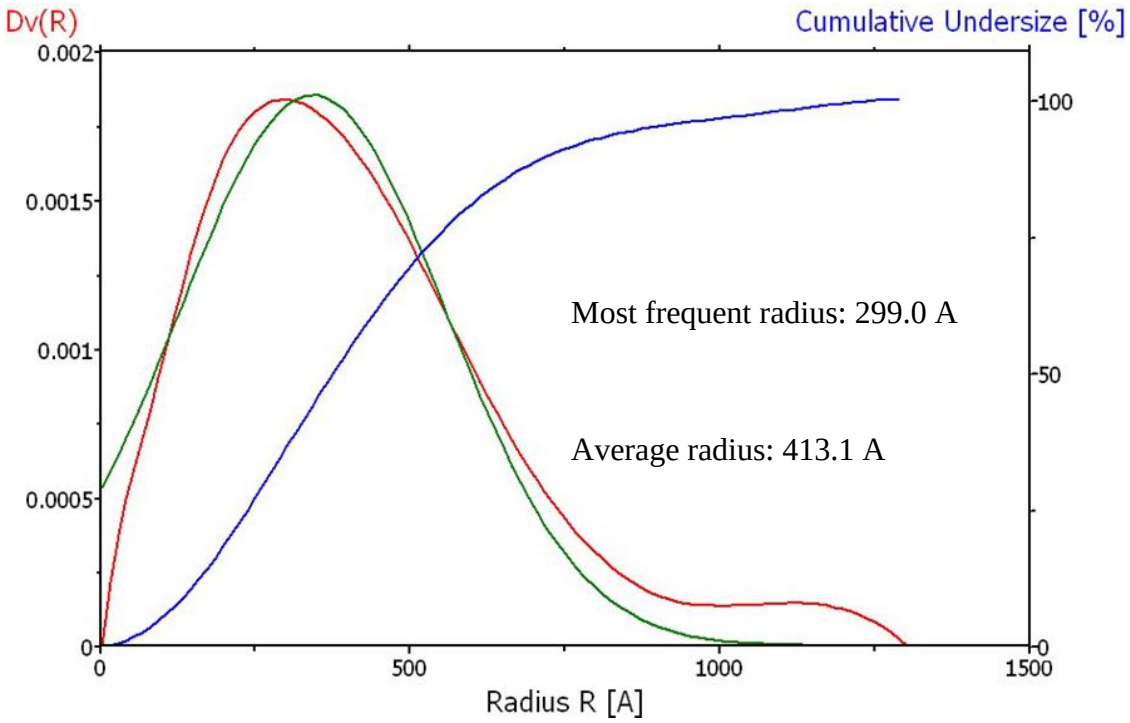

Figure 4.12: Small angle X-ray diffraction distribution of nano magnetite

The results indicated that the average particle size of nano-magnetite was ~40 nm and the most frequent size was 30 nm. Thus, we conclude that nano-magnetite was coagulated during the synthesis of MNCM-1.

For the case of MNCM-0.25 (figure 4.13), the image showed that all silica is still in the form of coagulated fine particles and there was no formation of mesopore structures. This was consistent with the XRD results and N_2 gas isotherms. Interestingly, the size of the coagulated particles was much smaller than those of MNCM-1, though it was not homogeneous. This indicates that nano-magnetite was dominantly dispersed to be coated by SiO_2 without severe coagulation during the synthesis of MNCM-0.25.

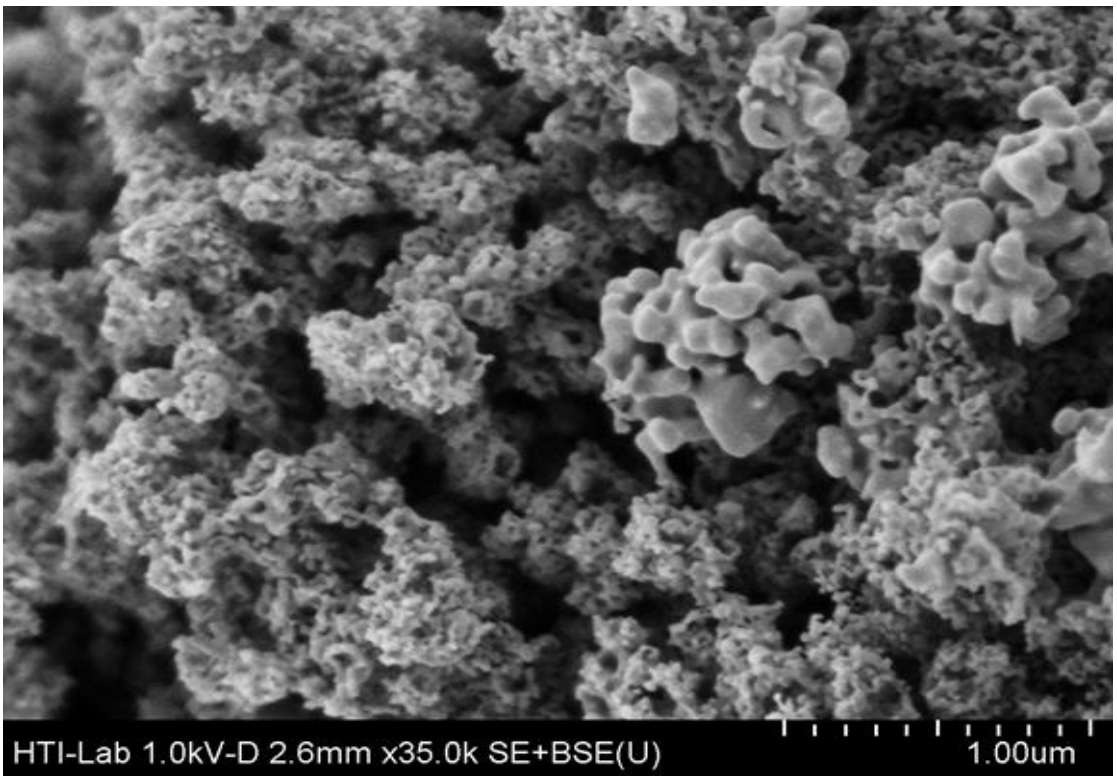

Figure 4.13: FESEM image of MNCM-0.25

The magnetic properties of MNCM-1 were investigated using a magnetometer with an applied field ranging from -5–5 KOe at room temperature (figure. 4.14). The hysteresis loop of the plot revealed a highest magnetic value of 2.9 emu/g. This value is higher than the sandwich structure $ZnCe_{0.03}Fe_{1.97}O_4$@nSiO_2@SBA-15 (< 2.0 emu/g) reported by Kuai and Nan (Kuai & Nan, 2014).

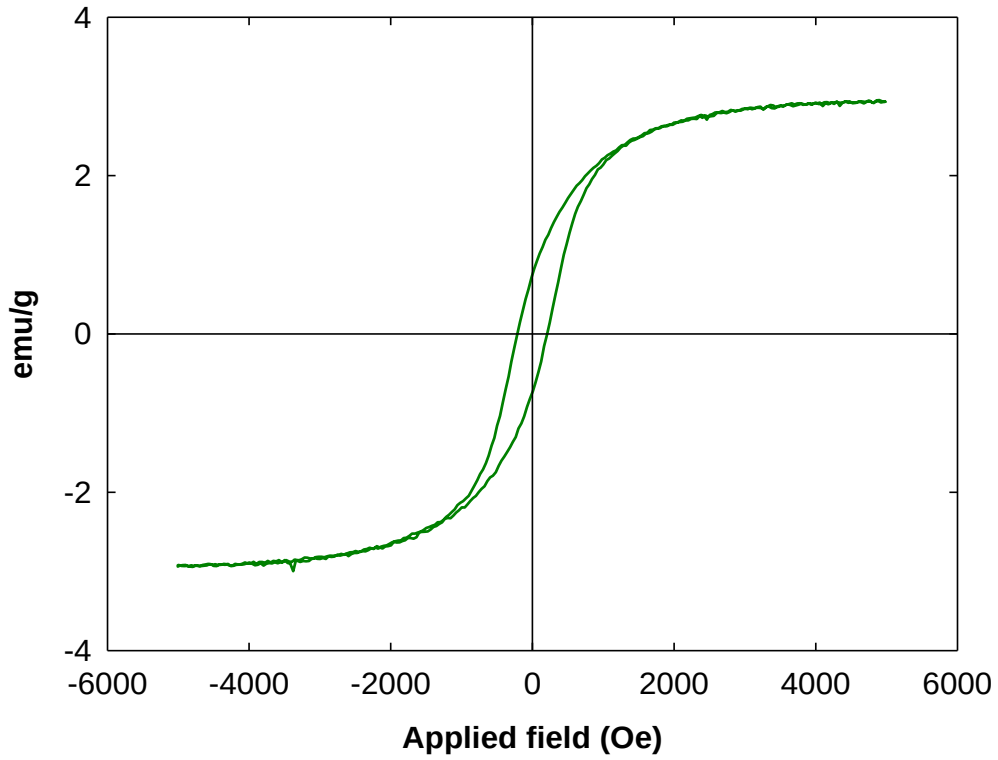

Figure 4.14: Magnetic properties of MNCM-1 investigated using a magnetometer

The FTIR spectrum of MNCM-1 is shown in figure 4.15; it showed a curved band in the hydroxyl region, ranging from 3500–3200 cm^{-1}, and a small peak around 900 cm^{-1} attributable to the hydroxyls of the silanol groups and water molecules adsorbed. Another two strong peaks were observed around 1100 and 800 cm^{-1}, indicating Si-O-Si asymmetric stretching and bending vibrations, respectively. No peaks related to nano-magnetite were observed in the FTIR spectrum due to complete coating by SiO_2 (Briceño et al., 2014).

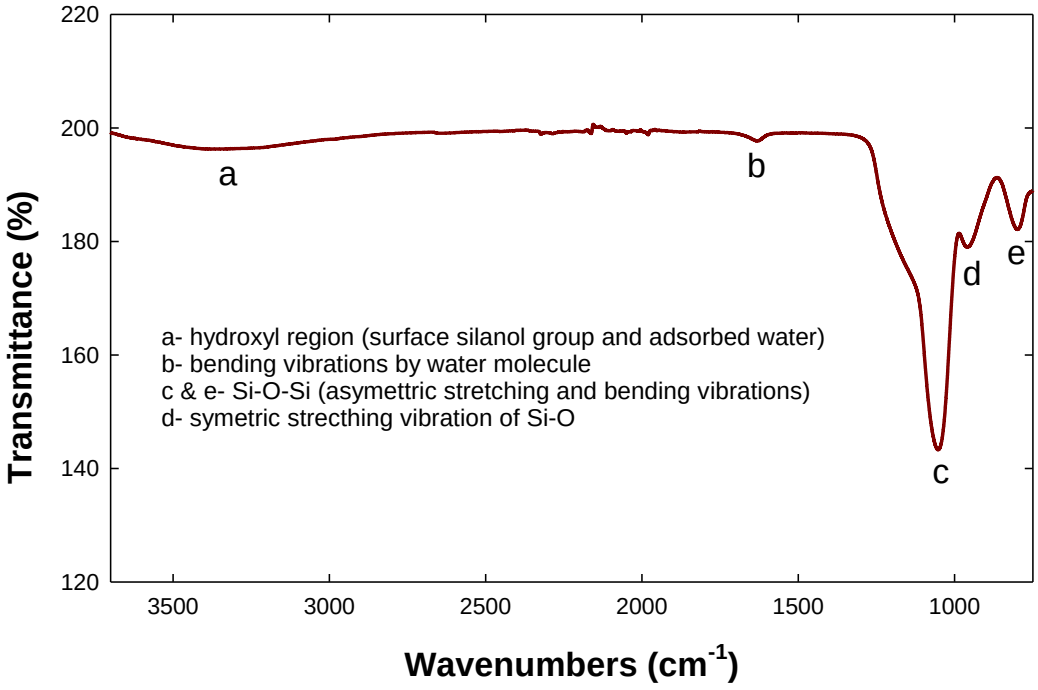

Figure 4.15: FTIR spectrum of MNCM-1

4.5 Mechanism of synthesis of MNCM-1

The synthesis of MNCM-1 is strongly dependent on the mass of the nano-magnetite. Among the synthesized materials, only MNCM-1 had meso-structure physical characteristics. Based on the synthesis route of MSM in section 4.2, the synthesis mechanism of MNCM can be illustrated as shown in schematic 4.2.

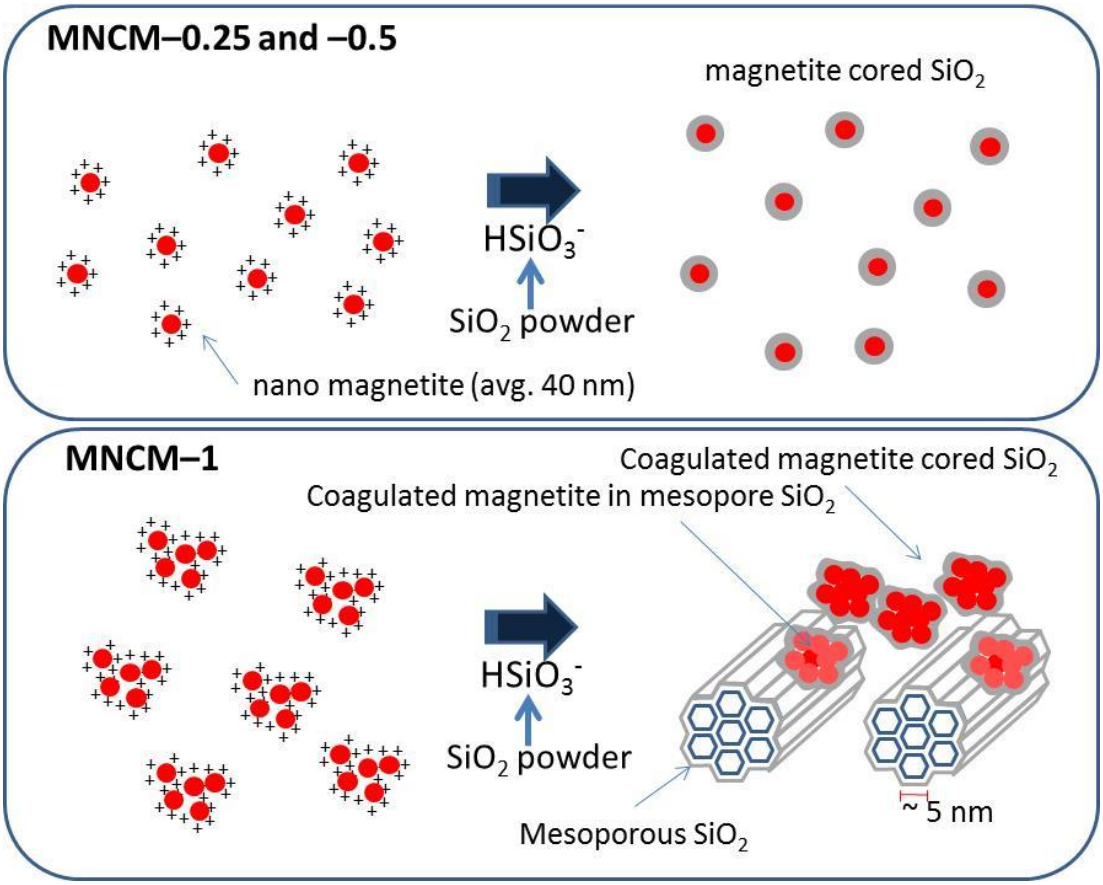

Schematic 4.2: Synthesis mechanism of MNCM (stoichiometric ratio for MNCM-1 was 0.14 Fe_3O_4: 1 SiO_2: 1 NaOH: 0.1 HCl: 0.013 Pluronic®: 167 H_2O)

When nano-magnetite is added to an acidic medium (pH <1), the surface charge of nano-magnetite is transformed to be positive ($\equiv Fe\text{-}OH_2^+$). Thus, a large amount of nano-magnetite affects the formation of mesoporous SiO_2 because negatively-charged $HSiO_3^-$ could instantly coordinate on to the surface of nano-magnetite as it is added into the magnetite suspended medium. Thus, the available surface area and charge of nano-magnetite is important in forming mesopore material. When smaller mass of nano-magnetite is added, they repel each other and do not coagulate. Therefore, most nano-magnetite can be coated by $HSiO_3^-$ so that no more $Si(OH)_4$ can be generated. This might be the main reason why mesopore materials were not formed with MNCM-0.25 and -0.5. When the mass of nano-magnetite is increased to 1g, the nano-magnetite coagulates, resulting in a reduction of available surface area and positive charge. This

limits the coating of $HSiO_3^-$ and the remaining $HSiO_3^-$ is transformed to $Si(OH)_4$. Finally, through a hydrothermal process, two $Si(OH)_4$ molecules formed a silicate dimer, which is further polymerized to form a mesoporous material framework within the synthesis of $S^oH^+Cl^-I^o$.

4.6 Removal of MB by MNCM-1

4.6.1 Effects of pH on adsorption of MB

Figure 4.16 (A) shows the kinetics of MB removal by MNCM-1 at different initial pH values of the solution. It is clear that the pH value have significantly affected the adsorption capacities of MNCM-1. At pH 2, the adsorption capacity at equilibrium was low, 16 mg/g. However, as the pH was increased to 10, the adsorption capacity increased significantly to 146 mg/g. This phenomenon was similar to those previous results reported by Kuai et al. and Zhao et al. (Kuai & Nan, 2014; M. Zhao, Tang, & Liu, 2008). The adsorption mechanism can be examined by observing the surface charge (pH of the isoelectric point, pH_{IEP}) of the MNCM-1. In Figure 4.17, the pH_{IEP} of MSM and MNCM-1 was observed similar at pH 1. This suggests that the incorporation of nano-magnetite in MNCM-1 did not affect the pH_{IEP}, indicating that the nano-magnetite was fully coated by SiO_2, which finding matched the result of FTIR (Fig. 20).

Under acidic conditions, pH 2–4, the surface became slightly negatively charged and H^+ ions competed with cationic MB on the sorption sites. At higher pH, above 4, the surface became more negative, which increased the electrostatic interaction between the MNCM-1 surface and positive charged MB molecule. This increased the adsorption amounts of MB by MNCM-1. Figure 4.16 B is an actual photograph of MB removal by MNCM-1 followed by separation using a magnet (1.25 Tesla). At 20 mg L^{-1} MB solution, 30 mg MNCM-1 was added at pH 10 for 30 min. Then, all MNCM-1 was

separated within 30 s using the magnet. Consequently, the solution became transparent. This is an important advantage of magnetized sorbents when compared with other non-magnetic materials, such as activated carbon, silicate, and zeolite.

4.6.2 Effects of initial concentration on adsorption

Figure 4.16 (C) shows the removal of MB by MNCM-1 at various MB concentrations. Increased MB concentration improved the adsorption capacities of MNCM-1. At 20, 25, 30, 35, and 40 mg/L, the equilibrated adsorption capacities were 134, 140, 151, 171, and 236 mg/g, respectively. The adsorption capacity for nano-magnetite was very low (~5 mg/g) compared to other synthesized materials. This inferred that most of the sorption sites for MB adsorption were Si-OH pore structure. The increase in the concentration of MB proposes that two MB molecules may approach each other to a distance allowed by their van der Waals radii. This causes a strong affinity between the MB molecules and surface of MNCM-1 (Goscianska, Marciniak, & Pietrzak, 2014).

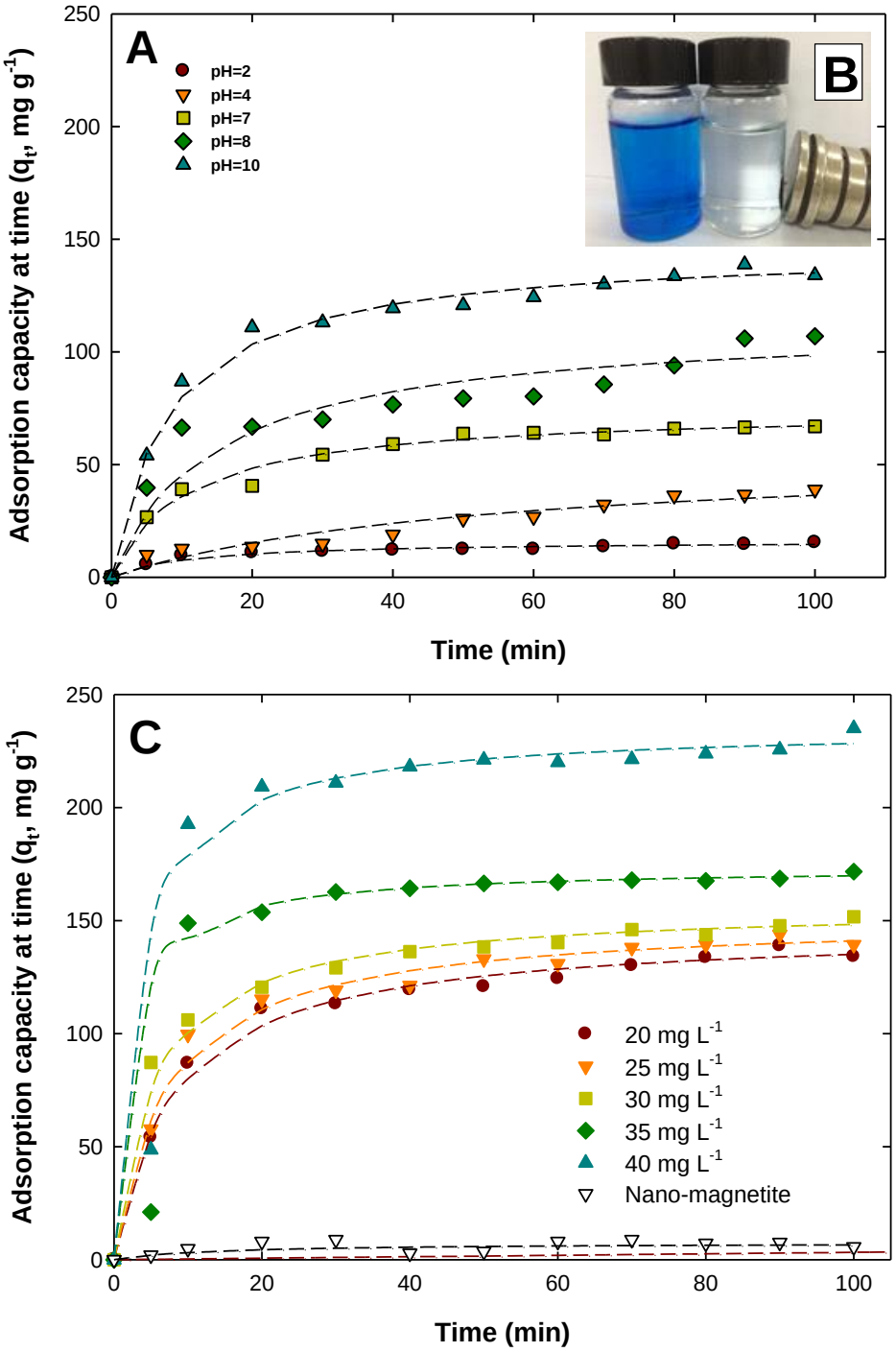

Figure 4.16: Effect of (A) pH and (B) actual photo of MB removal and separation of MNCM-1 using a magnet (1.25T) (C) concentration on adsorption of MB by MMSM-1, fitted lines from Pseudo 2nd order kinetic model

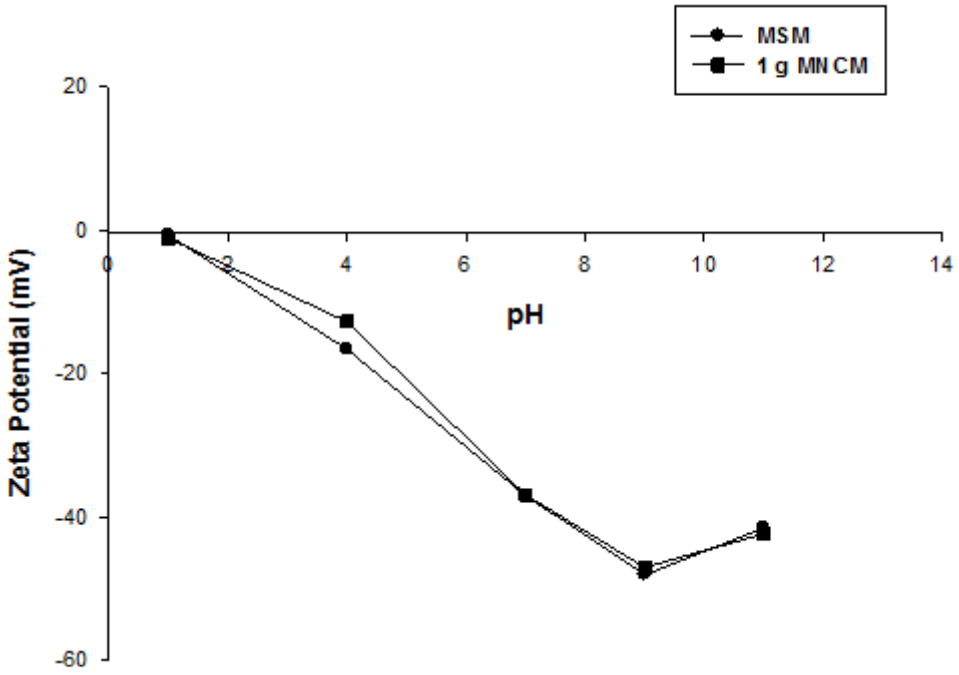

Figure 4.17: Zeta potential analysis of MNCM-1 and MSM

Experimental data from these isotherm experiments were fitted with two isotherm models, Langmuir and Freundlich, which was described in the earlier section. At equilibrium, K_L and q_{max} can be obtained from the intercepts and slopes of the plot of C_{eq}/q_{eq} versus C_{eq} (figure 23 A). The maximum adsorption capacity was calculated to be 248 mg/g, and K_L and R^2 were 1.13 L/mg and 0.997, respectively.

The plot in figure 4.18 B shows the correlation coefficient (R^2) of 0.955, smaller than that of the Langmuir isotherm. These results indicated that the Langmuir isotherm was more suitable for interpreting the adsorption of MB by MNCM-1, indicating a homogeneous monolayer adsorption process.

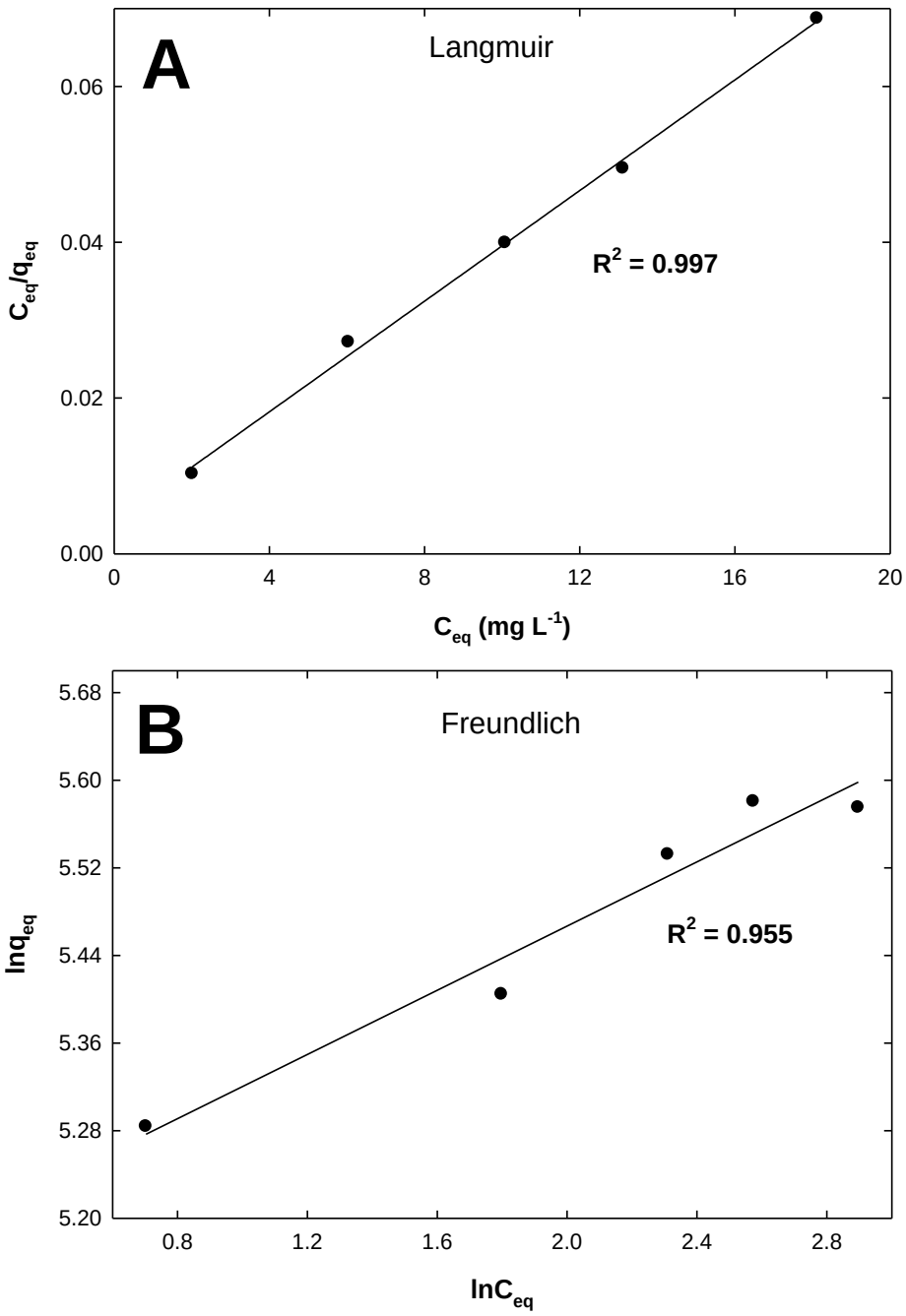

Figure 4.18: Linear Plots of (A) Langmuir and (B) Freundlich isotherm

4.6.3 Kinetics of methylene blue removal by MNCM-1

Pseudo-1st order, pseudo 2nd order, and intraparticle diffusion (IPD) models were used to evaluate the kinetic data obtained at different initial concentrations of MB. Data from the experiments were fitted with all three models, and all parameters are listed in table 4.5. The R^2 values (> 0.997) of the pseudo 2nd order kinetic models were larger than those (> 0.751) of the pseudo-first order, suggesting that the process is controlled by heterogeneous adsorption (Salem & El-Maazawi, 2000).

.

Table 4.5: Kinetic Parameters of MNCM-1 removal of MB

Initial conc. MB ($mg\ L^{-1}$)	Exp. q_e ($mg\ g^{-1}$)	Pseudo 1st order		Pseudo 2nd order			Intraparticle diffusion			
		$K_1 \times 10^{-2}$ (min^{-1})	R_2	$K_2 \times 10^{-4}$ ($g\ mg_{-1}\ min^{-1}$)	q_e ($mg\ g^{-1}$)	R^2	(t ≤ 10)	(t ≥ 10)		
							K_{d1} ($mg\ min^{-1/2} g^{-1}$)	K_{d2} ($mg\ min^{-1/2}$ g-1)	I ($mg\ g^{-1}$)	R^2
20	138.8	1.157	0.891	8.3	146.3	0.997	27.44	6.47	75.19	0.932
25	143.9	1.061	0.876	8.9	151.4	0.997	31.50	6.00	85.35	0.937
30	151.7	1.165	0.911	11.4	156.6	0.999	33.54	6.03	93.07	0.940
35	171.6	1.538	0.792	26.3	173.5	0.999	47.06	3.00	142.58	0.880
40	235.0	1.690	0.751	13.3	235.6	0.998	60.93	4.85	183.39	0.901

q_{eq}- experimental adsorption at equilibrium time
K_1-Pseudo 1st order rate constant, q_e- calculated adsorption at equilibrium time, K_2-Pseudo 2nd order rate constant

Figure 4.19 shows the plot of q_t versus $t^{1/2}$. The fit line obtained by the IPD model shows non-linearity, indicating that the adsorption process is a multi-step process: a fast increasing step at the beginning, then slowing down and becoming almost flat (M. Zhao et al., 2008). No linear plot at any concentration were observed passing through the origin of the graph, indicating that intraparticle diffusion is not the only rate-controlling step; other factors, such as surface area, pore size, and volume may also affect the adsorption rate (Kuai & Nan, 2014). The rate constants of these adsorption processes are listed in table 4.5.

The first step (K_{d1}) was the adsorption of MB on the external surface and the second was intraparticle diffusion (K_{d2}) of the MB through the solution to the internal pores of MNCM-1 (Xiao et al., 2015). K_{d1} was much higher than K_{d2}, signifying that surface adsorption was dominant for the first 10 min and diffusion, then became the rate-limiting step. The K_{d1} values of MNCM-1 ranged from 27.4–60.9 mg/min$^{1/2}$ g, which were relatively higher than the reference material $ZnCe_{0.03}Fe_{1.97}O_4@SiO_2@SBA\text{-}15$ (19.5-21.8 mg/min$^{1/2}$ g) under the same experimental conditions. This consequence could be associated with the fact that MNCM-1 had a larger surface area and pore volume than $ZnCe_{0.03}Fe_{1.97}O_4@SiO_2@SBA\text{-}15$.

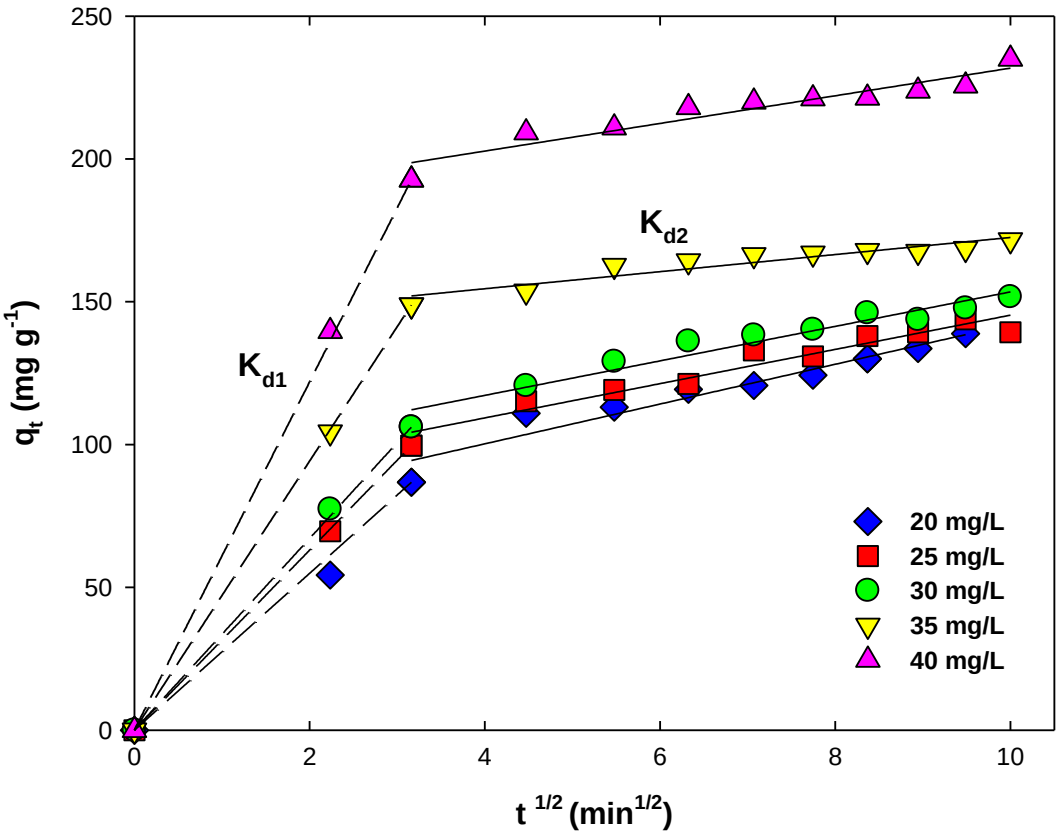

Figure 4.19: Intra particle mass transfer diffusion model for different MB concentration

4.6.4 Reuse of MNCM-1 for MB adsorption

MNCM-1 was regenerated and reused for MB adsorption three times (figure. 4.20). The adsorption capacities of the MNCM-1 remained almost same in each cycle and were not affected significantly by the regeneration process. The reusability of MMSM-1 is an important aspect for real waste water treatment because it can significantly reduce costs.

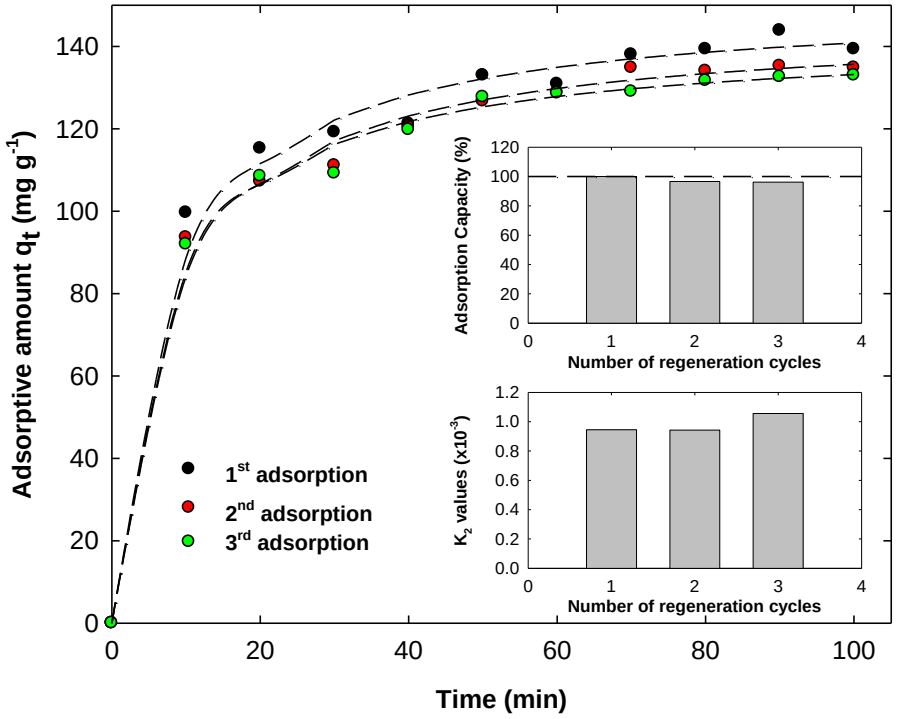

Figure 4.20: Regeneration test of MB adsorption by MNCM-1 at 25 mg L^{-1} with initial pH 10 with dotted line from pseudo 2nd order kinetic model.

The hydrothermal stability of MNCM-1 was investigated using TGA (figure. 4.21). MNCM-1 had good thermal stability up to 1,000°C with a low percentage of mass loss. Total weight loss of MNCM-1 was ~23% at 1,000°C, lower than that of SBA-15 (~27 %) (Kuai & Nan, 2014). In addition to the colour, the texture and magnetic properties of MNCM-1 remained almost the same after the TGA analysis, showing that the material was stable at a high temperature.

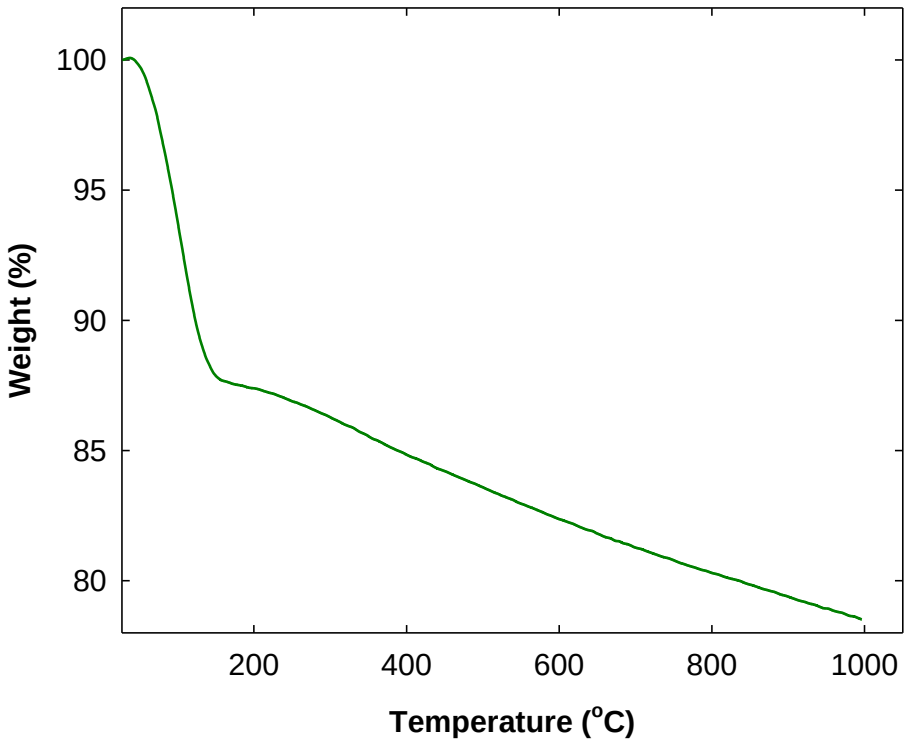

Figure 4.21: TGA of MNCM-1

4.6.5 Thermodynamic analysis

Thermodynamic analyses were conducted at four different temperatures: 298, 308, 318, and 328 K. Figure 4.22 A shows that the adsorption amount increased as the temperature of the solution increased.

Where m is the adsorbent dose (g/L), A is the Arrhenius factor, R is the gas constant (8.314 J/mol/K), and T is the temperature (in K). The adsorption affinity is defined as mq_{eq}/C_{eq}. The linear plot of $\ln(mq_{eq}/C_{eq})$ versus 1/T was plotted following equation (E12 from section 2.7). The thermodynamic parameters such as ΔH^o, ΔS^o, and ΔG^o were determined from the plot. The Arrhenius activation energy (ΔE_a) was calculated using equation (8). A linear plot of ln K_2 versus 1/T was prepared to determine E_a value (the slope). The thermodynamic parameters are listed in table 4.6.

The negative value of ΔG^o indicates a spontaneous process of MB adsorption by MNCM-1. The increase in the absolute value of negative ΔG^o with an increase of temperature means that the reaction is more favorable at higher temperatures. Additionally, because all ΔG^o were in the range of -20–0 kJ/mol, the MB adsorption by MNCM-1 can be concluded to be a physisorption process (Huang et al., 2011).

The positive value of ΔH^o (5.55 kJ/mol) indicates that adsorption of MB by MNCM-1 is an endothermic process in the bond formation between Si-OH and MB. However, the positive ΔS^o (42.57 J/mol K) indicates an increase in the randomness at the solid–liquid interphase when the reaction temperature increases, indicating that MB and MNCM-1 have good affinity during the adsorption process (Islam et al., 2015). The E_a (0.846 kJ/mol) was lower than the reference value for mesoporous SBA-15 (1.782 kJ/mol). This indicates that a lower energy barrier is required for MB adsorption by MNCM-1 (Huang et al., 2011).

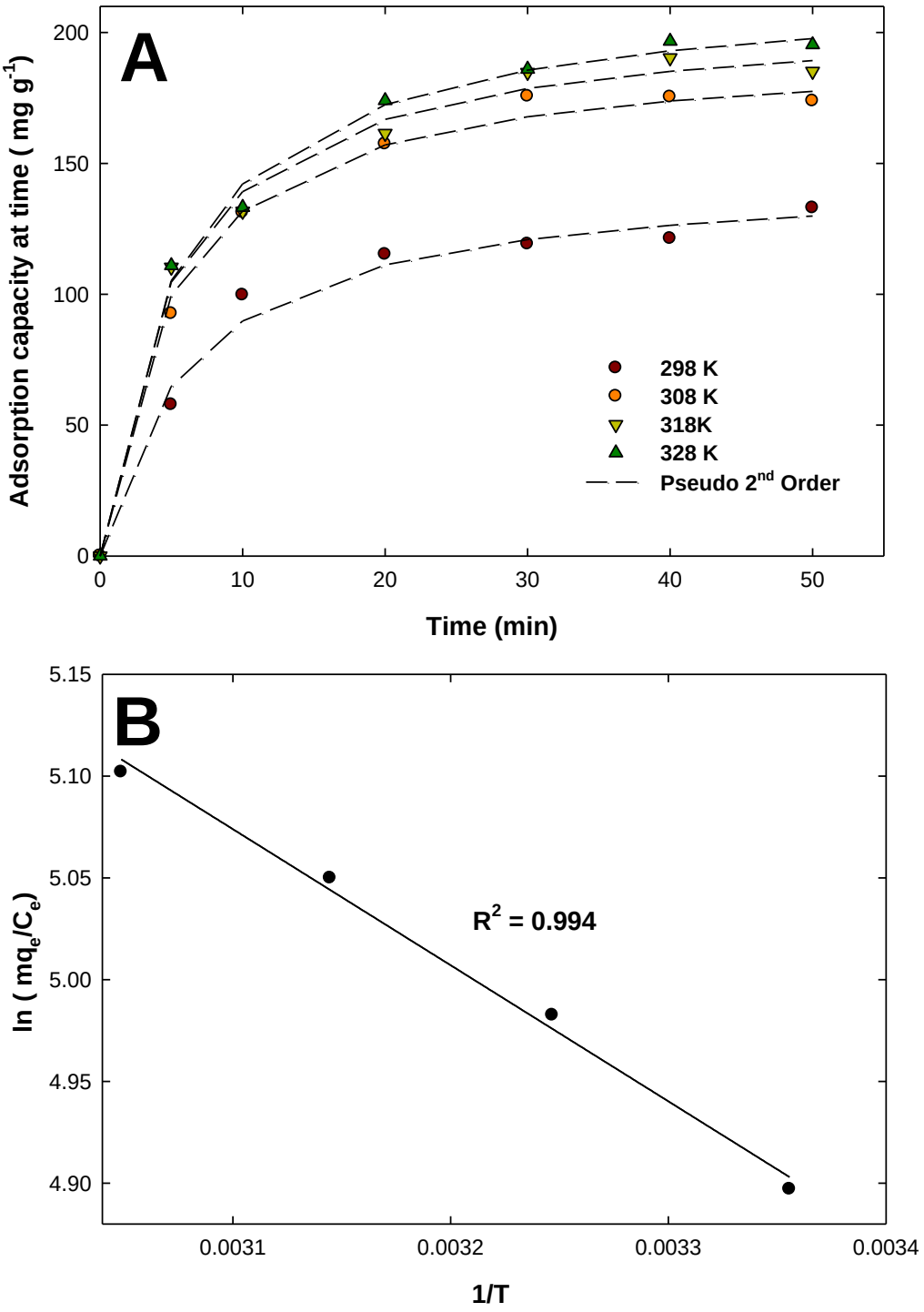

Figure 4.22: (A) Temperature effect on adsorption of MB and (B) temperature plot $\ln(mq_e/C_e)$ versus 1/T.

Table 4.6: Thermodynamic parameters for the adsorption of MB by MNCM-1

T (K)	ΔG^o (kJ/mol)	ΔH^o (kJ/mol)	ΔS^o (J/mol K)	ΔE_a (kJ/mol)
298	–12.13	5.55	42.57	0.846
308	–12.76			
318	–13.35			
328	–13.91			

4.6.6 Comparison of pore characteristics, sorption capacity of MB, and cost analysis

Table 4.7 shows the overall comparison of pore characteristics and sorption capacity of MB with other mesoporous materials. MNCM-1 exhibited more adsorption capacity than most of the media, except SBA-3. Upon analysis, we found that Q_{max} was correlated strongly with surface area for the case of non-magnetic mesoporous materials, while magnetized materials had particularly high Q_{max} even with smaller surface areas (figure 4.23). Thus, the surface area plays an important role in increasing Q_{max} of non-magnetic media. However, further study is needed to examine the exceptional characteristics of the magnetized materials.

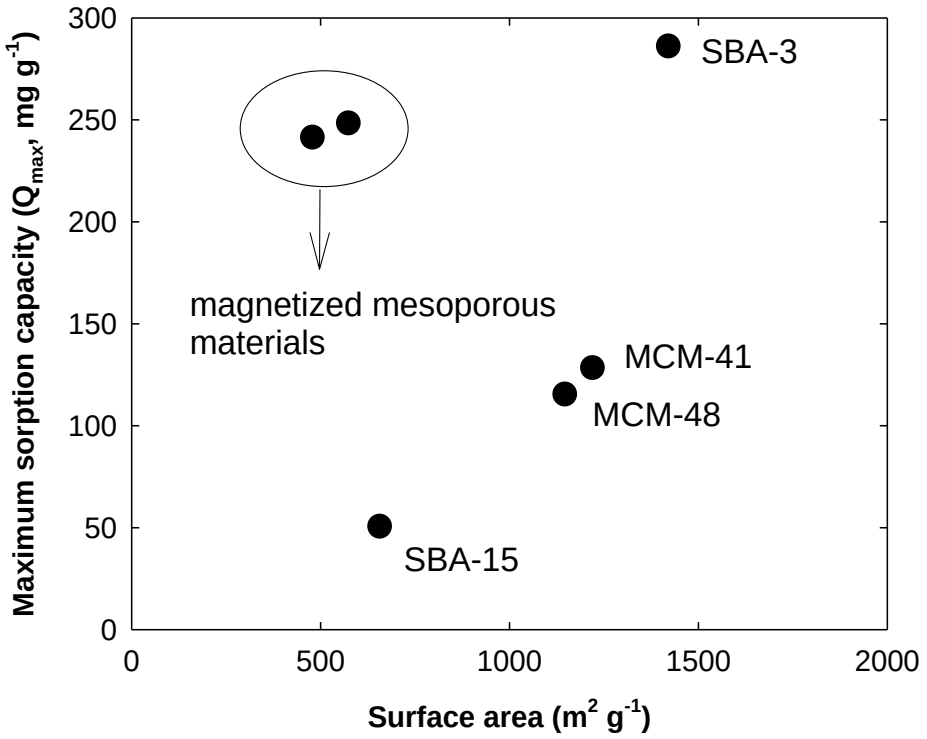

Figure 4.23: Comparison between mesoporous materials for Q_{max} vs. surface area

We calculated the costs for the initial synthesis of materials to estimate the treatment costs for MB containing water, for which the MB concentration and volume were 10 mg/L and 1 L, respectively. As shown in table 4.7, MNCM-1 involved the lowest cost ($ 0.018) when compared with other silica-based mesoporous media. For example, MNCM-1 is 82, 40, and 16 times less expensive than SBA-15, MCM-48, and $ZnCe_{0.03}Fe_{1.97}O_4@SiO_2@$SBA-15, respectively. The reduction in treatment cost was mainly due to the replacement of TEOS with a much less expensive silica source, SiO_2. The allocated price of TEOS is about 96% of the total cost of the synthesis and TEOS is about 200 times more expensive than SiO_2. Furthermore, the reusability and easy separation of MNCM-1 will further reduce treatment costs significantly. The synthesis and characteristics of MNCM and its application were summarised in the Schematic diagram 4.3

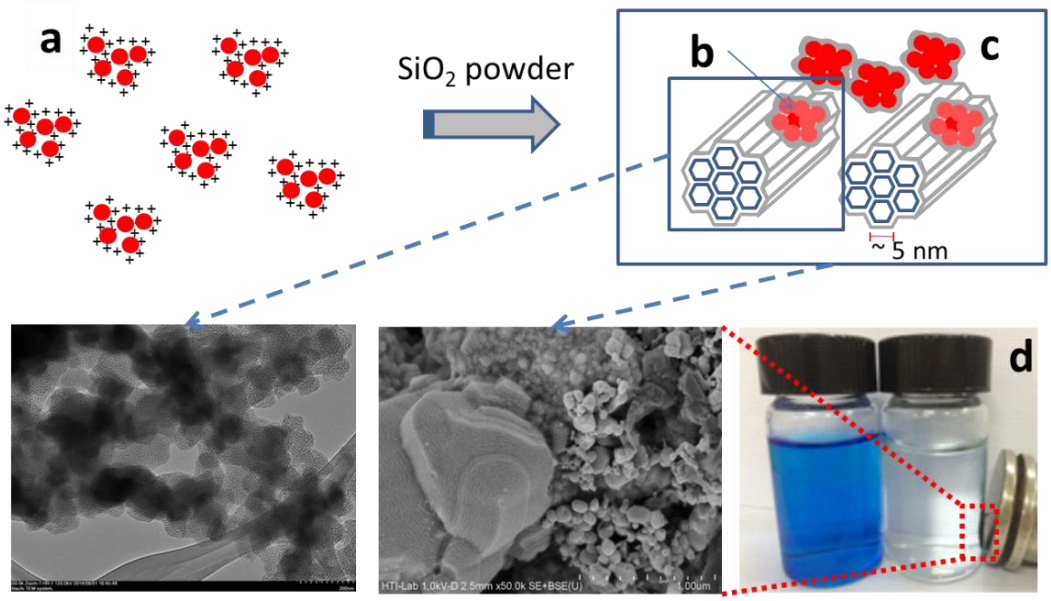

a: Coagulated nano magnetite
b: Coagulated nano magnetite in mesopore SiO_2
c: Coagulated magnetite cored SiO_2
d: Adsorption of methylene blue by MNCM-1 followed by magnetic separation

Schematic 4.3: MNCM syntheses, characteristics and application

Table 4.7: Comparison of pore characteristics, adsorption parameters and cost analyses for MB removal

Mesoporous materials	Surface Area ($m^2\ g^{-1}$)	Pore vol. ($cm^3\ g^{-1}$)	Conc. MB ($mg\ L^{-1}$)	t (min)	Q_{max} ($mg\ g^{-1}$)	Magnetic Property ($emu\ g^{-1}$)	[1]Mass (mg)	[2]Costs (USD)	Ref.
MCM–41	1222	1.0	3 ~30	120	128	[3]NM	78	0.615	(Huang et al., 2011)
MCM–48	1149	3.0	3 ~30	120	115	NM	86.9	0.772	(Kruk et al., 1997)
SBA–3	1423	0.93	50-150	20-60	285.7	NM	35	0.265	(B. C. Kim et al., 2011)
SBA–15	659	0.83	16-160	60	50.2	NM	199.1	1.528	(Bui & Choi, 2009c)
$ZnCe_{0.03}Fe_{1.97}O_4$ @SiO_2@SBA–15	481	0.53	20 ~ 40	60-90	241	2.0	41.5	0.280	(Kuai & Nan, 2014)
MCNM–1	576	0.65	20 ~ 40	20-80	248	2.9	40.3	0.018	This work

[1]Mass of media required for treating 1 L of water containing MB (10 $mg\ L^{-1}$), [2]Costs ($) of media for treating 1 L of MB containing water (10 $mg\ L^{-1}$), which do not include electricity consumption, manpower, regeneration and separation costs, [3]Non-magnetic

4.7 Characterization of MNCMT

The XRD patterns of MNCMT-1, -2 and -3 all displayed d_{100} peak at 2.79 of 2 theta (figure. 4.24). Compared to MNCM (figure. 4.8 A), amine modified media (MNCMT) had peaks shifted to the right with weak intensities; indicating that it has smaller pore size and higher heterogeneity in pore structure (Y.-H. Kim et al., 2014; H. Zhao, Hu, Wang, Zhou, & Liu, 2007).

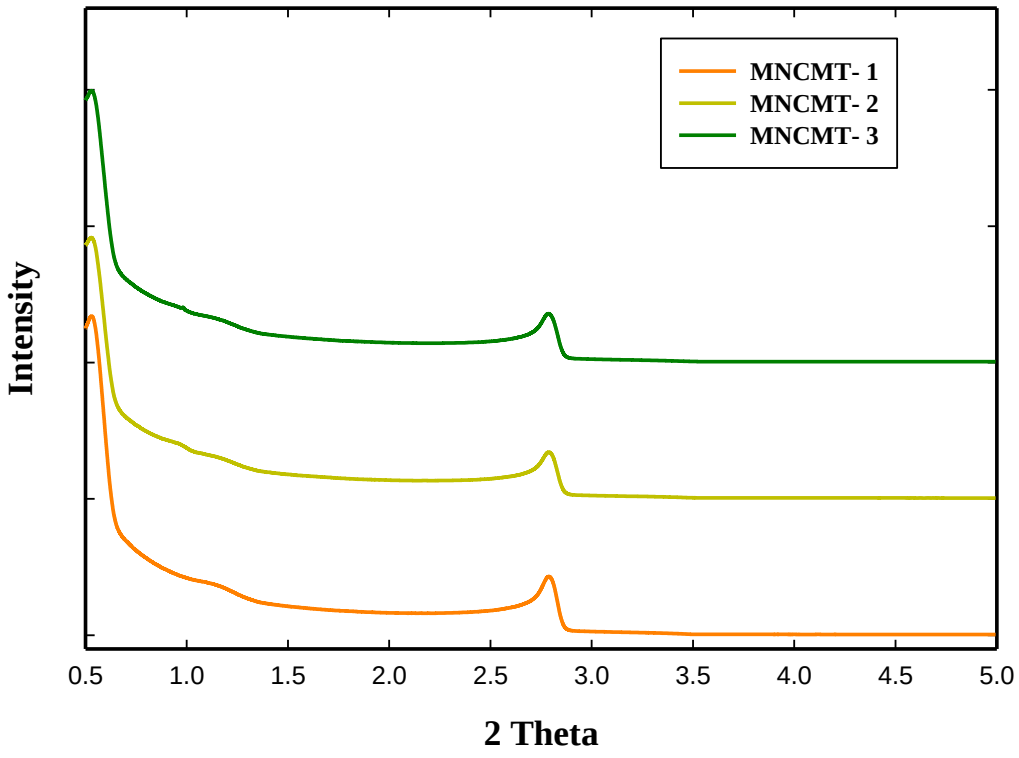

Figure 4.24: XRD analysis of MNCMTs

N_2 gas isotherms of MNCM, MNCMT-1, -2 and -3 are shown in figure. 4.25 (A). Adsorption isotherms of MNCM and MNCMT can be classified as type IV by IUPAC classification (Choma & Jaroniec, 2006). As expected, the surface area of MNCMT reduced largely after the impregnation of Tris. MNCM as synthesized had a large surface area of 576 m^2/g, while MNCMT-1, -2 and -3 had 72, 32 and 12 m^2/g of BET

surface area. However, MNCMT-1 still maintained a type IV hysteresis loop (figure 4.25 B).

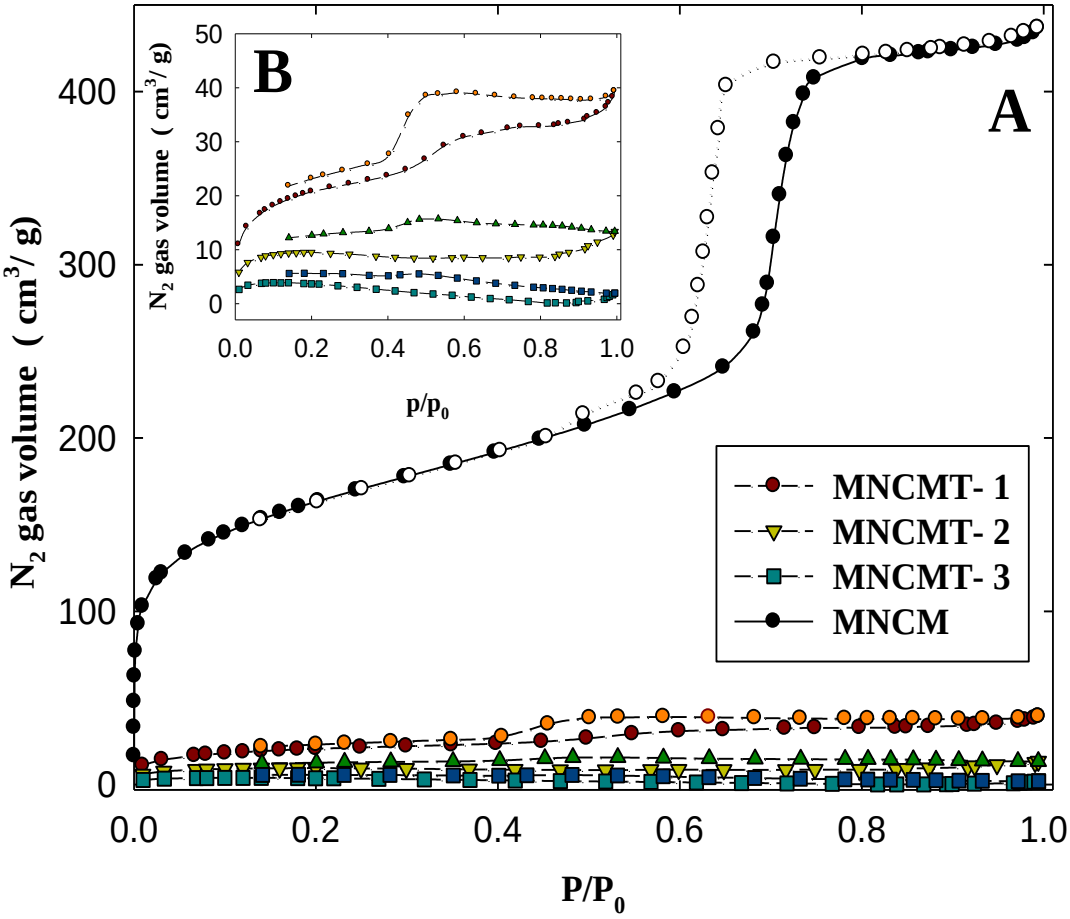

Figure 4.25: (A) BET surface area of MNCM and MNCMT-1, -2 and -3, (B) Enlarged expression of MNCMT-1, -2 and -3

Figure 4.26 shows the BJH pore size distribution of MNCM and MNCMTs after the impregnation of Tris. As a result, the pore size and volume of the materials sharply reduced after the impregnation of Tris. The primary pore width of MNCMT-1 was ~3 nm, which is less than the free-impregnated material MNCM (~5 nm). This shows that the pores may have been coated with Tris. However, once the amount of Tris is increased from 1 to 2 mmol, the pores were totally blocked, resulting in reduced pore size and volume (table 4.8)., The wall thickness of MNCMT is also reduced from 5 to

~3 nm (table 4.8). The reduction of wall thickness might be caused by the impregnation of Tris into the pores. Thus, during the impregnation process, the pores homogeneity was plausibly damaged. However, the wall thickness reduction was minimal < 2 nm, indicating that the MNCMT is still thermally stable.

From the XRD and N_2 gas isotherm data, Tris was successfully impregnated to clearly bind on both the surface and inside the pores of MNCM. Based on the physical characterization, MNCMT-1 can be considered as the best media compared to other Tris impregnated materials. In a comparable analogy, Zhao et.al have reported surface area and pore size reduction in the synthesis of amine modified SBA-15 (H. Zhao et al., 2007). The summary of physical characterization of MNCM and MNCMT is listed in table 4.8.

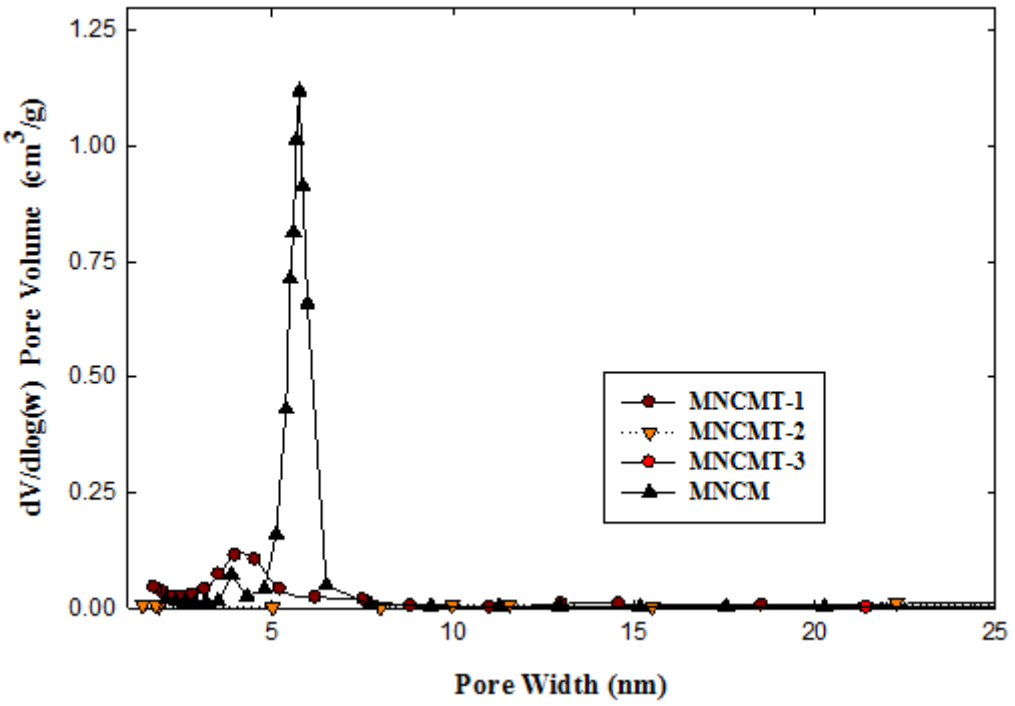

Figure 4.26: BJH pore size distribution of MNCM and MNCMT-1, -2 and -3

Table 4.8: Physical characteristics of MNCM, MNCMT-1,-2 and -3.

Materials	[b]Pore diameter (nm)	[d]BET surface area (m^2/g)	[e]Total pore volume (cm^3/g)	[a]*d* 100 (nm)	[c]Wall thickness (nm)	Ref.
MCM-41	2.54	1030	0.980	4.01	n/a	(Y.-H. Kim et al., 2011)
SBA-15	5.27	659	0.83	9.73	5.96	(Bui & Choi, 2009c)
MCM-41	4.80	1200	1.0	n/a	5.0	(Xiao et al., 2015)
MNCM	4.68	576	0.650	9.1	5.84	This work
MNCMT-1	4.19	75	0.061	6.65	3.49	This work
MNCMT-2	n/a	37.2	0.021	3.66	n/a	This work
MNCMT-3	n/a	15.8	0.003	3.67	n/a	This work

[a] the (100) interplanar spacing,[b] Calculated from the desorption of N_2 isotherm
[c] Determined from the difference between the unit cell parameter ($a_o = 2d_{100}/\sqrt{3}$) and the frame work pore size.
[d] BET surface area calculated from the adsorption of N_2 isotherm[e]V_t = total pore volume calculated using BJH

Surface charges of MNCM and MNCMT were measured using zeta potential analysis. Surface charge of MNCM was negative all the way from pH 1 to 12 (figure 4.27). After impregnation of Tris, the charge density shifted closer to zero potential. At pH 1 to 3, zeta potential of MNCMT was slightly positive due to the high concentration of H^+ ion coverage on the surface followed by formation of acidic amine functional groups such as $>NH_2^+$ and $-NH_3^+$. However, at pH 3 to 9 the surface charge was almost zero because of the neutrally charged functional group (>NH and $–NH_2$). However, at pH > 10 where the OH^- ions are electrostatically attracted to hydrogen of amine functional groups, the zeta potential becomes negative.

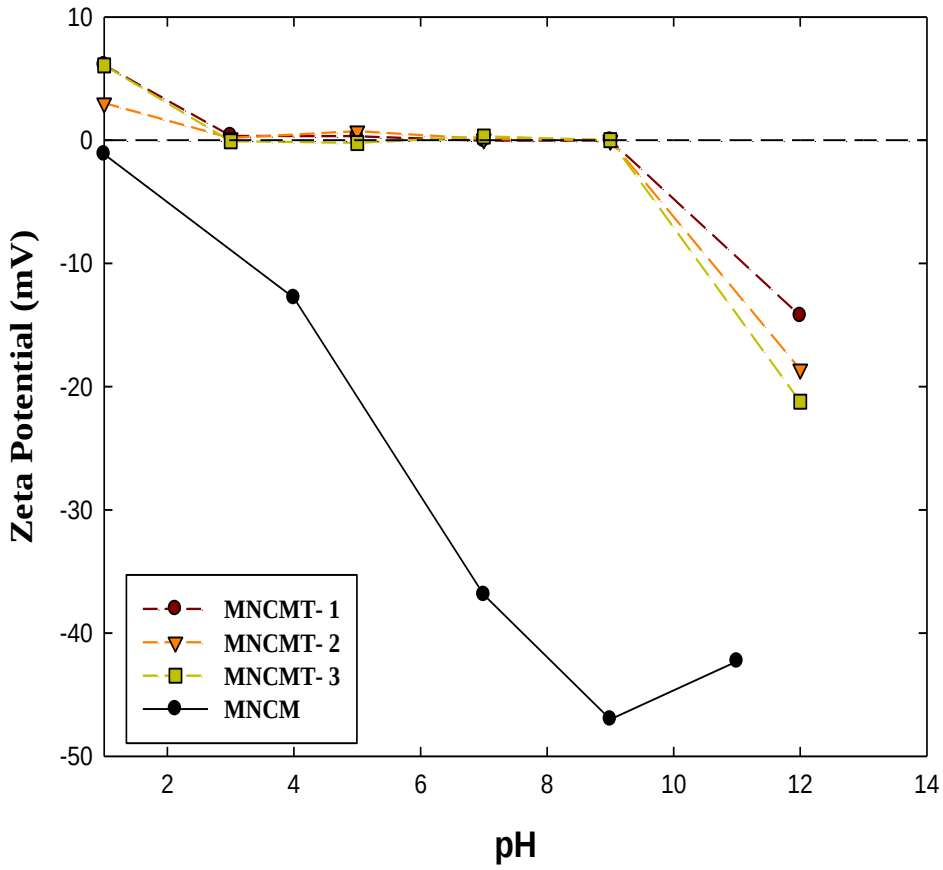

Figure 4.27: Zeta Potential analysis of MNCMT

4.8: Mechanism of synthesis of MNCMT

The mechanism of MNCMT synthesis (schematic 4.4) was proposed based on the characterization results (section 4.7). The synthesis of MNCMT was similar to the proposed mechanism by E. Borodine and N.H.N Kamaruddin et.al (Borodina et al., 2015; Kamarudin et al., 2013). The reaction was possible due to the interaction of silanol and three methoxygroups of Tris as described in schematic 4.4. Post synthesis of Tris into the MNCM reduced the number of free silanol groups; this can be proved by the disappearance of Si-OH bond at 963 cm^{-1} as shown in FTIR plot (figure. 4.28). The reduction in the intensity of Si−O−Si peaks at 790 cm^{-1}, 960 cm^{-1}, 1056 cm^{-1}, and formation of new amine group peak (>NH and $–NH_2$) at band 1651 cm^{-1} further supports this mechanism (H. Zhao et al., 2007).

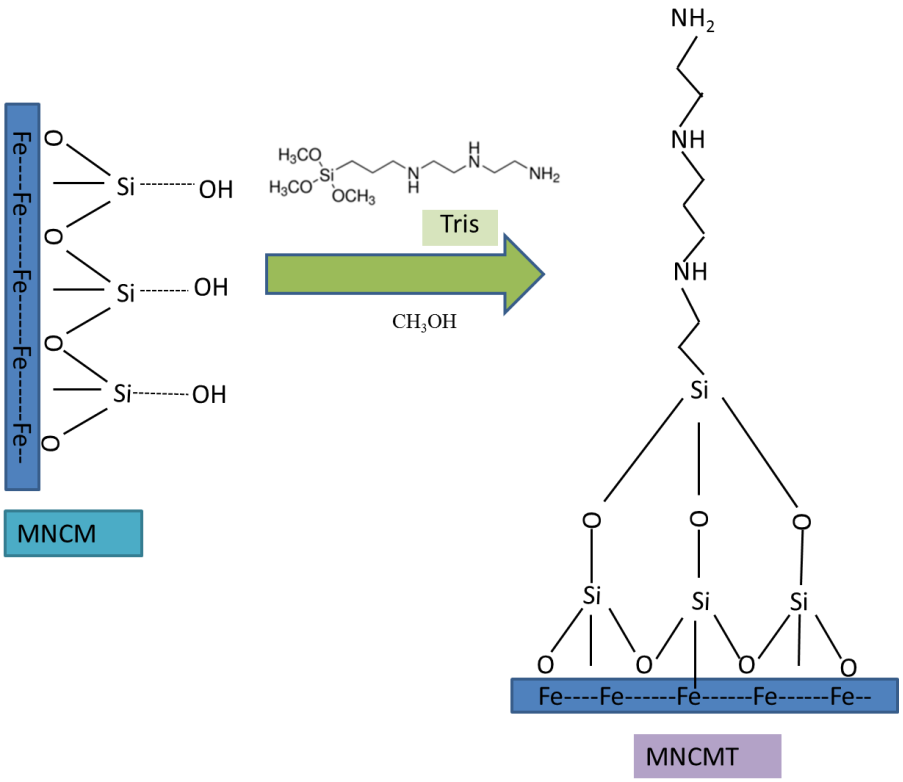

Schematic 4.4: Mechanism of synthesis of MNCMT

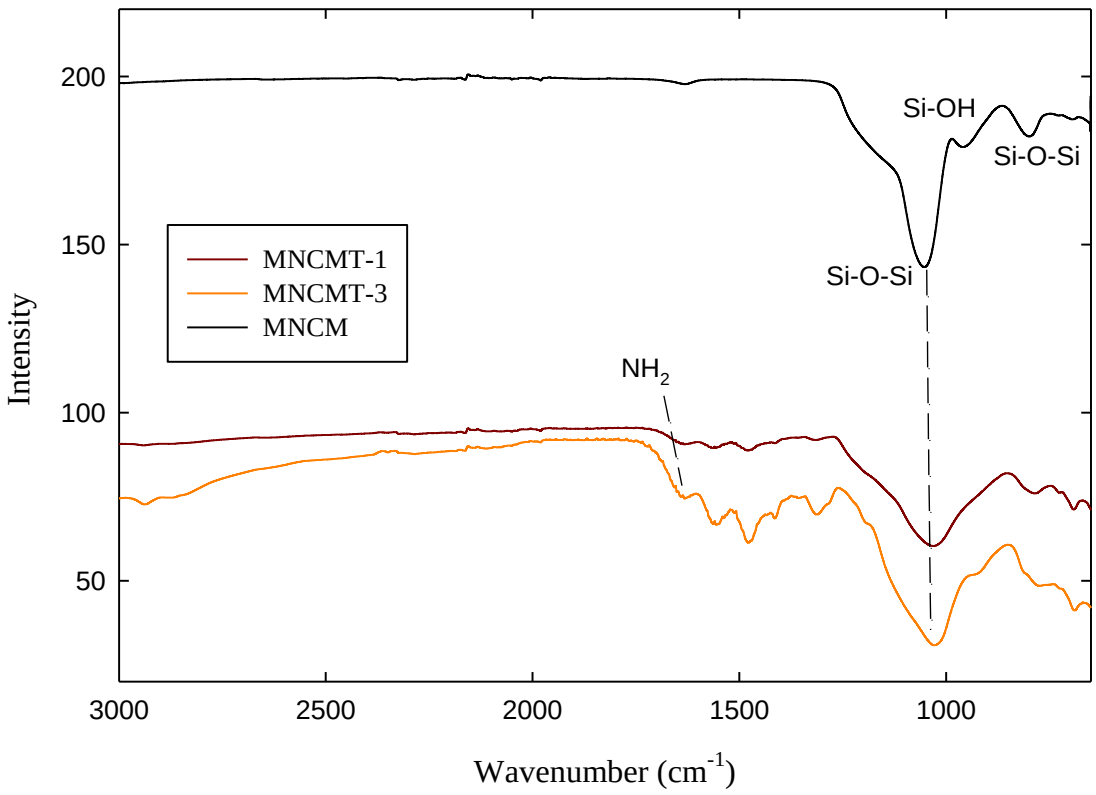

Figure 4.28: FTIR plots of MNCM and MNCMT

4.9 Removal of BPA by MNCMT

4. 9.1 Kinetics of BPA removal

The kinetics of BPA removal by MNCM, MNCMT-1, -2 and -3 were investigated (figure 4.29). MNCM presents smaller adsorption capacity for BPA compared to MNCMT-3, which displays the fastest and highest removal capacity then other materials. The equilibrium time required to reach plateau was around 300 min with adsorption capacity reaching up to 160 mg/g. The adsorption data was fitted with the pseudo 2nd order kinetic model with R^2 value of 0.991, signifying that the removal of BPA is a heterogeneous adsorption mechanism.

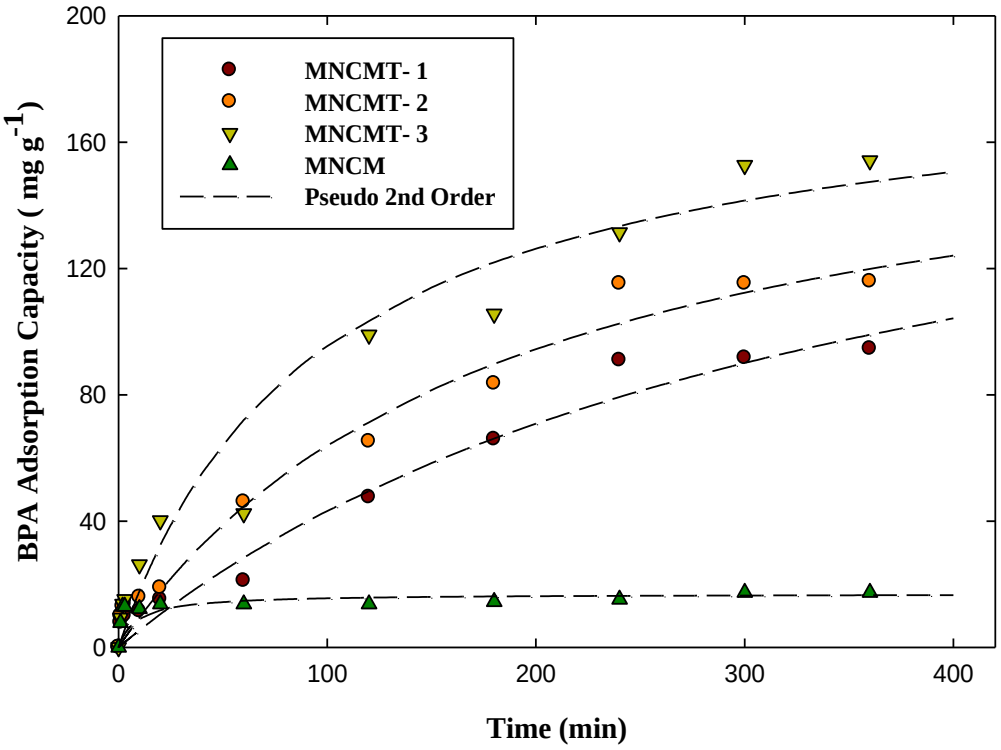

Figure 4.29: Time resolved uptake of BPA by MNCMT fitted with pseudo 2nd order kinetic line

MNCM's available surface area is 5.76×10^{20} nm^2 (576 m^2/g) and 1, 2 or 3 mmol Tris was coated into MNCM via an incipient wetness impregnation method so that all molecules of Tris are well incorporated to form MNCMTs. Based on the acid-base back titration method, Jung et al. presented that 1 molecule Tris can occupy 2.88 nm^2 of surface of nano-SiO_2 (H.-S. Jung, Moon, & Lee, 2012). This information was used to interpret that 1 molecule of Tris occupied 0.96 nm^2 surface area of MNCMT-1, deducing that the pore structure of MNCM was supersaturated with 1 mmol of Tris. Theoretically, the surface of MNCM can hold 0.3 mmol of Tris with a monolayer coating. Thus, pore blocking symptom might be well matched with the Tris coating condition. Since MNCMT-1 had a sorption capacity of 90 mg/g BPA, its sorption density for nitrogen was 0.13 mole BPA/mole N. The adsorption capacity of 160 mg/g BPA by MNCMT-3 was higher, but sorption density was 0.078 mole BPA/mole N. This

indicates that MNCMT-1 was much more efficient in removing BPA compared to other materials. All the kinetic parameters are listed in table 4.9.

4.9.2 Isotherm of BPA removal

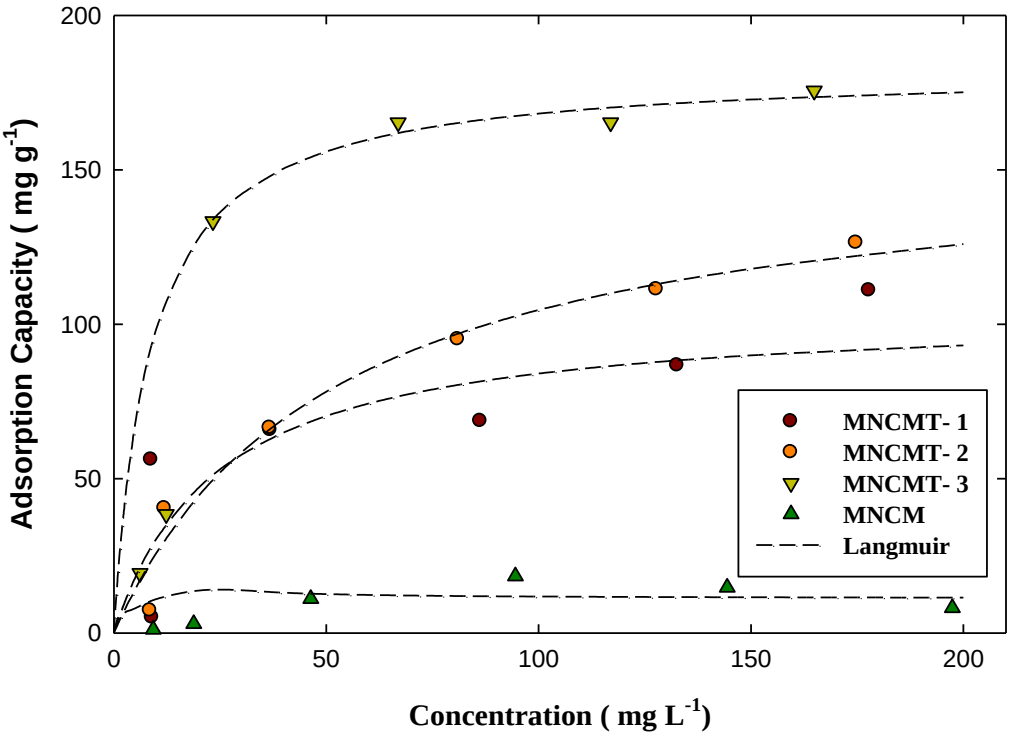

Figure 4.30: Isotherm analysis of BPA adsorption by MNCM-Tris fitted with Langmuir isotherm model.

The isotherm of BPA removal was carried out at the concentration ranging from 10 to 250 mg/L. MNCMT-3 had the highest adsorption capacity of 182 mg/g and the material was still magnetically active. The isotherm experimental data matched well with Langmuir isotherm model with R^2 value of 0.971 (Fig, 4.30). The removal capacity of MNCMT-3 from Langmuir isotherm model was 182 mg/g, listed in table 4.10. This value is higher than any reported value for many other silica based material such as SBA-15 and MCM-41 (Bhattarai, Muruganandham, & Suri, 2014; Y.-H. Kim et al., 2011; J. Yang et al., 2015). The pH effect on the BPA removal was also investigated (figure 4.31). The adsorption of BPA was highest at ~pH 6, but reduced at lower and higher pH levels.

MNCM as synthesized did not remove BPA effectively, but when MNCM was subsequently modified to MNCMT by introducing the amine group, the removal capacity of BPA increased. This infers that the BPA removal typically depends on the amine functional groups attached to MNCM, which is the sole removing source of BPA. The high adsorption capacity of BPA might be attributed to the increased hydrophobicity of MNCMT. As shown in zeta potential analysis in figure 4.27, the surface charge changed almost zero at pH 3 to 9. Zero surface charge indicates that the surface is hydrophobic, and hydrophobic BPA is more susceptible to be adsorbed by a hydrophobic adsorbate. However at pH > 9 or pH < 3, the surface charge of MNCMT become negative or positive, a hydrophilic condition and the BPA adsorption capacity reduced (figure. 4.31). The removal mechanism of BPA by MNCMT is discussed in the latter section of 4.11.4.

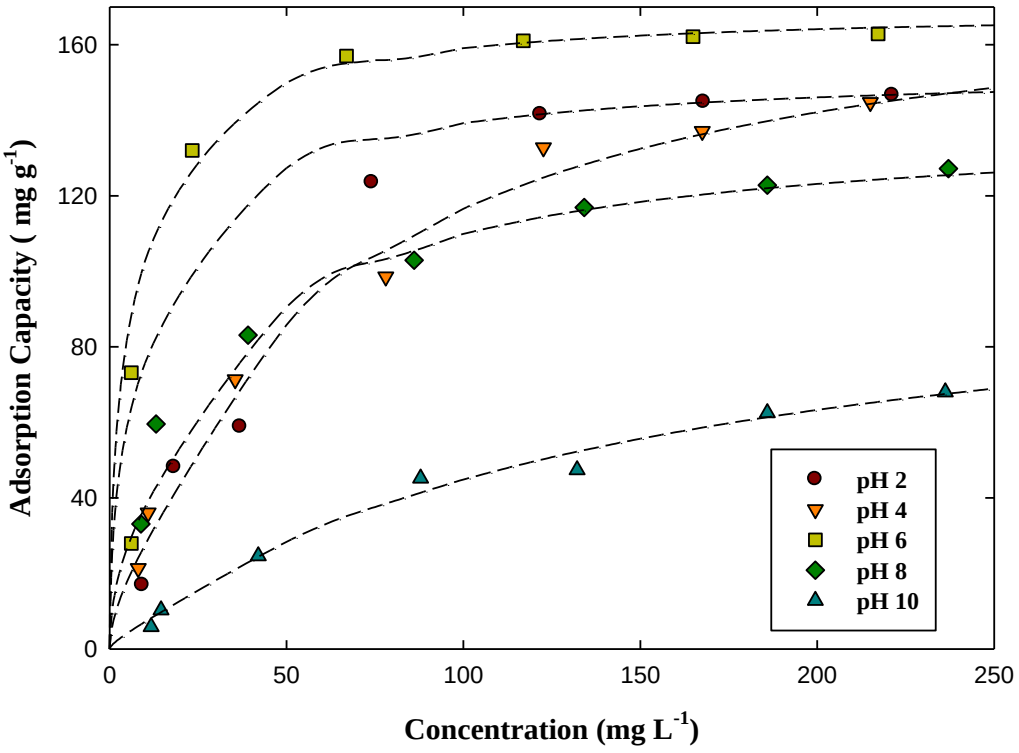

Figure 4.31: BPA adsorption pH effect of MNCMT

Table 4.9: Adsorption parameters determined from Pseudo 1st and 2nd Order kinetic model

Materials (pollutant)	Exp. q_{eq} (mg/g)	Pseudo 1st order		Pseudo 2nd order		
		K_1 (min^{-1})	R_2	K_2 (g/mg min)	q_e (mg/g)	R^2
MNCMT-3 (BPA)	154.12	6.58×10^{-3}	0.977	9.179×10^{-5}	169.86	0.892
MNCMT-1 (IBP)	184.10	9.11×10^{-1}	0.910	1.160×10^{-3}	195.99	0.991
MNCMT-1 (CFA)	78.40	7.59×10^{-3}	0.964	3.64×10^{-4}	83.88	0.985
MNCM (BPA)	92.4	5.8×10^{-3}	0.9725	1.28×10^{-4}	108.63	0.886
MNCM (IBP)	140.5	4.98×10^{-2}	0.925	4.84×10^{-3}	141.97	0.999
MNCM (CFA)	20.70	3.09×10^{-3}	0.8553	6.6×10^{-3}	16.92	0.988

q_{eq}- experimental adsorption at equilibrium time , K_1-Pseudo 1st order rate constant
q_e- calculated adsorption at equilibrium time, K_2-Pseudo 2nd order rate constant

4.10 Removal of IBP by MNCMT

4.10.1 Kinetic of IBP removal

Kinetic removal of IBP was investigated using MNCM, MNCMT-1, -2 and -3. MNCMT-1 shows the fastest and highest removal affinity for IBP (figure. 4.32). With an equilibrium time of ~ 40 min, adsorption capacity reached almost 190 mg/g. The adsorption data fitted the kinetic pseudo 2^{nd} order model with R^2 value of 0.991. Removal efficiency of MNCMT can be compared using the same theoretical calculation discussed in the BPA removal section.

MNCMT-1 has 3 molecules of nitrogen as the sorption site and its sorption capacity (180 mg/g) was higher than MNCMT-2 and MNCMT-3. The calculated sorption density of MNCMT-1 was 0.30 mole of IBP/mole N, which value is much higher than 0.15 or 0.06 mole of IBP/mole N for MNCMT-2 or -3, respectively. The adsorption capacity estimated using kinetic model was 195.6 mg/g, which was close to an isotherm value (184.10 mg/g) (table 4.9).

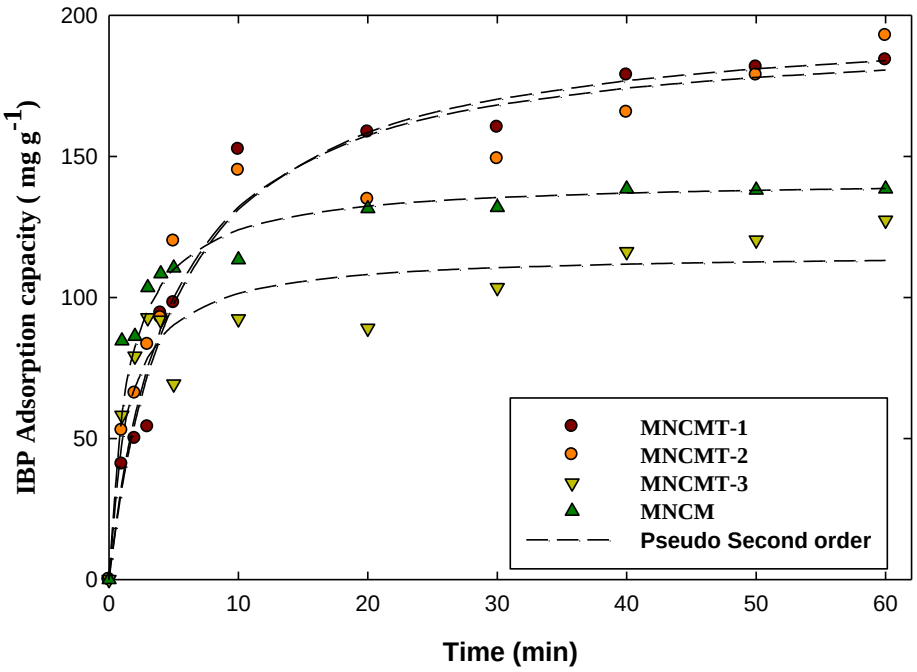

Figure 4.32: Kinetic analysis of IBP adsorption by MNCMTs fitted with Pseudo 2nd order

4. 10.2 Isotherm of IBP removal

The isotherm of IBP removal data matched well with Freundlich isotherm model with a R^2 value of 0.96. Adsorption capacities of MNCMT-1 and -2 were around 300 mg/g. The fitting of Freundlich isotherm indicates that IBP adsorption was a multi-layer adsorption process, unlike to Langmuir single layer adsorption of BPA. In comparison of removal efficiency between the synthesised materials, MNCMT-1 was much more efficient in removing IBP followed by MNCM-2 and -3, and the adsorption capacity (64.5 mg/g) for MNCM was lower than MNCMT-1 or -2.

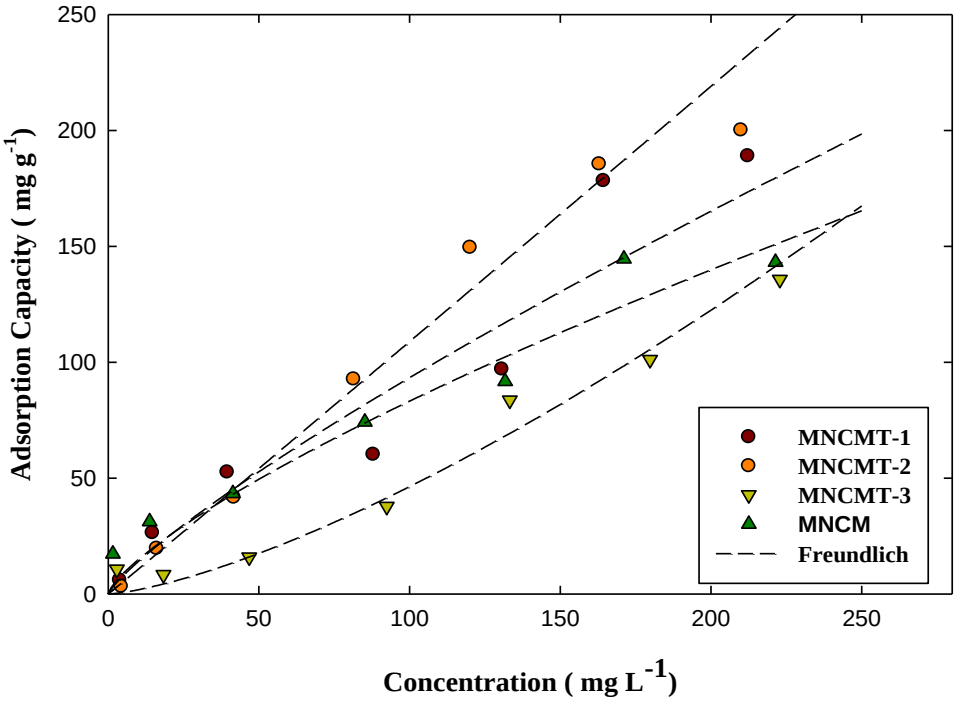

Figure 4.33: Isotherm analysis of IBP adsorption by MNCMT fitted with Freundlich isotherm model

The pH effect of the removal was also investigated and plotted in figure. 4.34. The results showed that adsorption of IBP was highest at the neutral condition ~pH 6, but reduced at lower or higher pH, which was a similar behaviour with BPA removal. Maximum adsorption capacity of MNCMT-1was 200 mg/g, which is compatible to commercially available adsorbents (Essandoh, Kunwar, Pittman, Mohan, & Mlsna, 2015).

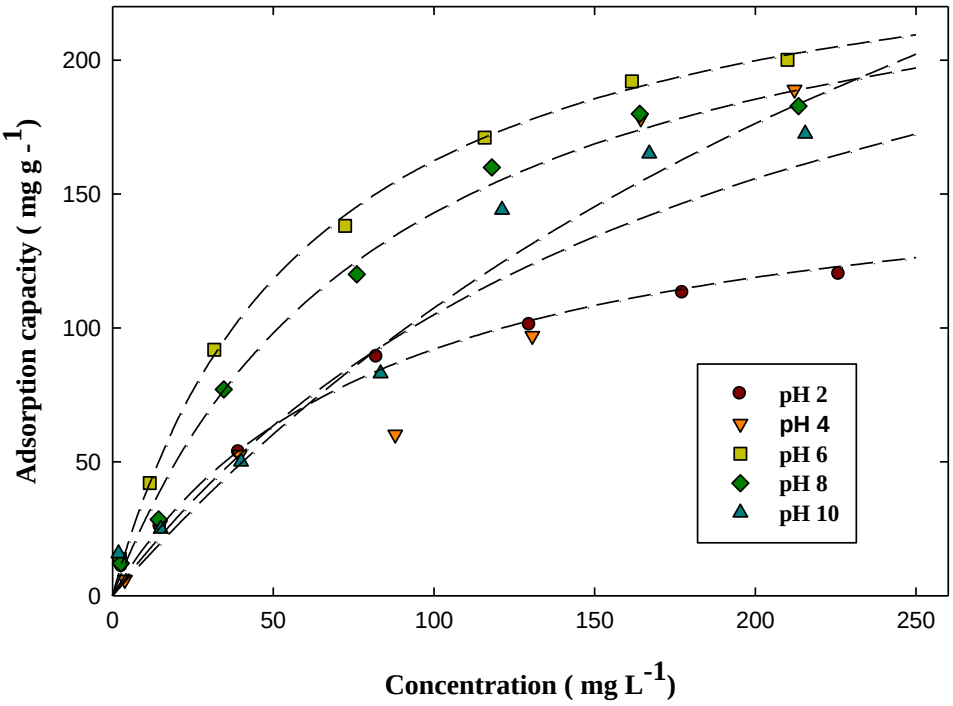

Figure 4.34: IBP adsorption pH effect of MNCMT

4.11 Removal of CFA by MNCMT

4.11.1 Kinetics of CFA removal

The removal of CFA was investigated using MNCM, MNCMT-1, -2 and -3 at different time intervals. MNCMT-1 showed the fastest and highest removal capacity for CFA, while MNCM showed a very low adsorption (<10 mg/g). As shown in figure. 4.35, the equilibrium reached at 200 min with an adsorption capacity of ~ 80 mg/g. The adsorption data fitted the pseudo 2^{nd} order model with a R^2 value of 0.985 and calculated adsorption capacity was 85.8 mg/g. The calculated sorption density revealed that MNCM-1 was more efficient in removing CFA with 0.13 mol CFA/mol N, compared to MNCMT-2 and -3 with 0.048 and 0.026 mol CFA/mol N of, respectively. The kinetic comparison data and experimental values were compared and listed in table 4.9.

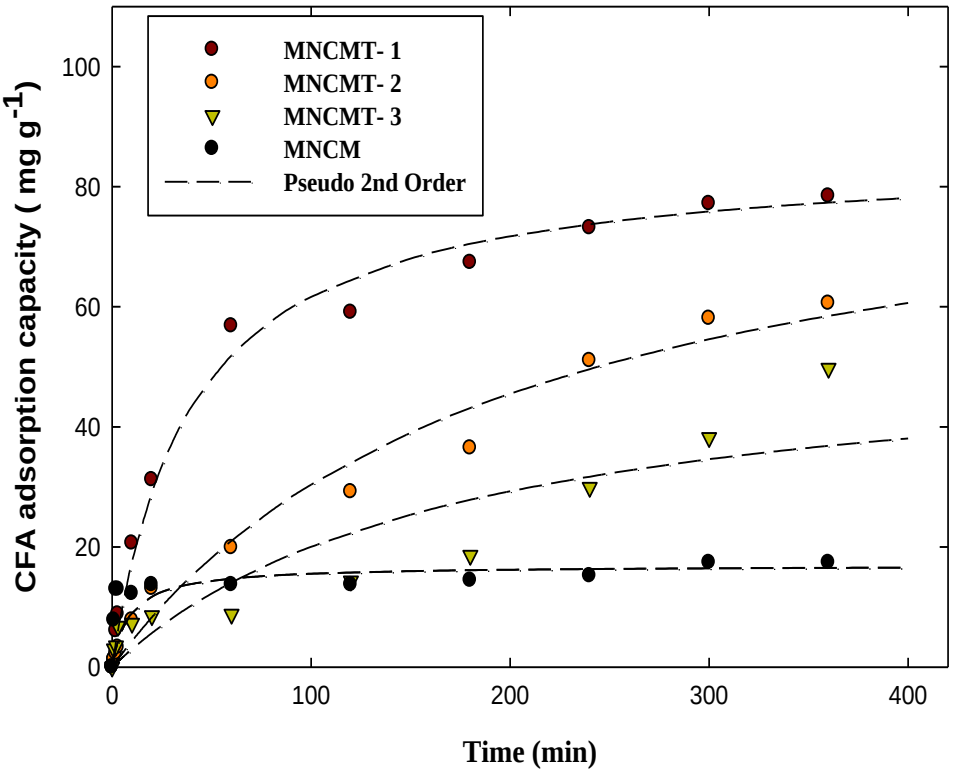

Figure 4.35: Kinetic analysis of CFA adsorption by MNCMTs fitted with Pseudo 2nd order

4.11.2 Isotherm of CFA removal

Isotherm removal of CFA was performed at various concentrations and the Langmuir isotherm model matched the experimental data with R^2 value of 0.958. MNCMT-1 showed the highest adsorption capacity (84.2 mg/g), while MNCM had the lowest adsorption capacity (44.5 mg/g). The experimental adsorption data of MNCMT-1 was close to the calculated value of 87.4 mg/g using Langmuir isotherm model. In a more acidic or basic condition, the adsorption of CFA reduced as shown in figure 4.37. Isotherm parameters for BPA, CFA and IBP adsorptions are summarised and listed in table 4.10.

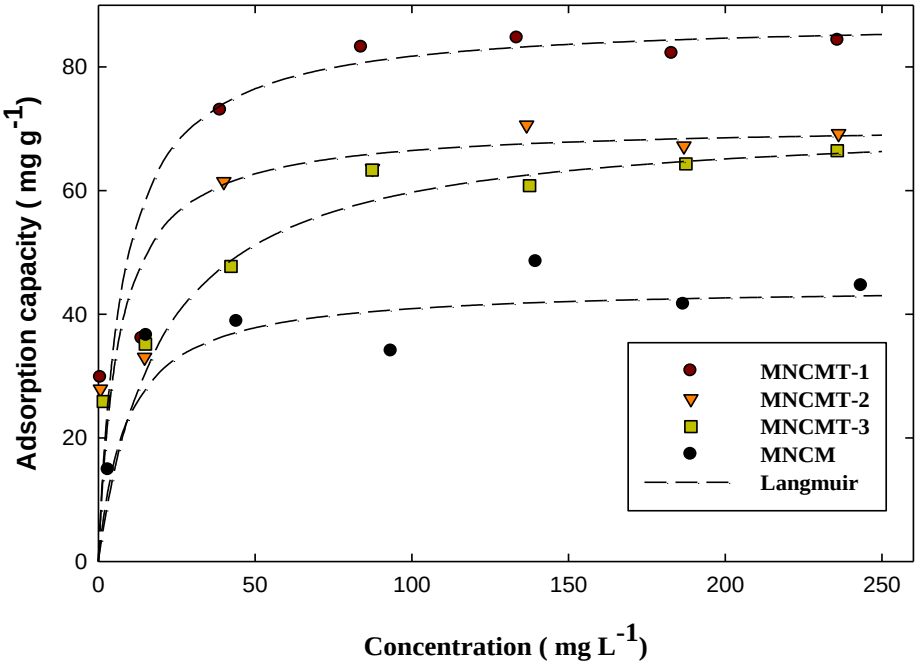

Figure 4.36: Isotherm analysis of CFA adsorption by MNCMT fitted with Langmuir isotherm model.

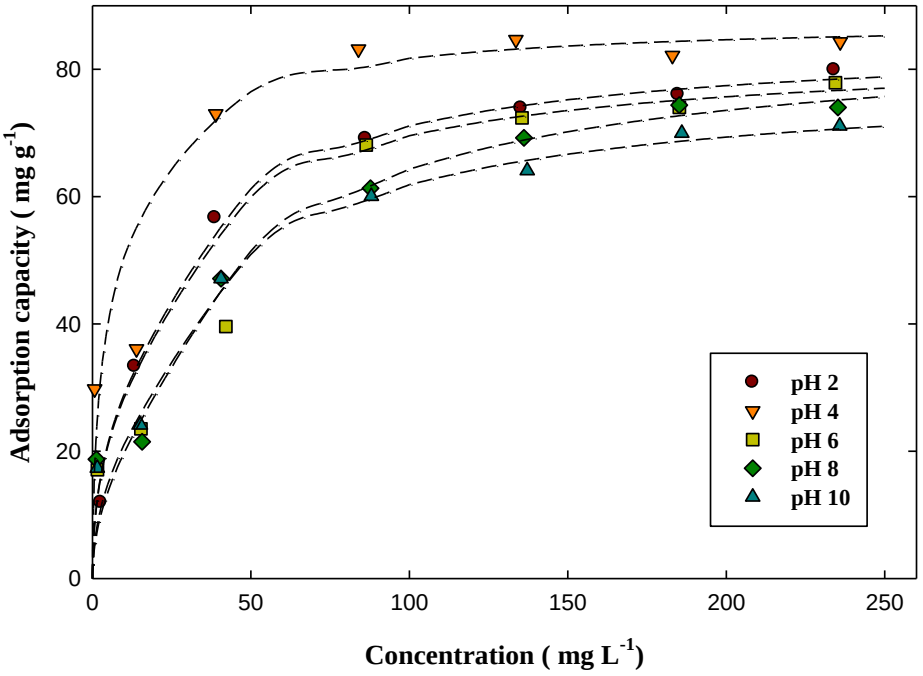

Figure 4.37: CFA adsorption pH effect of MNCMT

Table 4.10: Adsorption parameters determined from Langmuir and Freundlich isotherm model.

Sample	Langmuir equation			Freundlich Equation			Ref.
	K_L (L mg^{-1})	q_m (mg g^{-1})	R^2	^aK_F	1/n	R^2	
MNCMT-3 (BPA)	0.004	182.00	0.97	88.81	7.41	0.91	This work
MNCMT-1 (IBP)	0.005	301.82	0.99	2.10	1.24	0.83	This work
MNCMT-1 (CFA)	0.048	87.79	0.96	21.24	3.64	0.69	This work

4.11.3 The pH effect of adsorption

Figure 4.38 displayed the change in adsorption capacity at equilibrium (q_e) for adsorption of BPA, IBP and CFA. The increase in pH values caused significant changes in adsorption capacity of BPA and IBP. The adsorption capacity of BPA and IBP was highest at pH 6 and reduced drastically at higher pH passing the pK_a value of 9.8 and 4.5, respectively. The hydrophobic condition of MNCMT from pH 3 to 9 favoured the adsorption of both BPA and IBP.

Conversely, the CFA adsorption was not affected much by the change of pH with slightly higher at pH 4. The adsorption capacity of CFA reduced slightly at hydrophilic condition at pH < 3 and pH > 9. This phenomenon showed that the adsorption of BPA, IBP and CFA was not significantly affected by the pK_a value, but rather the surface charge and hydrophobicity of MNCMT.

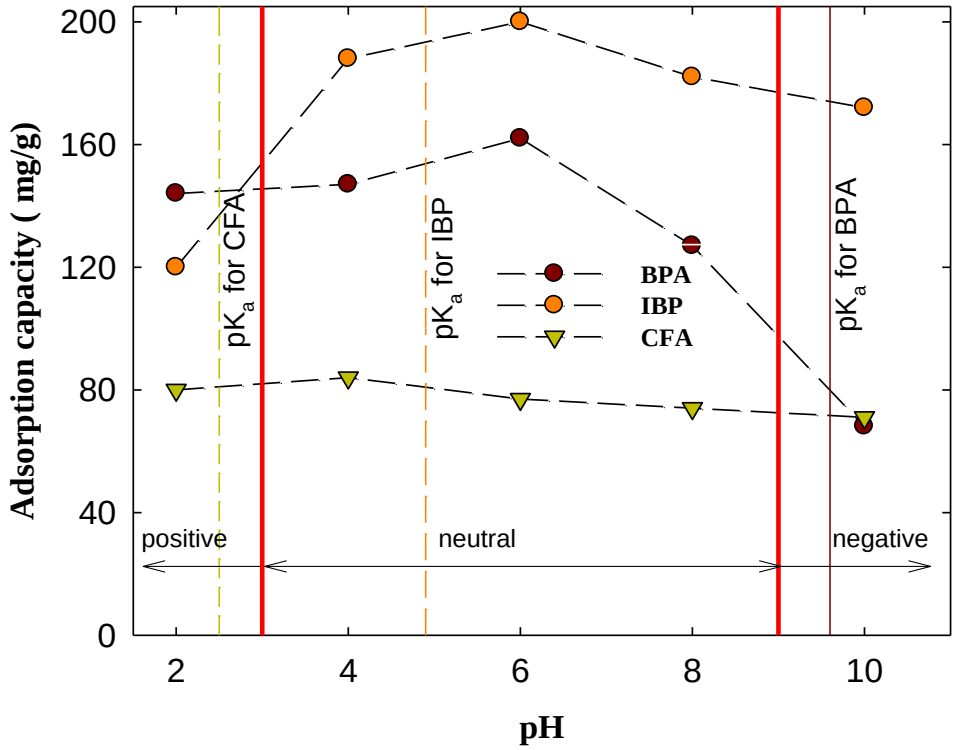

Figure 4.38: pH effects on adsorption capacities of BPA, IBP and CFA

4.11.4 The removal mechanism of BPA, IBP and CFA

In the aqueous solution at pH <3, MNCMT was likely to form protonated (NH_3^+) molecule as shown in schematic 4.5, but at pH 3 to 9 the molecule had a zero surface charge, a hydrophobic condition. At pH above 9, the surface became negatively charged due to the presence of OH^-. This molecular formation was inferred based on the surface charge results obtained from the zeta potential analysis (figure 4.27) and FTIR results (figure 4.28).

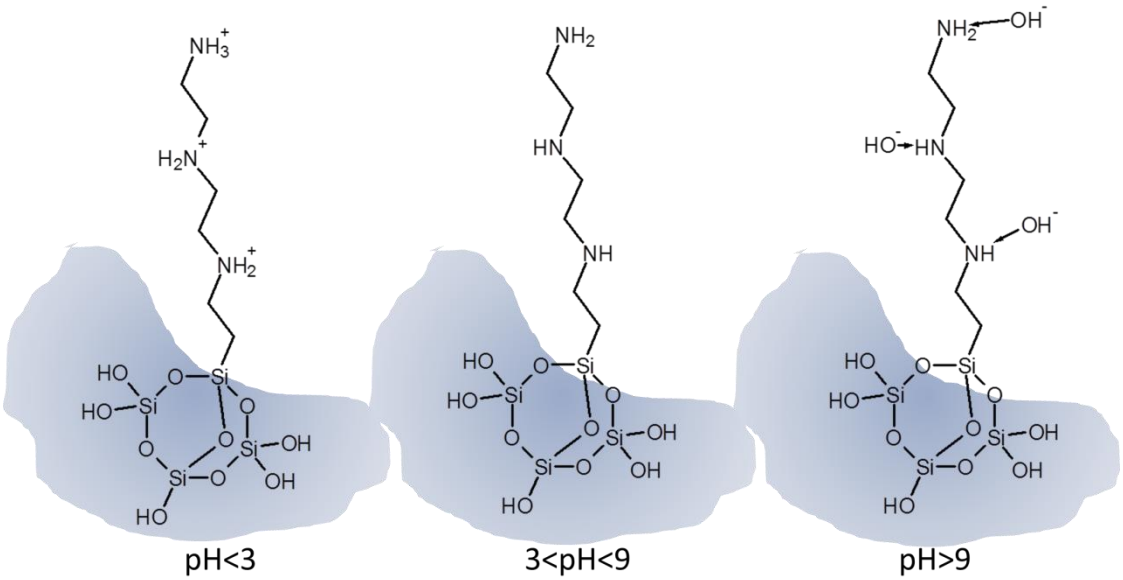

Schematic 4.5: MNCMT surface charge density at different pH

In earlier study, it was reported that hydrophobic and hydrophilic molecules worked independently for the adsorption of organic compounds onto alkyl-modified MCM-41 (Y.-H. Kim et al., 2011). The hydrophilic and hydrophobic groups of adsorbate interacted with hydroxyl groups and organic moieties on the pore surface of organic–inorganic silica, respectively (Inumaru, Inoue, Kakii, Nakano, & Yamanaka, 2003, 2004; Inumaru, Nakano, & Yamanaka, 2006).

The phenolic compounds, BPA and IBP both have hydrophilic hydroxyl and hydrophobic phenolic molecules. Though BPA has hydrophilic hydroxyl molecule, the removal of BPA being highest at pH 6, does suggest that the state is reflective of a hydrophobic condition. In the case of IBP adsorption, MNCMT adsorption of IBP was much higher than MNCM. This observation may be related to the formation of strong bond between hydrophobic group of BPA/IBP and amine group of MNCMT (X. Li et al., 2015).

A detailed physicochemical analysis of MNCMT adsorption of EDCs and comparison with similar studies have postulated that π–hydrogen bonds could be the dominant bond between BPA and MNCMT (schematic 4.6) (Bui et al., 2011; C. Jung et al., 2013). The removal mechanism of IBP by MNCMT was similar to the removal mechanism of BPA (Schematic diagram 4.6), but when more amounts of Tris were added to MNCMT, the surface area and pore volume decreased and resulted in the reduction of IBP adsorption capacity for MNCMT-2 and -3.

In the case of MNCMs, though MNCMs are more hydrophilic, the adsorption capacity for BPA/ IBP was lower, which was contrary to the finding of MNCMT adsorption. This finding could be due to the formation of hydrogen bond between MNCM and EDCs, which is considered relatively weak compared to the π–hydrogen bond and therefore the interaction between adsorbate and adsorbent may not be strong as encountered from π–hydrogen bond (Hasan & Jhung, 2015; Y.-H. Kim et al., 2011).

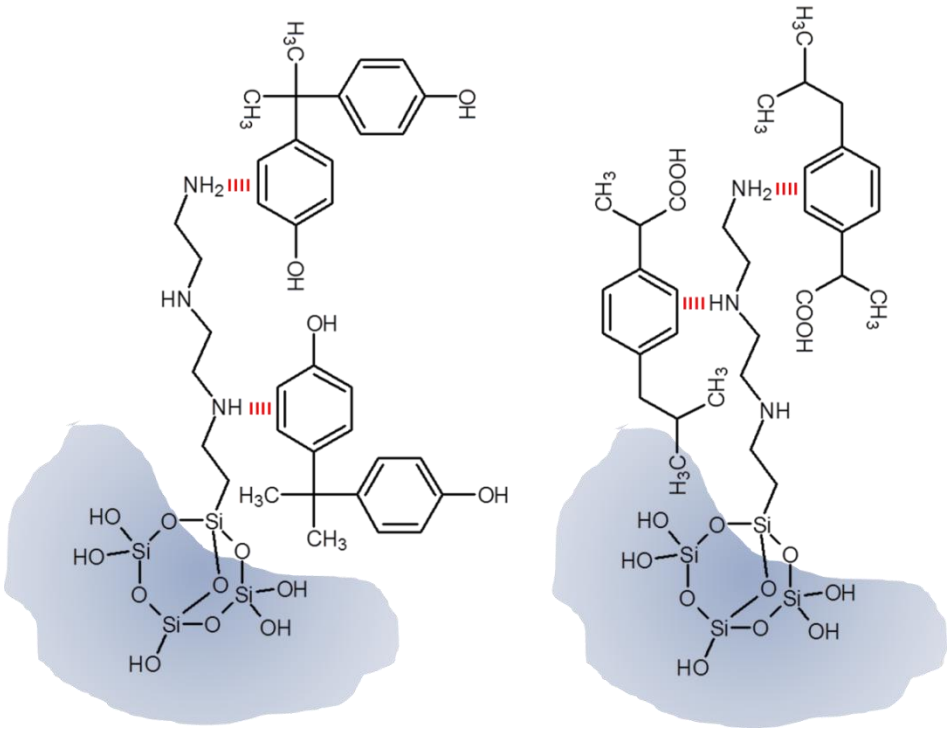

Schematic 4.6: Mechanism of BPA and IBP removals by MNCMT**.**

Based on previous studies, there are three different potential mechanisms that can be proposed for the adsorption of CFA (Suriyanon et al., 2015). First is the electrostatic interaction between negatively charged CFA molecule and positively charged surface of MNCMT; second is the hydrogen bonding interaction between hydroxyl group of CFA and amine group of MNCMT; and lastly, the hydrophobic interaction with π–hydrogen bonding between the phenolic group and amine group of MNCMT. The electrostatic interaction is not possible since the surface charge of MNCMT was varied and the pH > or < pK_a, did not affect the adsorption capacity of CFA. Although hydrogen bonding between $–O^-$ and hydrogen may be possible, it might be very unlikely due to the weak bond strength. In this case, the π–hydrogen bonding is more prominent because the surface of MNCMT was mostly in hydrophobic condition and as such, it may interact with the phenolic molecules in CFA. This interaction caused the formation of a strong π–hydrogen bonding between the adsorbate and adsorbent.

5. CONCLUSION

5.1 General conclusions

In this work, three types of mesoporous silica materials: MSM, MNCM and MNCMT were successfully synthesised using an economical and non-toxic silica precursor material, SiO_2 replacing TEOS. This research addressed the synthesis of MSM, a versatile, well-ordered and homogenous mesostructured material with large surface area and pore volume using a simple and direct method. The obtained MSM was further modified to produce magnetised materials MNCM and MNCMT, which have enhanced adsorption capacity and separation property. This study imply that not only in terms of physical and chemical properties, but also in economic value wise, the newly developed mesoporous materials have increased potential applications in the field of water treatment and biomedical engineering.

5.2 The key findings:

a) Adsorption isotherms and kinetics revealed that MSMs have relatively higher adsorption capacities and adsorption rates than other comparable silica-based media for IBP removal. The adsorption of IBP by MSM-500 was thermodynamically favourable at room temperature, but it involved relatively weak bonding because the calculated entropy was much smaller than other references. In consecutive sorption studies, MSM-500 showed 83–87% recovery efficiencies, although it had a slower pattern of uptake. Based on the FTIR results, the reaction mechanism was identified as a hydrophilic interaction between the COO^- of IBP and Si–OH of the pore surface. MSM-500 was also found suitable for IBP drug loading and unloading purposes, with a 41% loading capacity and almost 100 % unloading efficiency within a few hours. Moreover,

the production cost of MSM was low when compared to SBA-15, indicating that the synthesis route developed in this study could have high potential for cost-effective mass production. Hence, the MSM could be a suitable medium for industrial applications (for water treatment and drug delivery), as shown in the cost analysis study. Furthermore, the use of inert precursor SiO_2 is expected to produce non-toxic MSMs, which are more suitable for water treatment and biomedical application.

b) A magnetically separable MNCM was produced via a new synthetic route using silica and nano-magnetite substance. Among the media synthesized, MNCM-1 prepared with a molecular weight ratio of Fe_3O_4 to SiO_2 (0.14:1) had the highest specific surface area (576 m^2/g) and pore volume (0.65 cm^3/g). The mechanism of MNCM-1 formation was examined using XRD, N_2 gas isotherm, TEM, FESEM, and FTIR. Based on the physicochemical characterization and adsorption tests, it can be inferred that MNCM-1 has magnetic properties and structural strength, as well as higher and faster adsorptive capacity to remove MB than other mesoporous materials. The economic assessment indicated that the treatment costs for MB-containing water using MNCM-1 are much lower than other mesoporous materials, which is an encouraging finding as it effectively addresses the economically aspect of MNCM-1 production on a large scale. The MNCM-1 can be reused and regenerated without any defects after being easily separated using a magnet, which is an added advantage as it could have significant effects on the adsorption based treatment.

c) To further improve the removal process of EDCs, MNCMT was synthesized with different amounts of Tris impregnated into MNCM. Among the synthesis material, MNCMT-1 showed the best physicochemical properties. The obtained

MNCMT was able to remove the three EDCs BPA, IBP and CFA. The removal capacity for these three EDC's was higher than most of the earlier reported silica based material. The main removal mechanism of MNCMT was found to be π–hydrogen bonding for all the three EDCs.

5.3 Future Recommendations

The current research has contributed to an increased knowledge on the synthesis aspect of mesoporous silica-based materials. Despite the detailed research undertaken, there are certainly some areas that would require further investigation. They include:

- MSM, MNCM and MNCMT have great potentials to be produced in bulk and commercialized in the field of water treatment or drug loading and unloading. However, the application of these materials for real waste water treatment purposes needs to be further investigated using real waste water originated from pharmaceutical or municipal wastes. The behaviour of EDCs in real condition might be different due to the interaction within different species or presence of other species such as ions, and natural organic matters (NOMs). It is therefore suggested to perform a pilot-scale testing system using a reactor equipped with magnetic separator and pump, which will enable continues treatment system.

- To ascertain the cost involved for a large scale treatment and discover whether the process is cost effective, it is proposed that a detailed cost analysis including energy efficiency, material and production overheads be conducted.

- The study found that there is limited information on clinical aspects for drug loading and biomedical applications, thus recommends such studies should be initiated.

6. REFERENCES

Al-Khateeb, L. A., Obaid, A. Y., Asiri, N. A., & Salam, M. A. (2014). Adsorption behavior of estrogenic compounds on carbon nanotubes from aqueous solutions: Kinetic and thermodynamic studies. *J. Indus. Eng. Chem., 20*, 916-924.

Alyoshina, N. A., & Parfenyuk, E. V. (2013). Functionalized mesoporous silica materials for molsidomine adsorption: Thermodynamic study. *J. Solid State Chem., 205*, 211-216.

Anbia, Mansoor, & Hariri, Saba Asl. (2010). Removal of methylene blue from aqueous solution using nanoporous SBA-3. *Desalination, 261*(1), 61-66.

Andersson, Jenny, Rosenholm, Jessica, Areva, Sami, & Lindén, Mika. (2004). Influences of material characteristics on ibuprofen drug loading and release profiles from ordered micro-and mesoporous silica matrices. *Chem.Mater., 16*(21), 4160-4167.

Azaïs, Thierry, Tourné-Péteilh, Corine, Aussenac, Fabien, Baccile, Niki, Coelho, Cristina, Devoisselle, Jean-Marie, & Babonneau, Florence. (2006). Solid-state NMR study of ibuprofen confined in MCM-41 material. *Chem. Mater, 18*(26), 6382-6390.

Babonneau, Florence, Camus, Lydie, Steunou, Nathalie, Ramila, Ainhoa, & Vallet-Regi, Maria. (2003). *Encapsulation of ibuprofen in mesoporous silica: solid state NMR characterization.* Paper presented at the MRS Proceedings.

Borodina, E, Karpov, SI, Selemenev, VF, Schwieger, W, Maracke, S, Fröba, M, & Rößner, F. (2015). Surface and texture properties of mesoporous silica materials modified by silicon-organic compounds containing quaternary amino groups for their application in base-catalyzed reactions. *Microporous Mesoporous Mater, 203*, 224-231.

Briceño, S., Brämer-Escamilla, W., Silva, P., García, J., Del Castillo, H., Villarroel, M., Diaz, Y. (2014). $NiFe_2O_4$/activated carbon nanocomposite as magnetic material from petcoke. *J. Magn. Magn. Mater., 360*, 67-72.

Bui, Tung Xuan, & Choi, Heechul. (2009a). Adsorptive removal of selected pharmaceuticals by mesoporous silica SBA-15. *J.Hazard. Mater., 168*(2), 602-608.

Bui, Tung Xuan, Kang, Seo-Young, Lee, Sang-Hyup, & Choi, Heechul. (2011). Organically functionalized mesoporous SBA-15 as sorbents for removal of selected pharmaceuticals from water. *J.Hazard Mater, 193*, 156-163.

Cabrera-Lafaurie, Wilman A, Román, Félix R, & Hernández-Maldonado, Arturo J. (2014). Removal of salicylic acid and carbamazepine from aqueous solution with Y-zeolites modified with extraframework transition metal and surfactant cations: Equilibrium and fixed-bed adsorption. *Journal of Environmental Chemical Engineering, 2*(2), 899-906.

Cho, Hyun-Hee, Huang, Haiou, & Schwab, Kellogg. (2011). Effects of Solution Chemistry on the Adsorption of Ibuprofen and Triclosan onto Carbon Nanotubes. *Langmuir, 27*(21), 12960-12967.

Cho, Hyun-Hee, Smith, Billy A, Wnuk, Joshua D, Fairbrother, D Howard, & Ball, William P. (2008). Influence of surface oxides on the adsorption of naphthalene onto multiwalled carbon nanotubes. *Environ.Sci.Technol, 42*(8), 2899-2905.

Choma, J, & Jaroniec, M. (2006). Characterization of nanoporous carbons by using gas adsorption isotherms. *Interface Sci, 7*, 107-158.

Ciesla, Ulrike, & Schüth, Ferdi. (1999). Ordered mesoporous materials. *Microporous Mesoporous Mater, 27*(2), 131-149.

Clara, M, Strenn, B, Gans, O, Martinez, E, Kreuzinger, N, & Kroiss, H. (2005). Removal of selected pharmaceuticals, fragrances and endocrine disrupting compounds in a membrane bioreactor and conventional wastewater treatment plants. *Water Res., 39*(19), 4797-4807.

Cleuvers, Michael. (2004). Mixture toxicity of the anti-inflammatory drugs diclofenac, ibuprofen, naproxen, and acetylsalicylic acid. *Ecotoxicology and Environmental Safety, 59*(3), 309-315.

Connors, Sarah. (2013). Removal of ibuprofen from drinking water using adsorption. In P. J. Bergendahl (Ed.), (pp. 98). Website: Worcester Polytechnic Institute.

Dinu, Maria Valentina, & Dragan, Ecaterina Stela. (2010). Evaluation of Cu 2+, Co 2+ and Ni 2+ ions removal from aqueous solution using a novel chitosan/clinoptilolite composite: kinetics and isotherms. *Chem Eng J, 160*(1), 157-163.

Doadrio, AL, Sousa, EMB, Doadrio, JC, Pérez Pariente, J, Izquierdo-Barba, I, & Vallet-Regı, M. (2004). Mesoporous SBA-15 HPLC evaluation for controlled gentamicin drug delivery. *J Control Release, 97*(1), 125-132.

Doke, Suresh M, & Yadav, Ganapati D. (2014). Novelties of combustion synthesized titania ultrafiltration membrane in efficient removal of methylene blue dye from aqueous effluent. *Chemosphere, 117*, 760-765.

Essandoh, Matthew, Kunwar, Bidhya, Pittman, Charles U, Mohan, Dinesh, & Mlsna, Todd. (2015). Sorptive removal of salicylic acid and ibuprofen from aqueous solutions using pine wood fast pyrolysis biochar. *Chem. Eng. J*

Fent, Karl, Weston, Anna A, & Caminada, Daniel. (2006). Ecotoxicology of human pharmaceuticals. *Aquatic toxicology, 76*(2), 122-159.

Foo, KY, & Hameed, BH. (2010). Insights into the modeling of adsorption isotherm systems. *Chem.Eng.J., 156*(1), 2-10.

Fu, Xucheng, Chen, Xing, Wang, Jin, & Liu, Jinhuai. (2011). Fabrication of carboxylic functionalized superparamagnetic mesoporous silica microspheres and their application for removal basic dye pollutants from water. *Microporous Mesoporous Mater, 139*(1), 8-15.

Goscianska, Joanna, Marciniak, Michał, & Pietrzak, Robert. (2014). Mesoporous carbons modified with lanthanum (III) chloride for methyl orange adsorption. *Chem Eng J, 247*, 258-264.

Hameed, BH, Tan, IAW, & Ahmad, AL. (2008). Optimization of basic dye removal by oil palm fibre-based activated carbon using response surface methodology. *J. Hazard .Mater, 158*(2), 324-332.

Hameed, BH, Tan, IAW, & Ahmad, AL. (2009). Preparation of oil palm empty fruit bunch-based activated carbon for removal of 2, 4, 6-trichlorophenol: Optimization using response surface methodology. *J.Hazard. Mater*

Hasan, Zubair, Choi, Eun-Jeong, & Jhung, Sung Hwa. (2013). Adsorption of naproxen and clofibric acid over a metal–organic framework MIL-101 functionalized with acidic and basic groups. *Chem.Eng.J, 219*, 537-544.

Hasan, Zubair, Jeon, Jaewoo, & Jhung, Sung Hwa. (2012). Adsorptive removal of naproxen and clofibric acid from water using metal-organic frameworks. *J. Hazard.Mater, 209*, 151-157.

Hasan, Zubair, & Jhung, Sung Hwa. (2015). Removal of hazardous organics from water using metal-organic frameworks (MOFs): plausible mechanisms for selective adsorptions. *J.Hazard.Mater, 283*, 329-339.

Ho, YS, & Wang, CC. (2004). Pseudo-isotherms for the sorption of cadmium ion onto tree fern. *Process Biochemistry, 39*(6), 761-765.

Ho, Yuh-Shan, & McKay, Gordon. (1999). Pseudo-second order model for sorption processes. *Process biochemistry, 34*(5), 451-465.

Hong, Jun Ming, Lin, Bing, Jiang, Jie Shan, Chen, Bor Yann, & Chang, Chang Tang. (2013). Synthesis of pore-expanded mesoporous materials using waste quartz sand and the adsorption effects of Methylene Blue. *J Ind Eng Chem*.

Huang, Chih-Hung, Chang, Kai-Ping, Ou, Hong-De, Chiang, Yu-Chun, & Wang, Chu-Fang. (2011). Adsorption of cationic dyes onto mesoporous silica. *Microporous Mesoporous Mater, 141*(1), 102-109.

Inumaru, Kei, Inoue, Yuta, Kakii, Shintaro, Nakano, Tomoyasu, & Yamanaka, Shoji. (2003). Organic-inorganic cooperative molecular recognition in nanostructure of alkyl-grafted MCM-41. *Chemistry Letters*, *32*(12), 1110-1111.

Inumaru, Kei, Inoue, Yuta, Kakii, Shintaro, Nakano, Tomoyasu, & Yamanaka, Shoji. (2004). Molecular selective adsorption of dilute alkylphenols and alkylanilines from water by alkyl-grafted MCM-41: tunability of the cooperative organic–inorganic function in the nanostructure. *Physical Chemistry Chemical Physics, 6*(12), 3133-3139.

Inumaru, Kei, Nakano, Tomoyasu, & Yamanaka, Shoji. (2006). Molecular selective adsorption of alkylphenols and alkylanilines from water by alkyl-grafted mesoporous alumina: A comparative study to alkyl-grafted mesoporous silica. *Microporous .Mesoporous .Mater, 95*(1), 279-285.

Islam, Md Azharul, Tan, IAW, Benhouria, A, Asif, M, & Hameed, BH. (2015). Mesoporous and adsorptive properties of palm date seed activated carbon prepared via sequential hydrothermal carbonization and sodium hydroxide activation. *Chem Eng J, 270*, 187-195.

Jaroniec, Mietek. (2002). Characterization of Nanoporous Materials *Access in Nanoporous Materials* (pp. 255-272): Springer.

Jermann, Doris, Pronk, Wouter, Boller, Markus, & Schäfer, Andrea I. (2009). The role of NOM fouling for the retention of estradiol and ibuprofen during ultrafiltration. *J.Membrane. Sci., 329*(1), 75-84.

Jones, Oliver AH, Green, Pat G, Voulvoulis, Nikolaos, & Lester, John N. (2007). Questioning the excessive use of advanced treatment to remove organic micropollutants from wastewater. *Environ.sci.Technol., 41*(14), 5085-5089.

Juang, Ruey-Shin, Wu, Feng-Chin, & Tseng, Ru-Ling. (2002). Characterization and use of activated carbons prepared from bagasses for liquid-phase adsorption. *Colloids and Surfaces A: Physicochemical and Engineering Aspects, 201*(1), 191-199.

Jung, Chanil, Park, Junyeong, Lim, Kwang Hun, Park, Sunkyu, Heo, Jiyong, Her, Namguk, . . . Yoon, Yeomin. (2013). Adsorption of selected endocrine disrupting compounds and pharmaceuticals on activated biochars. *J.Hazard.Mater, 263*, 702-710.

Jung, Hak-Sung, Moon, Doo-Sik, & Lee, Jin-Kyu. (2012). Quantitative analysis and efficient surface modification of silica nanoparticles. *Journal of nanomaterials, 2012*, 48.

Jurado, E, Fernandez-Serrano, M, Nunez-Olea, J, Luzon, G, & Lechuga, M. (2006). Simplified spectrophotometric method using methylene blue for determining anionic surfactants: Applications to the study of primary biodegradation in aerobic screening tests. *Chemosphere, 65*(2), 278-285.

Kadhum, Safaa A, Ishak, Mohd Yusoff, Zulkifli, Syaizwan Zahmir, & binti Hashim, Rohasliney. (2015). Evaluation of the status and distributions of heavy metal pollution in surface sediments of the Langat River Basin in Selangor Malaysia. *Marine pollution bulletin*.

Kamarudin, NHN, Jalil, AA, Triwahyono, S, Salleh, NFM, Karim, AH, Mukti, RR, Ahmad, A. (2013). Role of 3-aminopropyltriethoxysilane in the preparation of mesoporous silica nanoparticles for ibuprofen delivery: Effect on physicochemical properties. *Microporous.Mesoporous Mater, 180*, 235-241.

Katiyar, Amit, Yadav, Santosh, Smirniotis, Panagiotis G, & Pinto, Neville G. (2006). Synthesis of ordered large pore SBA-15 spherical particles for adsorption of biomolecules. *Journal of Chromatography A, 1122*(1), 13-20.

Kim, Byoung Chan, Lee, Jinwoo, Um, Wooyong, Kim, Jaeyun, Joo, Jin, Lee, Jin Hyung, . . . Lee, Hongshin. (2011). Magnetic mesoporous materials for removal of environmental wastes. *J Hazard Mater, 192*(3), 1140-1147.

Kim, Seong-Su, Pauly, Thomas R, & Pinnavaia, Thomas J. (2000). Non-ionic surfactant assembly of ordered, very large pore molecular sieve silicas from water soluble silicates. *Chem.Commun.*(17), 1661-1662.

Kim, Seong-Su, & Pinnavaia, Thomas J. (2001). A low cost route to hexagonal mesostructured carbon molecular sieves. *Chem.Commun.*(23), 2418-2419.

Kim, Yohan, Bae, Jiyeol, Park, Jihae, Suh, Jeongkwon, Lee, Sanghyup, Park, Hosik, & Choi, Heechul. (2014). Removal of 12 selected pharmaceuticals by granular mesoporous silica SBA-15 in aqueous phase. *Chem Eng J, 256*, 475-485.

Kim, Yong-Ho, Lee, Byunghwan, Choo, Kwang-Ho, & Choi, Sang-June. (2011). Selective adsorption of bisphenol A by organic–inorganic hybrid mesoporous silicas. *Microporous.Mesoporous .Mater, 138*(1), 184-190.

Kim, Yong-Ho, Lee, Byunghwan, Choo, Kwang-Ho, & Choi, Sang-June. (2014). Adsorption characteristics of phenolic and amino organic compounds on nano-structured silicas functionalized with phenyl groups. *Microporous .Mesoporous Mater, 185*, 121-129.

Kimura, Katsuki, Hara, Hiroe, & Watanabe, Yoshimasa. (2007). Elimination of selected acidic pharmaceuticals from municipal wastewater by an activated sludge system and membrane bioreactors. *Environ.Sci.Technol, 41*(10), 3708-3714.

Kittappa, Shanmuga, Cui, Mingcan, Ramalingam, Malarvili, Ibrahim, Shaliza, Khim, Jeehyeong, Yoon, Yeomin, . . . Jang, Min. (2015). Synthesis Mechanism and Thermal Optimization of an Economical Mesoporous Material Using Silica: Implications for the Effective Removal or Delivery of Ibuprofen. *PloS one, 10*(7), e0130253.

Kresge, CT, Leonowicz, ME, Roth, WJ, Vartuli, JC, & Beck, JS. (1992). Ordered mesoporous molecular sieves synthesized by a liquid-crystal template mechanism. *Nature, 359*(6397), 710-712.

Kruk, M, Jaroniec, M, & Sayari, A. (1997). Application of large pore MCM-41 molecular sieves to improve pore size analysis using nitrogen adsorption measurements. *Langmuir, 13*(23), 6267-6273.

Kuai, Sanke, & Nan, Zhaodong. (2014). Formation of sandwich structured ZnCe0. 03Fe1. 97O4@ nSiO2@ SBA-15 and adsorptive removal of methylene blue from aqueous solution. *Chem Eng J, 244*, 273-281.

Kuo, WS, & Ho, PH. (2001). Solar photocatalytic decolorization of methylene blue in water. *Chemosphere, 45*(1), 77-83.

Li, Gang, Lu, Yongtao, Lu, Cheng, Zhu, Mingshan, Zhai, Chunyang, Du, Yukou, & Yang, Ping. (2015). Efficient catalytic ozonation of bisphenol-A over reduced graphene oxide modified sea urchin-like α-MnO 2 architectures. *J.Hazard.Mater, 294*, 201-208.

Li, Xiaona, Chen, Shuo, Fan, Xinfei, Quan, Xie, Tan, Feng, Zhang, Yaobin, & Gao, Jinsuo. (2015). Adsorption of ciprofloxacin, bisphenol and 2-chlorophenol on electrospun carbon nanofibers: In comparison with powder activated carbon. *J.Colloid Interf.Sci, 447*, 120-127.

Lim, Myong H, & Stein, Andreas. (1999). Comparative studies of grafting and direct syntheses of inorganic-organic hybrid mesoporous materials. *Chem.Mater., 11*(11), 3285-3295.

Liu, Yu, & Liu, Ya-Juan. (2008). Biosorption isotherms, kinetics and thermodynamics. *Sep. Purif.Technol, 61*(3), 229-242.

Margolese, D, Melero, JA, Christiansen, SC, Chmelka, BF, & Stucky, GD. (2000). Direct syntheses of ordered SBA-15 mesoporous silica containing sulfonic acid groups. *Chem.Mater., 12*(8), 2448-2459.

McLachlan, John A, Simpson, Erica, & Martin, Melvenia. (2006). Endocrine disrupters and female reproductive health. *Best Practice & Research Clinical Endocrinology & Metabolism, 20*(1), 63-75.

Md Paudi Abdullah, Yang Farina, Wan Mohd Afiq Wan Mohd Khalid, Nurfaizah Abu Tahrim. (2015, March 2015). Banned Pesticides In The Waters of Cameron Highlands. *Chemistry In Malaysia*, 32-35.

Mestre, A. S., Pires, J., Nogueira, J. M. F., Parra, J. B., Carvalho, A. P., & Ania, C. O. (2009). Waste-derived activated carbons for removal of ibuprofen from solution: Role of surface chemistry and pore structure. *Bioresource Technol., 100*, 1720-1726.

Mestre, A. S., Pires, R. A., Aroso, I., Fernandes, E. M., Pinto, M. L., Reis, R. L., . . . Carvalho, A. P. (2014). Activated carbons prepared from industrial pre-treated cork: Sustainable adsorbents for pharmaceutical compounds removal. *Chem. Eng. J., 253*, 408-417.

Mestre, Ana S, Pires, João, Nogueira, José MF, Parra, Jose B, Carvalho, Ana P, & Ania, Conchi O. (2009). Waste-derived activated carbons for removal of ibuprofen from solution: role of surface chemistry and pore structure. *Bioresource Technol., 100*(5), 1720-1726.

Munoz, B, Ramila, A, Perez-Pariente, J, Diaz, I, & Vallet-Regi, M. (2003). MCM-41 organic modification as drug delivery rate regulator. *Chem.Mater., 15*(2), 500-503.

Nakashima, Hiroshi, Omae, Kazuyuki, Sakai, Tohru, Yamazaki, Kazuto, & Sakurai, Haruhiko. (1994). Acute and subchronic inhalation toxicity of tetraethoxysilane (TEOS) in mice. *Archives of toxicology, 68*(5), 277-283.

Organization, World Health. (2002). IPCS global assessment of the state-of-the-science of endocrine disruptors. *WHO/PCS/EDC/02.2*, 35-50.

Park, Jayhyun, Han, Yosep, & Kim, Hyunjung. (2012). Formation of Mesoporous Materials from Silica Dissolved in Various NaOH Concentrations: Effect of pH and Ionic Strength. *J.Nano Mat., 2012*, 10. doi: 10.1155/2012/528174

Regel-Rosocka, Magdalena, & Szymanowski, Jan. (2005). Direct Yellow and Methylene Blue liquid–liquid extraction with alkylene carbonates. *Chemosphere, 60*(8), 1151-1156.

Reijenga, J. C., Ingelse, B. A., & Everaerts, F. M. (1997). Thermodynamics of chiral selectivity in capillary electrophoresis: Separation of ibuprofen enantiomers with b-cyclodextrin. *J. Chromatogr., 792*, 371-378.

Sadecka, Jana, Čakrt, Miroslav, Hercegová, Andrea, Polonský, Jozef, & Skačáni, Ivan. (2001). Determination of ibuprofen and naproxen in tablets. *Journal of pharmaceutical and biomedical analysis, 25*(5), 881-891.

Salem, Ibrahim A, & El-Maazawi, Mohamed S. (2000). Kinetics and mechanism of color removal of methylene blue with hydrogen peroxide catalyzed by some supported alumina surfaces. *Chemosphere, 41*(8), 1173-1180.

Serrano, D, Lema, JM, & Omil, F. (2010). Influence of the employment of adsorption and coprecipitation agents for the removal of PPCPs in conventional activated sludge (CAS) systems. *Water Science and Technology, 62*(3), 728.

Shan, Yan, Chen, Kezheng, Yu, Xuegang, & Gao, Lian. (2010). Preparation and characterization of biocompatible magnetic carbon nanotubes. *Applied Surface Science, 257*(2), 362-366.

Sun, Qiangqiang, Wang, Yu, Li, Laisheng, Bing, Jishuai, Wang, Yingxin, & Yan, Huihua. (2015). Mechanism for enhanced degradation of clofibric acid in aqueous by catalytic ozonation over MnOx/SBA-15. *J.Hazard.Mater, 286*, 276-284.

Sun, Qingye, & Yang, Linzhang. (2003). The adsorption of basic dyes from aqueous solution on modified peat–resin particle. *Water Research, 37*(7), 1535-1544.

Suriyanon, Nakorn, Permrungruang, Jutima, Kaosaiphun, Jidanan, Wongrueng, Aunnop, Ngamcharussrivichai, Chawalit, & Punyapalakul, Patiparn. (2015). Selective adsorption mechanisms of antilipidemic and non-steroidal anti-inflammatory drug residues on functionalized silica-based porous materials in a mixed solute. *Chemosphere, 136*, 222-231.

Tan, IAW, Hameed, BH, & Ahmad, AL. (2007). Equilibrium and kinetic studies on basic dye adsorption by oil palm fibre activated carbon. *Chem.Eng.J, 127*(1), 111-119.

Ternes, Thomas A. (2001). Analytical methods for the determination of pharmaceuticals in aqueous environmental samples. *TrAC Trends in Analytical Chemistry, 20*(8), 419-434.

Ternes, Thomas A, Joss, Adriano, & Siegrist, Hansruedi. (2004). Peer reviewed: scrutinizing pharmaceuticals and personal care products in wastewater treatment. *Environ.Sci.Technol, 38*(20), 392A-399A.

Ternes, Thomas A, Meisenheimer, Martin, McDowell, Derek, Sacher, Frank, Brauch, Heinz-Jürgen, Haist-Gulde, Brigitte, . . . Zulei-Seibert, Ninette. (2002). Removal of pharmaceuticals during drinking water treatment. *Environ.Sci.Technol, 36*(17), 3855-3863.

Thommes, Matthias. (2010). Physical adsorption characterization of nanoporous materials. *Chem.Ing.Tech., 82*(7), 1059-1073.

Tonghuan, Liu, Guojian, Duan, Xiaojiang, Duan, Wangsuo, Wu, & Ying, Yang. (2013). Adsorptive features of polyacrylic acid hydrogel for UO2 2+. *J.Radioanal.Nucl.Chem., 297*(1), 119-125.

Tsutsumi, Osamu. (2005). Assessment of human contamination of estrogenic endocrine-disrupting chemicals and their risk for human reproduction. *J.Steroid Biochem., 93*(2), 325-330.

Vallet-Regi, María, Balas, Francisco, & Arcos, Daniel. (2007). Mesoporous materials for drug delivery. *Angew. Chem. Int. Ed., 46*(40), 7548-7558.

Vallet-Regí, María, Balas, Francisco, & Arcos, Daniel. (2007). Mesoporous materials for drug delivery. *Angewandte Chemie International Edition, 46*(40), 7548-7558.

Walas, Stanley M. (1985). *Phase equilibria in chemical engineering* (Vol. 4): Butterworth Boston.

Wang, Jingjing, Lu, Jinming, Yang, Jianhua, Xiao, Wei, & Wang, Jinqu. (2012). Synthesis of ordered MCM-48 by introducing economical anionic surfactant as co-template. *Mater Lett, 78*, 199-201.

Wang, Shaobin, & Li, Huiting. (2006). Structure directed reversible adsorption of organic dye on mesoporous silica in aqueous solution. *Microporous.Mesoporous.Mater, 97*(1), 21-26.

Wang, Xiufang, Liu, Ping, & Tian, Yong. (2011). Ordered mesoporous carbons for ibuprofen drug loading and release behavior. *Microporous Mesoporous .Mesoporous.Mater., 142*(1), 334-340.

Wu, Feng-Chin, Tseng, Ru-Ling, & Juang, Ruey-Shin. (2009). Initial behavior of intraparticle diffusion model used in the description of adsorption kinetics. *Chem.Eng.J, 153*(1), 1-8.

Xiao, Xuechun, Zhang, Fei, Feng, Zhipeng, Deng, Shaojuan, & Wang, Yude. (2015). Adsorptive removal and kinetics of methylene blue from aqueous solution using NiO/MCM-41 composite. *Physica E, 65*, 4-12.

Xu, Zhizhong, Xia, Ao, Wang, Changchun, Yang, Wuli, & Fu, Shoukuang. (2007). Synthesis of raspberry-like magnetic polystyrene microspheres. *Materials chemistry and physics, 103*(2), 494-499.

Yang, Piaoping, Huang, Shanshan, Kong, Deyan, Lin, Jun, & Fu, Honggang. (2007). Luminescence functionalization of SBA-15 by YVO_4: Eu^{3+} as a novel drug delivery system. *Inorg. Chem., 46*(8), 3203-3211.

Yu, Lian, Yang, Xiaofang, & Wang, Dongsheng. (2015). TiO 2 incorporated in magnetic mesoporous SBA-15 by a facile inner-pore hydrolysis process toward enhanced adsorption–photocatalysis performances for As (III). *J.Colloid Interf.Sci, 448*, 525-532.

Zhang, L., Lv, J., Xu, T., Yang, L., Jiang, X., & Li, Q. (2013). High efficiency removal and recovery of an endocrine disrupting compound-bisphenol AF from wastewaters. *Sep. Purif. Technol., 116*, 145-153.

Zhang, Lei, Lv, Junna, Xu, Tianci, Yang, Lijun, Jiang, Xiaoqing, & Li, Qi. (2013). High efficiency removal and recovery of an endocrine disrupting compound–bisphenol AF from wastewaters. *Sep. Purif. Technol, 116*, 145-153.

Zhao, Dongyuan, Feng, Jianglin, Huo, Qisheng, Melosh, Nicholas, Fredrickson, Glenn H, Chmelka, Bradley F, & Stucky, Galen D. (1998). Triblock copolymer syntheses of mesoporous silica with periodic 50 to 300 angstrom pores. *Science, 279*(5350), 548-552.

Zhao, Dongyuan, Huo, Qisheng, Feng, Jianglin, Chmelka, Bradley F, & Stucky, Galen D. (1998). Nonionic triblock and star diblock copolymer and oligomeric surfactant syntheses of highly ordered, hydrothermally stable, mesoporous silica structures. *J.Am.Chem.Soc., 120*(24), 6024-6036.

Zhao, Huiling, Hu, Jun, Wang, Jianjun, Zhou, Lihui, & Liu, Honglai. (2007). CO 2 capture by the amine-modified mesoporous materials. *Acta Physico-Chimica Sinica, 23*(6), 801-806.

Zhao, Mingfei, Tang, Zhaobin, & Liu, Peng. (2008). Removal of methylene blue from aqueous solution with silica nano-sheets derived from vermiculite. *J Hazard Mater, 158*(1), 43-51.

Zhao, Wenru, Gu, Jinlou, Zhang, Lingxia, Chen, Hangrong, & Shi, Jianlin. (2005). Fabrication of uniform magnetic nanocomposite spheres with a magnetic core/mesoporous silica shell structure. *Journal of the American Chemical Society, 127*(25), 8916-8917.

Zhao, XS, Lu, GQ, Whittaker, AK, Millar, GJ, & Zhu, HY. (1997). Comprehensive study of surface chemistry of MCM-41 using 29Si CP/MAS NMR, FTIR, pyridine-TPD, and TGA. *J.Phys.Chem.B, 101*(33), 6525-6531.

Zhu, Yu-fang, Shi, Jian-lin, Li, Yong-sheng, Chen, Hang-rong, Shen, Wei-hua, & Dong, Xiao-ping. (2005a). Storage and release of ibuprofen drug molecules in hollow mesoporous silica spheres with modified pore surface. *Microporous .Mesoporous.Mater, 85*(1), 75-81.

PUBLICATIONS

1. Synthesis mechanism and thermal optimization of an economical mesoporous material using silica: Implications for the effective removal or delivery of ibuprofen, Shanmuga Kittappa, Mingcan Cui, Malarvili Ramalingam, Shaliza Ibrahim, Jeehyeong Khim, Yeomin Yoon, Shane A. Snyder, Min Jang*, ***PLOS ONE*** [1st Tier Journal with impact factor of 3.534 (2014)], Refer to **Appendix A,** **h**ttp://journals.plos.org/plosone/article?id=10.1371/journal.pone.0130253

2. Amine modified magnetised nano composite material for removal of Bisphenol A, Ibuprofen and Clofibric acid. Shanmuga Kittappa, Min Jang*, In preparation expected submission in December 2015

CONFERENCES, ORAL AND POSTER PRESENTED

1. Economical Synthesis of Magnetized Nano Structured Carbon Materials for Treatment of Ibuprofen in Water. Shanmuga Kittappa, Min Jang*, Oral Presentation at ***International Conference on Water and Wastewater Management (ICWWM)***. 8th – 10th October 2013, Kuala Lumpur, Malaysia.

2. Silica Powder based Mesoporous Materials: Its Application to Fast and Recyclable Removal of Pharmaceutical Compounds in Water. Shanmuga Kittappa, Min Jang, Published in the conference proceeding Oral Presentation at ***International Water Association (IWA) conference***, held in Dalian China19 – 20 May 2015-Refer to **Appendix B**

3. Mesoporous Silica Materials: Its Application in removal Ibuprofen from waste water. Shanmuga Kittappa, Min Jang*. Oral Presentation and Published in the conference proceeding. ***The 12th National Seminar of Laboratory Technology***, Balai Ungku Aziz, Dental Faculty, University of Malaya. 9-11 February 2015

APPENDIX A

PLOS | ONE

RESEARCH ARTICLE

Synthesis Mechanism and Thermal Optimization of an Economical Mesoporous Material Using Silica: Implications for the Effective Removal or Delivery of Ibuprofen

Shanmuga Kittappa[1], Mingcan Cui[2], Malarvili Ramalingam[3], Shaliza Ibrahim[1], Jeehyeong Khim[2], Yeomin Yoon[4], Shane A. Snyder[5], Min Jang[1,6]*

1 Department of Civil Engineering, Faculty of Engineering, University of Malaya, Kuala Lumpur, Malaysia, **2** School of Civil, Environmental, and Architectural Engineering, Korea University, Seoul, Republic of Korea, **3** Department of Chemistry, Jalan Sultan Petaling Jaya, Selangor, Malaysia, **4** Department of Civil and Environmental Engineering, University of South Carolina, Columbia, South Carolina, United States of America, **5** Department of Chemical and Environmental Engineering, University of Arizona, Tucson, Arizona, United States of America, **6** Nanotechnology and Catalysis Research Centre (NANOCAT), University of Malaya, Kuala Lumpur, Malaysia

* minjang@um.edu.my

OPEN ACCESS

Citation: Kittappa S, Cui M, Ramalingam M, Ibrahim S, Khim J, Yoon Y, et al. (2015) Synthesis Mechanism and Thermal Optimization of an Economical Mesoporous Material Using Silica: Implications for the Effective Removal or Delivery of Ibuprofen. PLoS ONE 10(7): e0130253. doi:10.1371/journal.pone.0130253

Editor: Heidar-Ali Tajmir-Riahi, University of Quebec at Trois-Rivieres, CANADA

Received: April 14, 2015

Accepted: May 19, 2015

Published: July 10, 2015

Data Availability Statement: All relevant data are within the paper.

Funding: This research was funded by the Malaysian Government Ministry of Higher Education through the High Impact Research Grant (D000062-16001), and partly supported by the Basic Science Research Program through a National Research Foundation of Korea (NRF) grant funded by the Korea government (MEST, No. KRF-2009-0092799). The funders had no role in study design, data

Abstract

Mesoporous silica materials (MSMs) were synthesized economically using silica (SiO_2) as a precursor via a modified alkaline fusion method. The MSM prepared at 500°C (MSM–500) had the highest surface area, pore size, and volume, and the results of isotherms and the kinetics of ibuprofen (IBP) removal indicated that MSM–500 had the highest sorption capacity and fastest removal speed *vs*. SBA–15 and zeolite. Compared with commercial granular activated carbon (GAC), MSM–500 had a ~100 times higher sorption rate at neutral pH. IBP uptake by MSM–500 was thermodynamically favorable at room temperature, which was interpreted as indicating relatively weak bonding because the entropy (Δ_{adsS}, –0.07 J mol^{-1} K^{-1}) was much smaller. Five times recycling tests revealed that MSM–500 had 83–87% recovery efficiencies and slower uptake speeds due to slight deformation of the outer pore structure. In the IBP delivery test, MSM–500 drug loading was 41%, higher than the reported value of SBA–15 (31%). The *in vitro* release of IBP was faster, almost 100%, reaching equilibrium within a few hours, indicating its effective loading and unloading characteristics. A cost analysis study revealed that the MSM was ~10–70 times cheaper than any other mesoporous silica material for the removal or delivery of IBP.

Introduction

Mesoporous silica materials (MSMs) have large, ordered pores, ranging from 2 to 50 nm, as classified by the International Union of Pure and Applied Chemistry (IUPAC) [1, 2]. MSMs have thick framework walls with interconnected channel structures and a high surface area

APPENDIX B

大连理工大学

Dalian University of Technology, Dalian 116024, P. R. China

Certificate of Oral Presentation

This is to certify that SHANMUGA SUNTHARAM KITTAPPA attended the IWA Nano and Water Regional Conference 2015, which was held from 20th to 23rd of May 2015 at Dalian, China, and presented paper entitled Silica powder based mesoporous materials, its application to fast and recyclable removal of pharmaceutical compounds in water in oral technical session.

Xie Quan, Professor, PhD, Chairman of the organization committee
Key Laboratory of Industrial Ecology & Environmental Engineering
Dalian University of Technology
Linggong Road 2#, Dalian, 116024, China
Phone: +86-411-84706140;
Fax: +86-411-84706263;
E-mail: quanxie@dlut.edu.cn